

CARNEGIE MELLON UNIVERSITY

ANALYSIS OF HEATING, VENTILATION, AND AIR
CONDITIONING DUCTS AS A RADIO FREQUENCY
COMMUNICATION CHANNEL

A DISSERTATION
SUBMITTED TO THE GRADUATE SCHOOL
IN PARTIAL FULFILLMENT OF THE REQUIREMENTS
for the degree
DOCTOR OF PHILOSOPHY
in
ELECTRICAL AND COMPUTER ENGINEERING

by

PAVEL V. NIKITIN

Pittsburgh, Pennsylvania

August, 2002

Copyright © 2002 by Pavel Nikitin
All Rights Reserved

I dedicate this work to my lovely wife Elena who kept inspiring me all these years.

Abstract

A typical HVAC duct system is a network of interconnected hollow metal pipes which can serve as waveguides and carry electromagnetic waves. This work presents an analysis of this system as a radio frequency communication channel. Two main parts of the analysis include channel modelling and antenna design.

The propagation modelling approach used here is based on the waveguide mode theory and employs the transfer matrix method to describe propagation through various cascaded HVAC elements. This allows one to model the channel response in the frequency domain. Impulse response characteristics of the ducts are also analyzed in this work.

The approximate transfer matrices of cylindrical straight sections, bends, and tapers are derived analytically. The transforming properties of cylindrical T-junctions are analyzed experimentally.

Antenna designs in waveguides and free-space are different. In waveguides, mode excitation characteristics are important as well as the impedance match. The criteria for antenna design in waveguides are presented here. Antennas analyzed in this work are monopole antennas, dipole antennas, and antenna arrays.

The developed model can predict both channel response and antenna characteristics for a given geometry and dimensions of the duct system and the antennas. The model is computationally efficient and can potentially be applied to duct systems of multiple story buildings. The accuracy of the model has been validated with extensive experimental measurements on real HVAC ducts.

Acknowledgements

I am grateful to all people whose direct and indirect contribution made this dissertation possible.

I consider myself lucky to have Daniel Stancil as my advisor. His guidance and influence can not be overestimated. Conversations with him always led to new ideas and insights, and his human behavior always set a personal example for me.

I would like to thank my committee members James Hoburg, Tuviah (Ed) Schlesinger, and Roy Nicolaides, who helped me to steer my research and showed me different angles of looking at the problems.

I acknowledge Asea Brown Bovari (ABB) Group for the financial support of this research and express my gratitude to all members of the HVAC project group. The team spirit helped me to achieve what I could not have done alone.

I am fortunate to have such friends as Ratish Punnoose, Richard Tseng, J. P. Van't Hof, Ahmet Cepni and Ariton Xhafa, who always were available to assist me with experiments or to resolve technical problems related to the research.

I am also greatly indebted to my wife and all of my family, whose constant love and support brought me to where I am now.

Table of Contents

1	Introduction	1
1.1	Motivation and background	1
1.2	Approaches and relevant work	4
1.3	Outline of the dissertation	6
2	Propagation model	9
2.1	Introduction	9
2.2	Assumptions	11
2.3	Arbitrary duct system	12
2.4	Straight duct	19
2.5	Discussion	21
2.6	Summary	22
3	Antennas	23
3.1	Introduction	23
3.2	Antenna impedance and current distribution	25
3.3	Selective mode excitation	27
3.4	Monopole antenna	29
3.5	Dipole antenna	36
3.6	Antenna array	40
3.7	Mode content analysis with a frequency-swept antenna	45
3.8	Summary	50
4	Transfer matrices	51
4.1	Introduction	51
4.2	Definitions	53
4.3	Matrix properties	55
4.4	Cascaded system	56

4.5	Straight sections	57
4.6	Bends	58
4.7	Tapers	59
4.8	T-junction	61
4.9	Summary	64
5	Impulse response	67
5.1	Introduction	67
5.2	Definitions	68
5.3	Physical mechanisms	69
5.4	Dispersion	71
5.5	RMS delay spread	75
5.6	Coherence bandwidth	78
5.7	Discussion	80
5.8	Summary	81
6	Comparison with experiment	83
6.1	Introduction	83
6.2	Experimental setup	83
6.3	Frequency response	87
6.4	Impulse response	99
6.5	Discussion	100
6.6	Summary	102
7	Summary	103
7.1	Summary	103
7.2	Suggestions for future work	104
A	Fields in waveguides	107
A.1	Introduction	107
A.2	Rectangular waveguide	109
A.3	Cylindrical waveguide	113
A.4	Bessel function roots	115
B	Design tool	119

List of Figures

1.1	Using an HVAC duct system for indoor communications.	3
2.1	Block diagram of the HVAC communication system.	10
2.2	Back-scattering in a cascaded system.	12
2.3	Transmitting and receiving antennas in an arbitrary duct system.	13
2.4	Circuit model of the HVAC communication system.	15
2.5	Equivalent circuit representations of the receiving antenna in a multimode duct. . .	16
2.6	Reflections in an arbitrary duct system terminated on the ends.	18
2.7	Transmitting and receiving antennas in a straight duct.	19
2.8	Channel gain as a function of frequency for two 3.1 cm long vertical monopole antennas located 15 m apart in a 30.5 cm cylindrical duct made of steel.	21
3.1	Equivalent circuit representations of the transmitting antenna in a multimode duct. .	25
3.2	Sinusoidal current distribution on a wire antenna.	27
3.3	Monopole antenna in a rectangular duct.	30
3.4	Parameters \mathcal{P} and \mathcal{T} as functions of the distance to the wall d ($l = 3.06$ cm) (A) and monopole length l ($d = 0.2$ m)(B) for a monopole antenna in a rectangular 0.4 m x 0.2 m duct at 2.45 GHz.	31
3.5	Mode distributions excited by monopole antennas with $l = 3.06$ cm, $d = 0.2$ m (A) and $l = 10$ cm, $d = 0.2$ m (B) in a rectangular duct 0.4 m x 0.2 m at 2.45 GHz. . .	32
3.6	Monopole antenna in a cylindrical duct.	33
3.7	Parameters \mathcal{P} and \mathcal{T} as functions of monopole length in a 30.5 cm cylindrical duct at 2.45 GHz.	35
3.8	Mode distributions excited by monopole antennas with $l = 3.06$ cm (A) and $l = 15.6$ cm (B) in a 30.5 cm cylindrical duct at 2.45 GHz.	35
3.9	Dipole antenna in a rectangular duct.	36
3.10	Dipole antenna in a cylindrical duct.	38

3.11	Parameters \mathcal{P} and \mathcal{T} for a dipole antenna as functions of the arc radius for $l = 3.06$ cm (A) and arm length for $r_d = 4$ cm (B) in a 30.5 cm cylindrical duct at 2.45 GHz.	39
3.12	Mode distributions excited by dipole antennas with $l = 3.06$ cm, $r_d = 4$ cm (A) and $l = 7$ cm, $r_d = 4$ cm (B) in a 30.5 cm cylindrical duct at 2.45 GHz.	40
3.13	Block diagram of a general transmitting antenna array.	40
3.14	Antenna array for selective mode excitation.	41
3.15	Attenuation (dB) as a function of distance between monopole antennas in a straight matched duct (A) and its spatial autocorrelation function (B) for two 3.06 cm monopole antennas in a 30.5 cm cylindrical duct at 2.45 GHz separated by 15 m.	42
3.16	A receiving 3-element antenna array.	44
3.17	Practical implementation of a passive receiving 3-element antenna array.	44
3.18	Frequency responses of the channel between a single transmitting antenna and each antenna in an array located 5 m away in a straight 30.5 cm cylindrical duct. Each probe is a 3.1 cm monopole probe. Spacing between array probes is 5 cm.	45
3.19	Swept-frequency mode content measurement with a single antenna.	46
3.20	Attenuation as a function of frequency (A) and its normalized frequency autocorrelation function (B) for two 3.06 cm monopole antennas located 15 m apart in a 30.5 cm straight cylindrical duct with matched ends.	47
3.21	Magnitude of normalized mode coefficients excited in a 30.5 cm cylindrical duct by a 3.06 cm monopole antenna as functions of frequency in 2.4-2.5 GHz band.	48
3.22	Normalized magnitude of theoretically generated mode coefficients excited in a 30.5 cm cylindrical duct by a 3.1 cm monopole antenna and their values extracted via the mode extraction technique.	49
4.1	A general HVAC element with multiple ports.	54
4.2	A symmetrical HVAC element: Y-junction.	56
4.3	Cascaded system of HVAC elements.	56
4.4	HVAC element in the form of a straight section.	57
4.5	HVAC element in the form of a bend.	58
4.6	HVAC element in the form of a taper.	59
4.7	HVAC element in the form of a symmetrical T-junction.	62
4.8	Mode distribution coming into port 1 and mode distributions coming out of ports 2 and 3 of the T-junction made of 30.5 cm cylindrical ducts in the 2.4-2.5 GHz band.	65
5.1	Propagation of two modes in a straight terminated duct with three types of dispersion present.	70

5.2	Different types of dispersion in the calculated power delay profiles: intramodal (A), intermodal and intramodal (B), multipath and intramodal (C), and combined (D).	74
5.3	Calculated and analytically approximated RMS delay spread and coherence bandwidth as functions of transmitter-receiver separation distance for 30.5 cm diameter cylindrical ducts and 3.5 cm monopole antennas in the 2.4-2.5 GHz band.	76
5.4	“Striped” impulse response profile.	77
5.5	Normalized RMS delay spread of the “striped” impulse response as a function of $\xi_0 = T_0/T$ and $\xi_1 = T_1/T$, defined for $T_0 \geq T_1$.	79
5.6	Normalized RMS delay spread and mean excess delay of the “striped” impulse response for $T_0 = 2T_1$.	79
6.1	Cylindrical duct 30.5 cm (12 in.) in diameter, used in experiments.	84
6.2	General experimental setup.	84
6.3	Agilent E8358A network analyzer used for measurements.	85
6.4	Experimental setup for bend and taper measurements.	86
6.5	Experimental setup for T-junction measurements.	86
6.6	Straight section, metal end cap, bend, taper, and T-junction used in experiments.	88
6.7	Monopole and dipole antennas used in experiments.	89
6.8	Mounting of monopole and dipole antennas on the duct.	89
6.9	Outside and inside view of the monopole probe antenna mounted on the duct.	89
6.10	Theoretical and experimental frequency responses for two monopole antennas in a straight open-ended duct with antenna separation distance 4.58 m (A), 7.54 m (B), 9.20 m (C), 11.63 m (D), and other parameters given in Table 6.3.	91
6.11	Comparison of the experimental frequency response for two monopole antennas in a straight open-ended duct and the theoretical frequency response computed using the end reflection coefficient $G = 0$ (A), $G = 0.2$ (B), $G = 0.4$ (C), $G = 0.6$ (D), and other parameters given in Table 6.3.	92
6.12	Comparison of the theoretical and experimental frequency responses for two monopole antennas in a straight open-ended duct with distance to the farthest open end 10.39 m (A) and 1.24 m (B), with other parameters given in Table 6.3.	93
6.13	Theoretical and experimental frequency responses for two monopole antennas in a straight open-ended duct with antenna length 0.9 cm (A) and 14.8 cm (B), and other parameters given in Table 6.3.	94
6.14	Theoretical and experimental frequency responses for two dipole antennas in a straight cylindrical open-ended duct (A) and for two monopole antennas in a straight rectangular open-ended (B), with other parameters given in Table 6.3.	94

6.15	Theoretical and experimental frequency responses for two monopole antennas in a straight duct short-terminated on one end with separation distance 2.44 m (A) and 4.53 m (B), with other parameters given in Table 6.3.	95
6.16	Theoretical and experimental frequency responses for two monopole antennas in a straight duct short-terminated on both ends, with other parameters given in Table 6.3.	96
6.17	Theoretical and experimental frequency responses for two monopole antennas in an open-ended bent duct (A) and tapered duct (B), with other parameters given in Table 6.3.	97
6.18	Experimental frequency responses for two monopole antennas in an open-ended duct with a T-junction and other parameters given in Table 6.3.	97
6.19	Theoretical and experimental power delay profiles for two monopole antennas in a straight duct with open ends (A) and closed ends (B) (other parameters are given in Table 6.5).	100
6.20	RMS delay spread: comparison of theoretical model with experimental data for two 3.5 cm monopole antennas in a 30.5 cm steel cylindrical duct with open ends ($G =$) and closed ends ($G = -0.9$).	101
A.1	Rectangular waveguide.	109
A.2	Mode cutoff frequencies in a 2:1 rectangular waveguide.	110
A.3	First 18 modes of a 2:1 rectangular waveguide (courtesy Andrew Greenwood, University of Illinois at Urbana-Champaign).	112
A.4	Cylindrical waveguide.	113
A.5	Mode cutoff frequencies in a cylindrical waveguide.	113
A.6	First 15 modes of a cylindrical waveguide (courtesy Andrew Greenwood, University of Illinois at Urbana-Champaign).	116
B.1	The program structure of the Duct Explorer.	119
B.2	The graphical user interface of the Duct Explorer	122

List of Tables

1.1	Number of modes in rectangular and cylindrical ducts at 915 MHz, 2.4835 GHz, and 5.825 GHz.	2
1.2	Attenuation in different communications media at 2.4 GHz, dB for 100 m.	3
5.1	The RMS delay spread σ_τ due to different types of dispersion.	74
5.2	Parameters of the modes excited in a 30.5 cm cylindrical duct by a 3.5 cm monopole probe antenna at 2.5 GHz.	75
6.1	Parameters of ducts used in experiments.	84
6.2	Parameters of bends, tapers, and T-junctions used in experiments.	85
6.3	Parameters of the frequency response experiments.	90
6.4	Comparison of theoretical predictions and experimental measurements of the average channel gain in the band.	98
6.5	Parameters of the impulse response experiments.	99
A.1	Values of p'_{nm} for TE modes in a cylindrical waveguide	117
A.2	Values of p_{nm} for TM modes in a cylindrical waveguide	117

Chapter 1

Introduction

1.1 Motivation and background

There are several different ways to provide network access inside a large office building. High-speed connection can be provided by Ethernet line or fiber optics, which may be a costly option. Wireless is an attractive alternative but the design of a wireless network in large buildings is still a difficult task due to the nature of indoor propagation [1, 2]. As an alternative, existing infrastructures, such as powerlines [3, 4, 5, 6, 7] or phonelines [8, 9], can be used for data communications. Recently, Stancil and coworkers proposed to use heating, ventilation, and air conditioning (HVAC) ducts for signal distribution inside buildings [10, 11, 12].

HVAC ducts are designed for the distribution of air. They also present a new indoor communication channel with potentially high data transmission capacity at radio frequencies (RF), which can satisfy the need for high-speed network access. This technology can be used with any standards (IEEE 802.11b, IEEE 802.11a, HIPERLAN, and HIPERLAN2) as long as the band used is above the duct system cutoff frequency.

The HVAC duct system in most buildings consists of interconnected hollow metal pipes of rectangular or circular cross-section, which behave as multimode waveguides when driven at RF frequencies. A typical duct used in the U.S. is a cylindrical pipe of 12 inches (approximately 30.5

cm) in diameter with the cutoff frequency of 577 MHz. The most common frequencies used for unlicensed wireless communications are Industrial, Scientific, and Medical (ISM) and Unlicensed National Information Infrastructure (UNII) bands (902-928 MHz, 2.4-2.4835 GHz, 5.15-5.35 GHz, 5.725-5.825 GHz), which are above the aforementioned cutoff. Table 1.1 lists the number of modes in rectangular and cylindrical ducts of various sizes at the upper frequencies of the mentioned frequency bands.

Table 1.1: Number of modes in rectangular and cylindrical ducts at 915 MHz, 2.4835 GHz, and 5.825 GHz.

Duct	Size	915 MHz	2.4835 GHz	5.825 GHz
Cylindrical	6 in. diameter	-	5	24
Cylindrical	12 in. diameter	2	17	91
Cylindrical	18 in. diameter	6	40	197
Cylindrical	24 in. diameter	10	66	313
Rectangular	6 in. x 3 in.	-	5	25
Rectangular	12 in. x 6 in.	1	21	108
Rectangular	18 in. x 9 in.	5	44	243
Rectangular	24 in. x 12 in.	10	81	438

There are many advantages of using an HVAC duct system for indoor signal distribution. First, the HVAC duct system, used as a communication infrastructure, is already present in almost any building. Second, the power loss in the ducts is very low compared to free-space propagation and even a coaxial cable, as shown in Table 1.2. Third, the HVAC duct channel is electrically shielded from the rest of the indoor environment and not affected by time-varying factors, such as moving people and rearrangement of furniture and other objects. Fourth, various transmitting powers or frequencies can potentially be used inside the ducts without violating emittance and interference regulations, provided that leakage from the duct system into the building space can be controlled. Fifth, the data capacity of the HVAC duct channel is high, which means that all of building services (data, voice, security, controls, alarms) can potentially be integrated into a single duct-based communication system. Finally, the HVAC ducts are robust to damage and will continue to carry RF signals even if some parts of the duct system were damaged.

Table 1.2: Attenuation in different communications media at 2.4 GHz, dB for 100 m.

HVAC ducts	Coaxial cable	Free space
1-10	30-70	80

On September 11, 2001, the leaky coaxial cable system in one of the World Trade Center towers was destroyed [13]. That system provided wireless communications between the floors of the skyscraper. After it was destroyed, hand-held radio communication between fire-fighters on different floors became impossible. In the absence of a repeater system, hand-held radios can penetrate only a few floors in a high-rise building made of concrete and steel. An HVAC duct system used for communications could also serve as a reliable repeater system in skyscrapers.

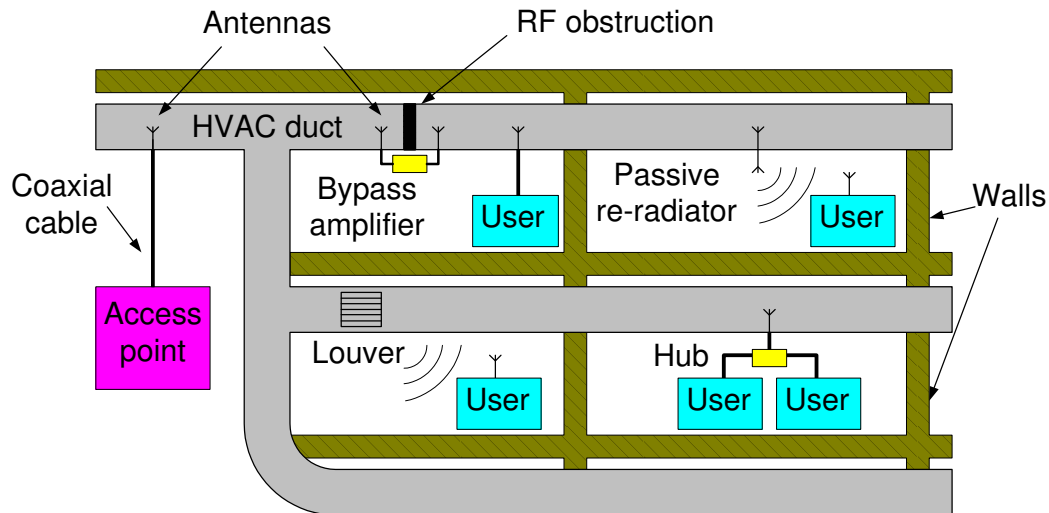


Figure 1.1: Using an HVAC duct system for indoor communications.

Figure 1.1 shows an example of an HVAC system used for signal distribution. The access point is connected to the transmitting antenna which excites waveguide modes in the duct system. These modes propagate through the duct system with different group velocities and attenuation constants, experiencing multiple reflections from terminations and non-uniformities, and are received in the end by the receiving antenna. The number of modes may vary depending on geometry and dimensions of HVAC duct system elements. Users access the system either directly (via a cable connected

to the office antenna) or wirelessly (passive office antenna or duct louver re-radiate into the office space). Coupling around various RF obstructions can be achieved with bypass amplifiers. HVAC ducts can be modified to improve their RF propagation characteristics. One can envision that in buildings of the future the HVAC system will be co-designed not only to satisfy the air flow requirements but also to serve as a good radio communication channel (be “radio-friendly”).

To design an effective signal distribution system based on HVAC ducts, a solid understanding of physical properties of ducts at RF frequencies is needed. It is also highly desirable to have a reliable propagation model, which would allow one to interactively investigate the dependence of channel frequency and impulse responses on duct network layout and dimensions, antenna geometry and locations, frequency band, etc. Having such a model is crucial for planning and performance optimization of HVAC communication system.

1.2 Approaches and relevant work

A channel model describes how the signal changes when it propagates through a certain environment. There are two general approaches to modelling radio wave propagation. One approach is based on fitting an empirical formula or parameters of an assumed statistical distribution to measured data, which allows one to model the behavior of scalar quantities, such as power or delay spread [14, 15]. This approach does not possess a physical insight but allows one to model complex systems. Another approach is based on electromagnetic (EM) theory computations using specific information about the environment and can reproduce in detail complicated physical phenomena [16]. This approach is based on physical principles but may be difficult to use in case of complex systems.

Traditional indoor and outdoor propagation environments have been extensively studied using both approaches [17, 18, 19, 20, 21, 22, 23]. Using HVAC ducts for indoor signal propagation has been proposed only recently, and the channel characteristics of this unique communication environment have not yet been explored.

An HVAC duct system is a network of multimode waveguides whose layout and dimensions may

vary in different buildings but are known for each particular case. Empirical approaches to HVAC channel modelling are not very efficient because for each case considered (certain duct dimensions, antenna geometries, operating frequencies, etc.), a new set of measurements needs to be performed, although only once. Theoretical approaches are more attractive because they do not require measurements to predict the channel response and allow optimization of the system performance based on derived parameter dependence.

Theoretical approaches to modelling propagation in multimode waveguides include ray tracing [24], numerical modelling [25], parabolic equation modelling [26, 27], and mode theory [28]. Ray tracing methods use the geometrical optics approximation, which is not applicable when the wavelength is comparable to the duct cross-section. Numerical methods, such as finite element method (FEM), typically require generating a mesh that covers the whole problem space. For duct systems this can be very computationally expensive. Parabolic equation methods neglect back-scattering and model forward propagation in a heterogeneous media step by step. Homogeneous empty ducts of either rectangular or circular cross-section allow normal mode solution, which eliminates the necessity of using the parabolic equation approach.

Multimode waveguides are widely used in optics [29, 30, 31] but are less common in traditional RF and microwave engineering [32, 33]. Using multimode waveguides for long distance communications was proposed in the early 50's [34, 35]. Later, using hollow metallic waveguides for optical transmission was studied [36].

The current applications of multimode waveguides are usually power flow and energy distribution [37, 38, 39], typically to and from high-power microwave devices [40] and waveguide antennas [41] or for waveguide discontinuity problems [42]. Problems involving multimode propagation exist in other areas of engineering. At FM frequencies, automobile, railway, and coal mine tunnels behave as multimode waveguides [43, 44, 45]. The problem of radio wave propagation in a tunnel environment has been analyzed using modal theory [46, 47, 48, 49], geometrical optics [50, 51, 52, 53, 54, 55], and statistical analysis [56, 57]. A good comparison of modal and ray-tracing approaches for modelling propagation in tunnels can be found in [58].

The phenomena of multimode wave guiding is also observed in atmospheric propagation in the form of evaporation and oceanic surface-based ducts [59, 60, 61] as well as in acoustic oceanic floor propagation [62, 63, 64].

Reviews of specific literature pertaining to channel models, antenna design, transfer matrix methods, and impulse response characteristics in HVAC ducts are included in the appropriate chapters.

1.3 Outline of the dissertation

This work presents an analysis of HVAC ducts as an RF communication channel. The approach uses waveguide mode theory to calculate coupling in and out of the duct and employs the transfer matrix method to describe propagation through various HVAC elements (straight, bends, tapers, etc.). The transfer matrix of a specific HVAC element can either be measured experimentally or calculated using any of the approaches mentioned in the previous section.

The analysis described here is based on the traditional waveguide theory which has been well developed over the last fifty years. Novel contributions of this work include the treatment of a double probe waveguide system as a communication channel, the derivation of a channel frequency response in a general multimode waveguide using the transfer matrix method, the analysis of channel impulse response characteristics, the investigation of selective mode excitation with various antennas, the technique of the mode content measurement with a single antenna, and the development of an interactive software tool for planning an indoor communication system using HVAC ducts as a propagation channel.

The model presented in this work can predict both channel characteristics and antenna characteristics for given geometry and dimensions of duct system and antennas. The model is computationally efficient and can potentially be applied to duct systems of multiple story buildings. The accuracy of the model has been validated with extensive experimental measurements on real HVAC ducts.

The rest of the dissertation is organized as follows. Chapter 2 describes a propagation model. Antennas for HVAC ducts are discussed in Chapter 3 together with an antenna-based mode content measurement technique. Chapter 4 explains the transfer matrix method and presents matrices for certain HVAC elements. The impulse response is discussed in Chapter 5. Chapter 6 describes an experimental setup and presents comparison between data and theory. Conclusions are given in Chapter 7.

Chapter 2

Propagation model

2.1 Introduction

The simplest HVAC duct communication channel can be viewed as a waveguide with two probes coupled into it. This specific problem has been considered in literature before. The mutual impedance of two probes in an infinite rectangular waveguide was first found by Ittipiboon and Shafai [65] using a vector potential. Wang [66, 67] found the mutual impedance of two infinitely thin probes in semi-infinite rectangular and circular waveguides for the multimode case using a general dyadic Green's function. Li and coworkers [68, 69] analyzed the mutual impedance of two probes in an infinite rectangular waveguide with a dielectric discontinuity.

From a communications point of view, we are interested in the frequency response of the channel between two probes coupled into an HVAC duct system rather than in their mutual impedance. It is known that a communication channel can be completely characterized by its frequency response, i.e. transfer function. The latter can in principle be found via mutual impedance. However, mutual impedance formulas derived by the authors mentioned above are very complex even for special cases considered. For the purposes of design of a wireless HVAC distribution system, it is highly desirable to have a simple analytical model. This model must be valid for ducts of different cross-sections and allow one to investigate easily the frequency response dependence on such parameters

as antenna geometry, transmitter-receiver separation distance, duct cross-section size, conductivity of the duct material, reflection coefficient of the terminated duct ends, etc.

Aside from the special cases mentioned above, where a mutual impedance between monopole probes was derived, the problem of finding a transfer function of an arbitrary multimode waveguide system with two antennas coupled into it has not been analyzed in the literature. The model presented here allows one to predict a frequency response between two antennas coupled into an arbitrary duct system. The response is given by an analytical formula dependent on duct layout and dimensions, antenna geometry and locations, and operating frequency. The influence of specific HVAC elements between the transmitter and the receiver is taken into account via their transfer matrices, which can be measured or calculated as shown in Chapter 4.

Figure 2.1 shows a block diagram of a communication system using HVAC ducts. The transmitter is connected to the transmitting antenna, which excites a number of waveguide modes that propagate in the duct. The receiving antenna senses those modes and provides a signal for the receiver.

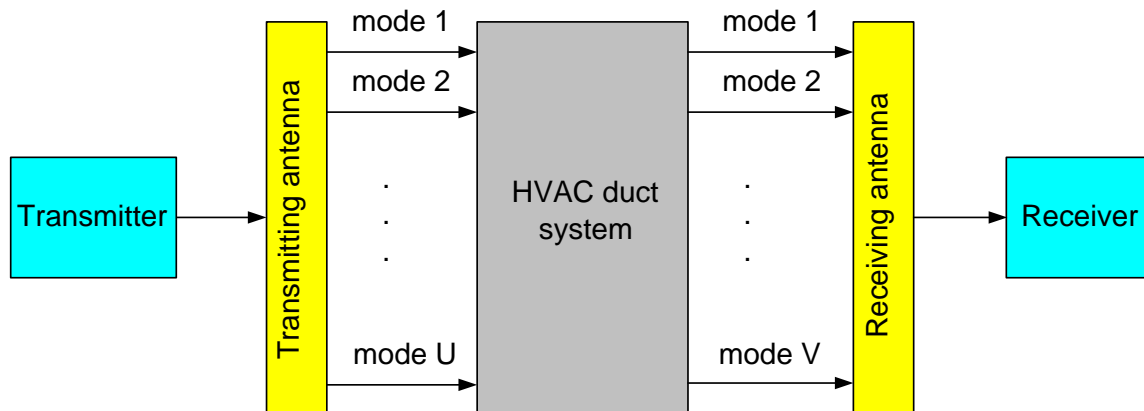


Figure 2.1: Block diagram of the HVAC communication system.

2.2 Assumptions

A rigorous solution to the double probe waveguide system involves calculating a Green's function of the waveguide, including both evanescent and non-evanescent modes, matching the EM boundary conditions on waveguide walls and antenna surfaces, and computing self-consistently currents on the antennas.

Finding a Green's function of an arbitrary waveguide system and computing exact currents on the antenna coupled into such a system are not easy tasks. To make the problem tractable, we make several approximations.

First, we assume that the current distributions on both transmitting and receiving antennas are known. In most cases, this assumption is valid. For example, the current distribution on single wire antennas can be assumed to be sinusoidal, even when such an antenna is inserted into a waveguide [70].

Second, we assume that the amplitudes of excited waveguide modes can be calculated for a transmitting antenna in a straight infinite waveguide (waveguide with matched loads on the ends). This allows one to find excited mode coefficients as functions only of antenna parameters and of waveguide cross-section at the antenna location.

Third, we assume that the back-scattering from the internal waveguide structure can be neglected. This assumption is valid when the reflection from the junctions between two elements is relatively small. This allows the use of a forward beam propagation approach, similar to the one used in optics.

Figure 2.2 illustrates this on the example of three cascaded HVAC duct elements. Suppose that only mode is propagating. Assume that the reflection coefficient from any of the two ports of elements 1 and 2 is G . Let the transmission coefficient (equivalent of a transfer matrix for a single mode case) of the element 1 and the element 2 be T . Assume for simplicity that the elements are connected via a lossless transmission line, which is sufficiently short to neglect the phase change. If the wave with a normalized amplitude of 1 arrives from the left, the forward beam propagation

approach predicts that the output wave amplitude will be T after the element 1 and T^2 after the element 2. If we were to take into account the reflections between elements 1 and 2, the output wave amplitude would be $T^2 + T^2 G^2 + T^2 G^4 + \dots = T^2 [1 + O(G^2)]$, showing that reflections are a second order effect provided that G is small. Including the internal reflections into consideration increases

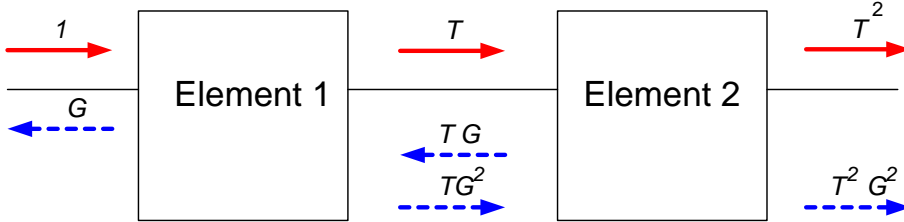


Figure 2.2: Back-scattering in a cascaded system.

the complexity of the problem exponentially with the number of potential reflection points [71]. Thus, we will consider only reflections from the terminated waveguide ends, which may have large reflection coefficients.

Last, we assume that antennas are sufficiently far apart to neglect coupling via evanescent modes. Power in evanescent modes decays sharply with the distance, thus only modes whose cutoff frequency is below the operating frequency are considered.

The intuitive approach of propagating the excited EM field in a waveguide and adding the reflections from the ends is similar to summing up the multipath reflections of an antenna radiating in an outdoor environment. The frequency response solution obtained via this approach delivers a good agreement with experimental measurements, which can be viewed as a validation of this approach.

2.3 Arbitrary duct system

There are many possible HVAC duct architectures. The duct system in a building is a three-dimensional structure, which extends to all floors and has multiple branches. We will consider only a certain class of duct systems. From the point of view of RF propagation, many other types of duct architectures can be reduced to this class. Figure 2.3 shows the type of duct systems that we

will consider: an arbitrary duct system with two terminated ends.

The current in the transmitting antenna radiates in the duct and excites modes, which travel to the right and to the left from the transmitting antenna. Both left and right ends of the waveguide are terminated with arbitrary loads. The system consists of three parts: the section to the left of the transmitter, the section between the receiver and the transmitter, and the section to the right of the receiver. Each section can be characterized by its transfer matrix, which describes a transformation of an incoming mode distribution into the outgoing mode distribution (see Chapter 4). The transfer matrices of the three parts of the system are \hat{P} , \hat{Q} , and \hat{R} . The load terminations are characterized by reflection matrices \hat{F} and \hat{G} .

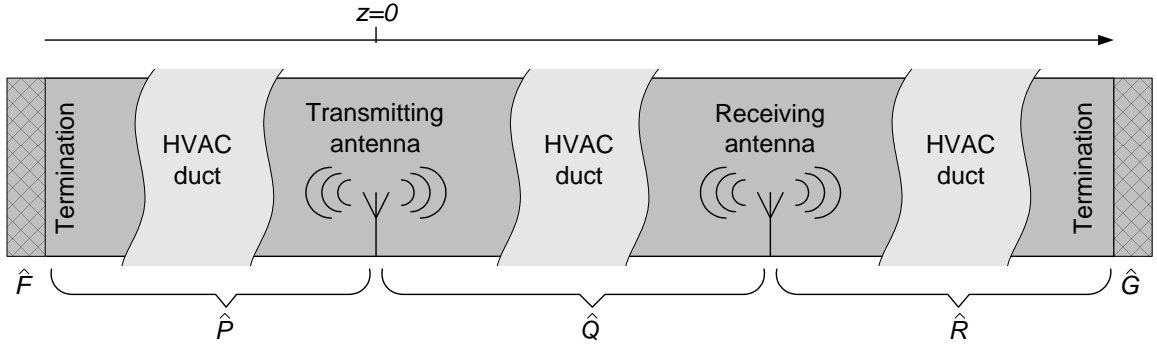


Figure 2.3: Transmitting and receiving antennas in an arbitrary duct system.

The number of propagating modes is determined by the dimensions of a waveguide and the excitation frequency. The waveguide with U propagating modes is considered to be multimode if $U > 1$. An arbitrary propagating electric field \vec{E} in such a waveguide can be represented in terms of normal waveguide modes as

$$\vec{E} = \sum_{u=1}^U \vec{E}_u = \sum_{u=1}^U C_u \vec{e}_u e^{\pm\gamma_u z}, \quad (2.1)$$

where u is the mode index, \vec{E}_u is electric field of waveguide mode u , C_u is the mode coefficient of mode u , \vec{e}_u is the normalized electric field of mode u , γ_u is the complex propagation constant of mode u , and z is the longitudinal coordinate along the direction of propagation. Mode index u represents separate degenerate and non-degenerate TE and TM modes and their conventional

indices n and m , all combined into one. Mode coefficient C_u is the electric field amplitude measured in volts per meter (V/m).

To find the channel response, we need to know what is the amplitude of each mode excited by the transmitting antenna. Mode coefficients excited by an antenna with a known current distribution in a waveguide can be computed using a standard microwave technique for probe-waveguide coupling [32, 72]. This technique is based on the power density flow conservation, which says that the power dissipated on the antenna must be equal to the power carried by the mode in both directions:

$$P_u + P_u = -\frac{1}{2} \int_A \vec{E}_u \cdot \vec{J} dS, \quad (2.2)$$

where P_u is the time-average power carried by mode u in one direction, \vec{J} is the surface current density on the transmitting antenna measured in amperes per meter (A/m), and the integral is taken over the surface A of the transmitting antenna. For thin wire antennas, this integral becomes

$$P_u + P_u = -\frac{1}{2} \int \vec{E}_u \cdot \vec{J} dl, \quad (2.3)$$

where \vec{J} is the current through the transmitting antenna cross-section measured in amperes (A) and the integral is taken over the length of the transmitting antenna. To preserve the generality of derivations, we will consider antennas in the form of a conducting surface with a given surface current density distribution.

The time-average power P_u can be represented as

$$P_u = |C_u|^2 p_u, \quad (2.4)$$

where p_u is the normalized power carried by mode u in one direction. The surface current density on the transmitting antenna can be represented as

$$\vec{J} = I_o \vec{j}, \quad (2.5)$$

where I_o is the current amplitude at the antenna terminals and \vec{j} is the normalized surface current density distribution. Mode coefficients excited by the transmitting antenna then can be expressed as

$$C_u = -\frac{I_o}{4p_u} \int_A \vec{\epsilon}_u \cdot \vec{j} dS. \quad (2.6)$$

To distinguish between the transmitting and the receiving antennas, we will use a superscript $'$. The EM field at the receiving antenna can also be decomposed into the sum of normal modes. Denote the mode coefficients at the receiving antenna as C'_v , where v is the mode index. Assume that the presence of the receiving antenna does not perturb the field in a waveguide. From the time reversal [73] and reciprocity principles [74, 75, 76], the relationship between the mode coefficient and the current it induces on the receiving antenna is the same as in Equation 2.6:

$$C'_v = -\frac{I'_v}{4p'_v} \int_{A'} \vec{\epsilon}'_v \cdot \vec{j}' dS', \quad (2.7)$$

where $\vec{\epsilon}'_v$ is the normalized electric field of waveguide mode v at the receiver, \vec{j}' is the normalized surface current distribution on the receiving antenna, and the integral is taken over the surface A' of the receiving antenna.

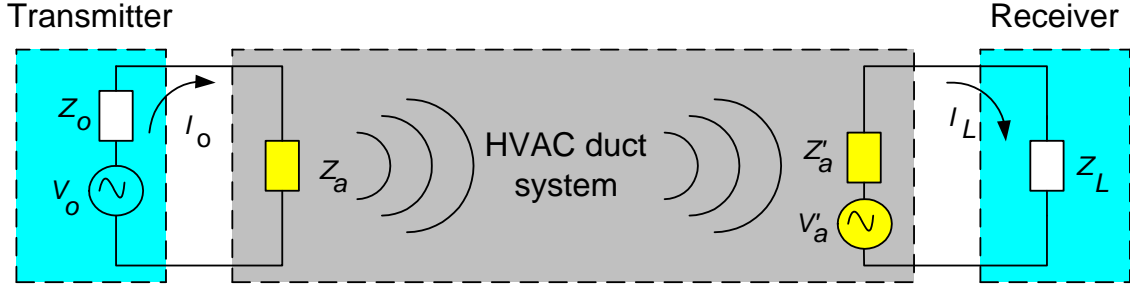


Figure 2.4: Circuit model of the HVAC communication system.

Figure 2.4 shows the circuit model of the HVAC communication system, where V_o is the voltage of the transmitter source, Z_o is the internal impedance of the transmitter, Z_a is the transmitting antenna impedance, Z'_a is the receiving antenna impedance, V'_a is the voltage induced on the receiving antenna, and Z_L is the internal impedance of the receiver load. We assume that the transmitter and the receiver are connected to the antennas by cables that are matched to their internal impedances. The current in the transmitting antenna can be found as

$$I_o = \frac{V_o}{Z_o + Z_a}. \quad (2.8)$$

Figure 2.5 shows three equivalent circuit representations of the receiving antenna in a multimode waveguide. The first representation is a series of Norton circuits, where each circuit corresponds to

a specific mode v , inducing a current I'_v on the receiving antenna. The second representation is a series of equivalent Thevenin circuits. The induced voltage V'_v in each circuit is computed as

$$V'_v = I'_v Z'_v, \quad (2.9)$$

where Z'_v is the impedance of the receiving antenna due to mode v . The third representation is a combined Thevenin equivalent circuit. The total voltage on the receiving antenna is

$$V'_a = \sum_{v=1}^V V'_v, \quad (2.10)$$

where the summation is performed over all propagating modes at the cross-section of the receiving antenna. The sum of voltages is linear because the waveguide modes are orthogonal. The voltage appearing at the receiver load can be found as

$$V_L = I_L Z_L, \quad (2.11)$$

where the current in the receiver load is

$$I_L = \frac{V'_a}{Z'_a + Z_L}. \quad (2.12)$$

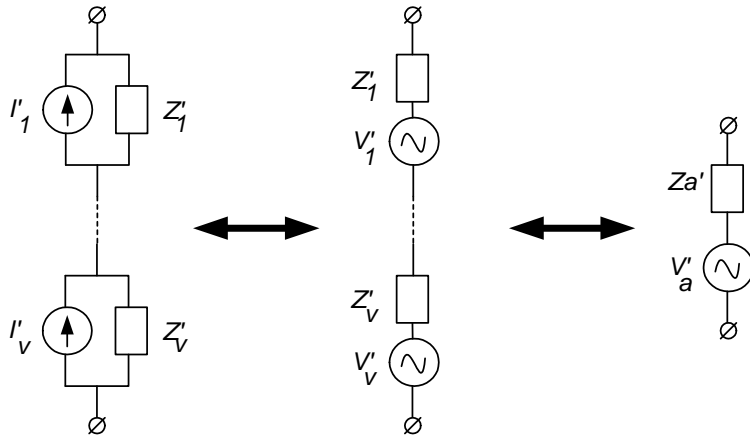


Figure 2.5: Equivalent circuit representations of the receiving antenna in a multimode duct.

We need a channel model that can be compared with experimental data. Experimentally, the channel response is usually measured with respect to some reference. A typical reference case is

where both the transmitter and the receiver are connected directly by a lossless matched cable. In this case, the reference measured voltage on the receiver load is

$$V_{REF} = \frac{V_o Z_L}{Z_o + Z_L}. \quad (2.13)$$

The real cables are not lossless, but the loss is usually calibrated out by the measuring equipment. The frequency response can then be determined as

$$H(\omega) = \frac{V_L}{V_{REF}}. \quad (2.14)$$

Combining Equations 2.11, 2.12, 2.13, and 2.14 allows one to express the frequency response as

$$H(\omega) = \frac{(Z_o + Z_L)V'_a}{(Z'_a + Z_L)V_o}. \quad (2.15)$$

Using Equations 2.7, 2.9, and 2.10 allows one to write the transfer function as

$$H(\omega) = \frac{Z_o + Z_L}{(Z_o + Z_a)(Z'_a + Z_L)} \sum_{v=1}^V \frac{-4p'_v Z'_v C'_v}{I_o \int_{A'} \vec{\epsilon}_v \cdot \vec{j} dS'}. \quad (2.16)$$

The mode distribution \vec{C} excited by the transmitting antenna and the mode distribution \vec{C}' observed at the receiving antenna are related as

$$\vec{C}' = \hat{T} \vec{C}, \quad (2.17)$$

where \hat{T} is the system transfer matrix, which describes the change in mode content from the transmitter to the receiver and \vec{C}' and \vec{C} are column vectors. The transfer matrix of a cascaded system can be found as a product of the respective transfer matrices (see Chapter 4).

Let us introduce a special notation for the integral that defines the interaction of the antenna current with the mode electric field:

$$\mathcal{I}_u = \int_A \vec{\epsilon}_u \cdot \vec{j} dS. \quad (2.18)$$

Using this notation together with Equations 2.7 and 2.17 allows one to write the final expression for the frequency response as

$$H(\omega) = \frac{Z_o + Z_L}{(Z_o + Z_a)(Z'_a + Z_L)} \sum_{v=1}^V \frac{Z'_v p'_v}{\mathcal{I}'_v} \sum_{u=1}^U \frac{T_{vu} \mathcal{I}_u}{p_u}, \quad (2.19)$$

where T_{vu} are the elements of the transfer matrix \hat{T} .

In the system shown in Figure 2.3, each mode will experience multiple reflections from the loads on terminated duct ends. The mode distribution observed at the receiving antenna can be found as a sum of an infinite geometric series, which converges because of the conductor wall loss and the loss at each reflection. Using a method of time-domain reflectometry [77, 78, 79, 80], we can construct a picture of reflections. Figure 2.6 shows possible reflection paths in the system, which allows one

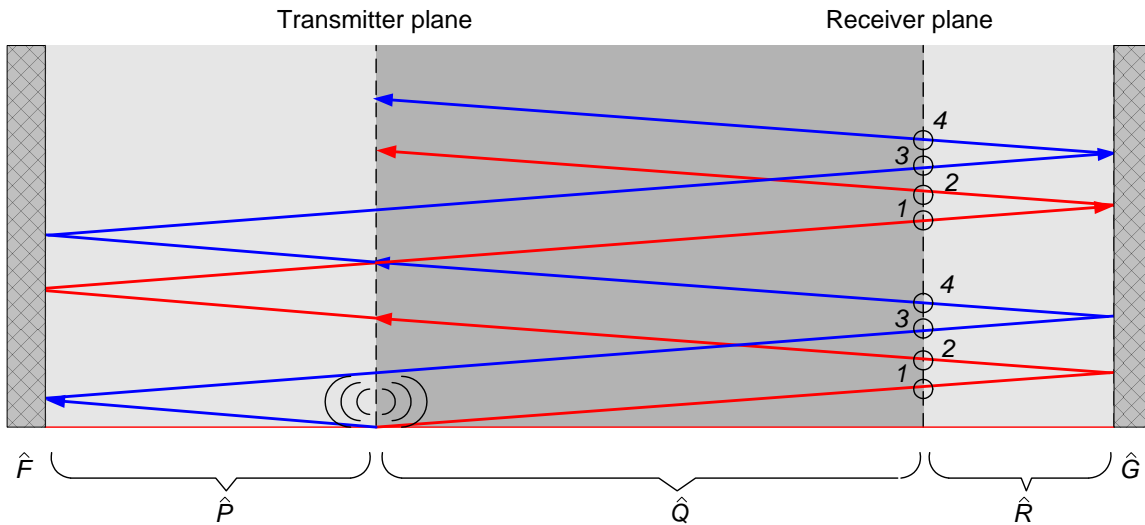


Figure 2.6: Reflections in an arbitrary duct system terminated on the ends.

to identify four main terms in a series plus their periodic replicas.

The first term corresponds to the direct propagation path transmitter-receiver and can be characterized by the transfer matrix \hat{Q} . The second term corresponds to the propagation path transmitter-right termination-receiver and can be characterized by the transfer matrix $\hat{R}\hat{G}\hat{R}\hat{Q}$. The third term corresponds to the propagation path transmitter-left termination-receiver and can be characterized by the transfer matrix $\hat{Q}\hat{P}\hat{F}\hat{P}$. The fourth term corresponds to the propagation path transmitter-left termination-right termination-receiver and can be characterized by the transfer matrix $\hat{R}\hat{G}\hat{R}\hat{Q}\hat{P}\hat{F}\hat{P}$.

The overall system transfer matrix \hat{T} is

$$\hat{T} = \left(\hat{Q} + \hat{R}\hat{G}\hat{R}\hat{Q} + \hat{Q}\hat{P}\hat{F}\hat{P} + \hat{R}\hat{G}\hat{R}\hat{Q}\hat{P}\hat{F}\hat{P} \right) \left(\hat{I} + \hat{Y} + \hat{Y}^2 + \dots \right), \quad (2.20)$$

where \hat{I} is the identity matrix and \hat{Y} is the matrix that describes one roundtrip propagation of the mode pack, which originates at the receiver, reflects once from each duct end, and arrives to the receiver again:

$$\hat{Y} = \hat{R}\hat{G}\hat{R}\hat{Q}\hat{P}\hat{F}\hat{P}\hat{Q}. \quad (2.21)$$

If the loads are matched, there are no reflections from the terminated ends ($\hat{F} = \hat{G} = 0$). In this specific case, the system transfer matrix is the transfer matrix of the section between the transmitter and the receiver ($\hat{T} = \hat{Q}$).

2.4 Straight duct

Consider a straight duct terminated at both ends with arbitrary loads as shown in Figure 2.7. This system is analyzed in [81]. Assume that terminations have constant reflection coefficients G_1 and G_2 for all waveguide modes. The distance between the transmitter and the receiver is L , and the respective distances to the terminated ends are L_1 and L_2 .

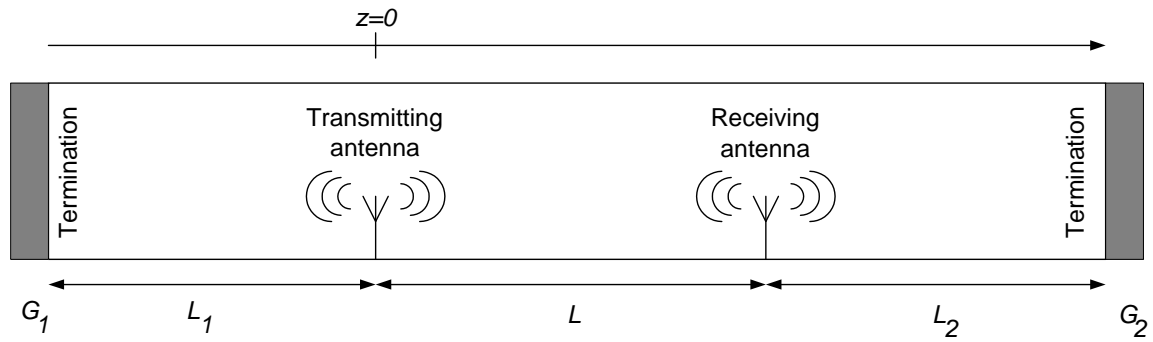


Figure 2.7: Transmitting and receiving antennas in a straight duct.

In such a system, matrices \hat{P} , \hat{Q} , \hat{R} , \hat{F} , and \hat{G} are square and diagonal:

$$P_{vu} = e^{-\gamma_u L_1} \delta_{vu}, \quad (2.22)$$

$$Q_{vu} = e^{-\gamma_u L} \delta_{vu}, \quad (2.23)$$

$$R_{vu} = e^{-\gamma_u L_2} \delta_{vu}, \quad (2.24)$$

$$F_{vu} = G_1 \delta_{vu}, \quad (2.25)$$

$$G_{vu} = G_2 \delta_{vu}, \quad (2.26)$$

where δ_{uv} is the Kronecker delta, and no summation over indices is implied. Matrix \hat{Y} is also square and diagonal

$$\Upsilon_{uv} = G_1 G_2 e^{-2\gamma_u(L+L_1+L_2)} \delta_{vu}. \quad (2.27)$$

The sum of matrix products can then be found as

$$\hat{Q} + \hat{R}\hat{G}\hat{R}\hat{Q} + \hat{Q}\hat{P}\hat{F}\hat{P} + \hat{R}\hat{G}\hat{R}\hat{Q}\hat{P}\hat{F}\hat{P} = \hat{I}(1 + G_1 e^{-2\gamma_u L_1})(1 + G_2 e^{-2\gamma_u L_2}). \quad (2.28)$$

The sum of the infinite geometric series in Equation 2.20 can be calculated as

$$\hat{I} + \hat{Y} + \hat{Y}^2 + \dots = \frac{\hat{I}}{1 - G_1 G_2 e^{-2\gamma_u(L+L_1+L_2)}}. \quad (2.29)$$

To further simplify the problem and obtain elegant results, let us make two assumptions. First, assume that the transmitter and the receiver have the same internal impedance ($Z_o = Z_L$), which is often the case. Second, assume that the transmitting and the receiving antennas are identical ($Z_a = Z'_a, \vec{j} = \vec{j}'$).

The frequency response of a straight terminated duct in this case can be expressed as

$$H(\omega) = \frac{2Z_o}{(Z_o + Z_a)} \sum_{v=1}^V Z_v e^{-\gamma_v L} \frac{(1 + G_1 e^{-2\gamma_v L_1})(1 + G_2 e^{-2\gamma_v L_2})}{1 - G_1 G_2 e^{-2\gamma_v(L+L_1+L_2)}}. \quad (2.30)$$

A typical frequency response generated with Equation 2.30 for the channel contained between two monopole antennas inserted into a straight cylindrical duct with matched ends is shown in Figure 2.8.

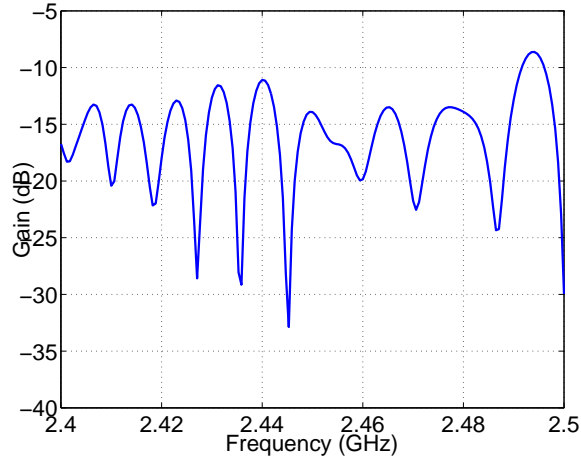


Figure 2.8: Channel gain as a function of frequency for two 3.1 cm long vertical monopole antennas located 15 m apart in a 30.5 cm cylindrical duct made of steel.

2.5 Discussion

Equation 2.19 gives a complex frequency response of the HVAC duct channel. The dependence on the antenna parameters is contained in interaction integrals \mathcal{I}_u and \mathcal{I}'_v and impedances Z'_v , Z_a and Z'_a . The dependence on the duct shape and size at the cross-sections, where the transmitter and the receiver are located, is contained in impedances Z'_v , Z_a , and Z'_a , interaction integrals \mathcal{I}_u and \mathcal{I}'_v , and normalized power densities p_u and p'_v . The dependence on the properties of the duct system between the transmitter and the receiver is contained in the transfer matrix elements T_{vu} .

To analyze the propagation characteristics of the HVAC duct system, quantities Z'_v , \mathcal{I}_u , \mathcal{I}'_v , p_u , p'_v , Z_a , Z'_a have to be computed only one time. Once they are determined, the dependence of the frequency response on the transfer matrix \hat{T} can be investigated. This capability is especially useful for optimal system design purposes which may require multiple computations of the transfer function. E.g., to optimize the antenna performance in a given HVAC duct channel, quantities \hat{T} , p_u , p'_v may be fixed and other quantities, dependent on the antenna characteristics, may be varied.

2.6 Summary

This Chapter presented a channel model for the complex frequency response between two antennas inserted into an arbitrary HVAC duct system in terms of the system transfer matrix. The system may contain multiple cascaded elements of various geometry. The derived frequency response depends on the parameters of the transmitting and receiving antennas, the transfer matrix of the duct system, and the impedances of the transmitter and the receiver. For the straight duct with two terminated ends the solution simplifies and results in an elegant formula.

Chapter 3

Antennas

3.1 Introduction

To transmit and receive the signal, antennas are needed to couple into the duct waveguide. The theory and design of antennas radiating into free-space is well established. The main differences between the waveguide propagation environment and free-space are: 1) the waves can propagate only along the guide; 2) the propagating field can always be decomposed into a finite sum of normal modes. An antenna in free space can be characterized by the far-field radiation pattern. In waveguides, a characteristic analogous to the antenna radiation pattern is the excited mode distribution [35].

One efficient way of coupling in and out of a microwave guide is a monopole probe fed by a coaxial cable. This technique has been mentioned as early as in the late 40's by Marcuvitz [82], Marchand [83], and Montgomery, Dicke, and Purcell [74].

Most researchers were interested in the impedance of waveguide probes coupled into a single-mode waveguide. Self-impedance of a coaxially fed short monopole probe coupled into a waveguide was first found by Lewin [84] and Collin [72], and then studied extensively by Otto [85], Williamson [86, 87], Williamson and Otto [88, 89], Keam and Williamson [90], Rollins [91], Jarem [92, 93], Liang and Zaki [94], Lee and Yung [95], and others [96]. The above authors con-

sidered both rectangular and cylindrical waveguides but restricted their consideration to monopole probe-like antennas. Hejase et al. [97] analyzed a circular loop antenna in a parallel-plate waveguide. Recently, dipole antennas in parallel-plate [98] and rectangular [99] waveguides were analyzed from the point of view of finding a Green's function in each case although no impedance expressions were given.

We are interested not only in the antenna impedance, but also in the mode distribution that the antenna excites in a duct. Designing an antenna with a good impedance match is important but it is also critical to be able to excite a desired mode distribution to build an effective waveguide communication system.

Both the excited mode distribution and the antenna resistance can be expressed via an interaction integral. The antenna reactance can be obtained from the resistance via the Hilbert transform, widely used in engineering [100, 101, 102, 103]. Hence, to calculate the channel response using the approach presented in Chapter 2, only an antenna interaction integral needs to be found.

Below, we will derive an interaction integral for monopole and dipole antennas in rectangular and cylindrical ducts. The impedance results obtained here for a monopole antenna in a rectangular waveguide and in a cylindrical duct can be reduced to those derived by Lewin [84] and Lee and Yung [95] respectively (latter assumed that the monopole length is smaller than the waveguide radius). The expressions for the impedance of a dipole antenna in rectangular and cylindrical duct and the impedance of a monopole antenna with length longer than the waveguide radius have not appeared in the literature before.

A useful application of antennas in waveguides is selective mode excitation. While many mode selection techniques are known [104], selective mode excitation with simple monopole and dipole antennas coupled into a multimode waveguide has not previously been studied. Yet it seems to be the most viable, practical, and economically effective solution for HVAC communication purposes.

Even more effective mode excitation characteristics can potentially be obtained with antenna arrays. While many experimental mode content measurement techniques employ probe arrays [105, 106], using antenna arrays for waveguide excitation has been addressed only recently. Antenna array

excitation of a TEM mode in a parallel-plate waveguide was explored by Tomasic and Hessel [107, 108]. Stepanov [109] studied multi-element chamber excitation for improvement of uniformity of microwave energy distribution. Lienard et al. [110] studied antenna array performance in a tunnel environment. It appears that the analysis of an antenna array for selective mode excitation in a general multimode waveguide has not appeared in literature yet.

3.2 Antenna impedance and current distribution

The complex impedance of a general antenna is

$$Z_a = R_a + jX_a, \quad (3.1)$$

where R_a is the resistance and X_a is the reactance. In a multimode waveguide with an orthogonal set of normal modes, the antenna can be viewed as a series network of loads, with each load corresponding to a specific mode, as shown in Figure 3.1. The impedance of each load is defined by the interaction between the antenna current and the electric field of a specific waveguide mode. The

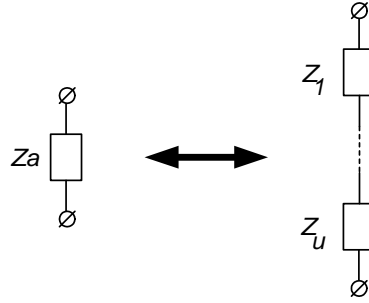


Figure 3.1: Equivalent circuit representations of the transmitting antenna in a multimode duct.

antenna impedance is

$$Z_a = \sum_{u=1}^U R_u + j \sum_{u=1}^U X_u, \quad (3.2)$$

where R_u is antenna radiation resistance due to mode u and X_u is antenna reactance due to mode u .

The radiation resistance R_u can be found in terms of the power radiated into mode u . If the power carried by mode u in one direction is P_u , then the total power radiated into mode u can be

expressed as

$$\frac{1}{2} I_o^2 R_u = 2 P_u = 2 p_u |C_u|^2 . \quad (3.3)$$

In terms of an interaction integral \mathcal{I}_u and a normalized power density p_u , the resistance R_u is

$$R_u = \frac{|\mathcal{I}_u|^2}{4p_u} . \quad (3.4)$$

The normalized power density p_u for rectangular and cylindrical waveguides is given by Equations A.25 and A.39. The parameter that needs to be computed for a specific antenna is an interaction integral \mathcal{I}_u .

If the antenna resistance R_u is known, the antenna reactance X_u can be found via the Hilbert transform, which relates real and imaginary parts of a causal analytic response function as

$$X_u(\omega) = \frac{1}{\pi} \int_{-\infty}^{+\infty} \frac{R_u(y)}{\omega - y} dy . \quad (3.5)$$

This integral can be estimated using various series expansion or numerical quadrature methods. We propose to use a simple approximation that leads to a closed-form result.

Assume that the band-limited resistance $R_u(\omega)$ is known for N frequency points $(\omega_1, \omega_2, \dots, \omega_N)$. Let us approximate the impedance $Z_u(\omega) = R_u(\omega) + jX_u(\omega)$ with step functions at each frequency point:

$$Z_u(\omega) = \begin{cases} 0 & \text{if } \omega < \omega_1 - \frac{\Delta\omega}{2} \\ r_n + j x_n & \text{if } \omega_n - \frac{\Delta\omega}{2} \leq \omega < \omega_n + \frac{\Delta\omega}{2} \\ 0 & \text{if } \omega_N + \frac{\Delta\omega}{2} \leq \omega \end{cases} , \quad (3.6)$$

where $\Delta\omega = \omega_n - \omega_{n-1}$. The values x_n of an unknown reactance $X_u(\omega)$ can be found by calculating the integral given by Equation 3.5 as a discrete sum over the frequency band of interest $(\omega_1 \dots \omega_N)$.

The closed-form expression for the reactance then is:

$$x_n = -\frac{2}{\pi} \sum_{k=1}^N \int_{f_k - \frac{\Delta f}{2}}^{f_k + \frac{\Delta f}{2}} \frac{r_k}{f_n^2 - y^2} dy = -\frac{2}{\pi} \sum_{k=1}^N r_k \ln \left| \frac{(\omega_n + \frac{\Delta\omega}{2})^2 - \omega_k^2}{(\omega_n - \frac{\Delta\omega}{2})^2 - \omega_k^2} \right| . \quad (3.7)$$

In most cases, a sinusoidal current distribution can be assumed on a wire antenna. This approximation has been successfully applied by many authors to modelling antennas in rectangular and cylindrical waveguides [95, 66, 70]. The sinusoidal current on a thin wire antenna is

$$\vec{J}(\xi) = I_o \frac{\sin k(l - \xi)}{\sin kl} \vec{\xi}, \quad (3.8)$$

where I_o is the current amplitude at the antenna terminals, $k = \omega/c$ is the free-space wave number, l is the probe length, and ξ is the coordinate along the antenna length ($0 \leq \xi \leq l$). Figure 3.2 shows a segment of the wire antenna with a sinusoidal current distribution on it. The interaction integral \mathcal{I}

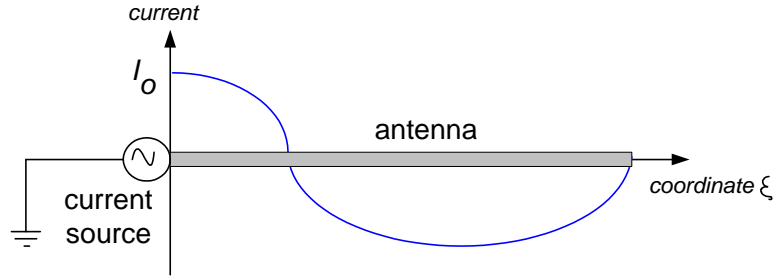


Figure 3.2: Sinusoidal current distribution on a wire antenna.

can be calculated by simply integrating along the length of the antenna:

$$\mathcal{I} = \int_0^l \vec{e}_\xi(\xi) \frac{\sin k(l - \xi)}{\sin kl} d\xi, \quad (3.9)$$

where \vec{e}_ξ is the electric field component along the antenna.

3.3 Selective mode excitation

One of the mechanisms that affects the capacity of the HVAC duct channel is multimode dispersion. Multimode dispersion between different modes in the ducts can significantly affect the inter-symbol interference (ISI) and, hence, the capacity of the channel. Redistribution of energy between different modes when the signal passes through HVAC elements with non-trivial geometry (T-junctions, Y-junctions, etc.) can also affect the signal-to-noise ratio (SNR) in our channel.

An effective way to reduce dispersion and control the excited mode distribution is to use antennas designed for selective mode excitation. “Selective mode” means either a single mode excitation or a preferred mode excitation.

Single mode excitation refers to exciting mostly one mode and is useful for HVAC systems where inter-mode coupling and conversion is non-significant. In such systems, exciting a single low order low-loss mode (e.g., TE_{01}) allows one to significantly reduce both attenuation and dispersion in the channel.

Preferred mode excitation refers to exciting a specific mode distribution which propagates through the duct system favorably. It is useful for HVAC systems which contain a number of complex elements, which cause mode coupling and conversion (e.g., T-junctions).

We will concentrate on studying single mode excitation characteristics. To design an effective single mode antenna, the power radiated into some mode must be maximized. The power carried by mode u is proportional to the radiation resistance R_u . Let us introduce a mode power coefficient, which is the power carried by the most excited mode normalized by the power carried by all modes:

$$\mathcal{P} = \frac{\max_{u=1\dots U} R_u}{\sum_{u=1}^U R_u}. \quad (3.10)$$

The parameter \mathcal{P} can vary between almost 0 (a very large number of comparably excited modes) and 1 (all power is carried by one mode). An alternative parameter that can be used instead of a mode power coefficient is the next mode rejection ratio, which is the power carried by the most excited mode normalized by the power carried by the next most excited mode. Optimization results would depend on what parameter was chosen for optimization. We will use the mode power coefficient.

The impedance match is also very important since it allows one to maximize the power delivered from the transmitter to the antenna. The mismatch between the antenna impedance Z_a and the transmitter impedance Z_o can be characterized by the reflection coefficient Γ :

$$\Gamma = \frac{Z_a - Z_o}{Z_a + Z_o}. \quad (3.11)$$

The parameter that indicates the quality of the impedance match is the power transmission coeffi-

cient \mathcal{T} :

$$\mathcal{T} = 1 - |\Gamma|^2. \quad (3.12)$$

The parameter \mathcal{T} varies on the same scale as the parameter \mathcal{P} , between 0 (all power is reflected back) and 1 (a perfect impedance match).

To maximize both parameters simultaneously, we can introduce a linear cost function \mathcal{C} :

$$\mathcal{C} = \mathcal{W}_{\mathcal{P}} \mathcal{P} + \mathcal{W}_{\mathcal{T}} \mathcal{T}, \quad (3.13)$$

where $\mathcal{W}_{\mathcal{P}}$ and $\mathcal{W}_{\mathcal{T}}$ are weights which indicate the importance of the relative power delivered to a single mode and the power delivered to the whole antenna. If the weights are properly chosen, maximizing the cost function allows one to design an optimal antenna.

The peak of the cost function should be smooth rather than sharp. The reason for this is when the real antenna is manufactured, its physical parameters may be different from the specifications. A smooth peak results in less sensitivity to manufacturing variations.

For illustrative purposes, we prefer to explore the behavior of \mathcal{P} and \mathcal{T} independently to separate the underlying physical phenomena.

3.4 Monopole antenna

A simple way of coupling in and out of the duct is to use a coaxially fed monopole probe antenna. A typical monopole antenna used for communications is a quarter-wavelength monopole, which in free space has a good impedance match with the 50Ω load. The current is zero at the tip of such monopole and maximum at the antenna source terminals. When such an antenna is inserted into a duct, its radiation characteristics change.

Consider a monopole antenna inserted into a rectangular waveguide as shown in Figure 3.3. The parameters of this antenna are its length l , its distance from the waveguide wall d , and its orientation (vertical). The coordinate ξ along the antenna is $\xi = y$. The interaction integral of interest \mathcal{I} is

$$\mathcal{I} = \int_0^l \epsilon_y(y)|_{x=d} \frac{\sin k(l-y)}{\sin kl} dy, \quad (3.14)$$

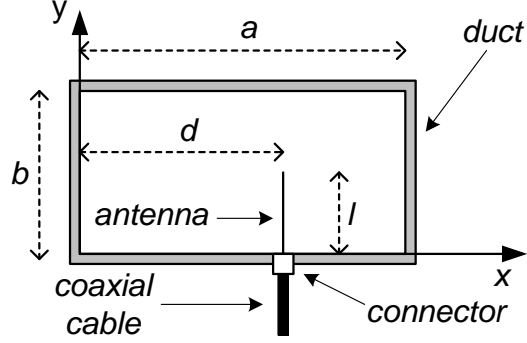


Figure 3.3: Monopole antenna in a rectangular duct.

where k is the free space wave number. First, let us calculate an intermediate result needed for further computations:

$$\mathcal{D} = \int_0^l \cos \frac{m\pi y}{b} \sin k(l-y) dy = \frac{1}{k} \left[\frac{\cos \frac{m\pi l}{b} - \cos kl}{1 - \left(\frac{m\pi}{kb}\right)^2} \right]. \quad (3.15)$$

Using this result together with the normalized field expressions given by Equations A.14 and A.19, we can find the interaction integral \mathcal{I} to be

$$\mathcal{I} = -\frac{j\pi \mathcal{D}}{g^2 \sin kl} \sin \frac{n\pi d}{a} \times \begin{cases} \frac{kn}{a} & \text{if } TE \\ \frac{\beta m}{b} & \text{if } TM \end{cases}, \quad (3.16)$$

where β is the waveguide wave number of the mode (see Appendix A) and g is different for TE and TM modes ($ga = p'_{nm}$ for TE and $ga = p_{nm}$ for TM). The mode radiation resistance can be found to be

$$R = \eta \frac{\pi^2 \mathcal{D}^2 \chi_n \chi_m}{2\beta a b g^2 \sin^2 kl} \sin^2 \frac{n\pi d}{a} \times \begin{cases} \frac{kn^2}{a^2} & \text{if } TE \\ \frac{\beta m^2}{b^2} & \text{if } TM \end{cases}, \quad (3.17)$$

where χ_n is given by Equation A.24. Equation 3.17 can be reduced to the one derived by [84] for the special case of a probe completely spanning a rectangular guide.

A monopole antenna inserted vertically into a rectangular duct has two variable parameters - antenna length l and the distance to the wall d . Let us set the dimensions of a rectangular duct to be $a = 0.4$ m, $b = 0.2$ m and the monopole length to be $l = 3.06$ cm (quarter-wavelength at 2.45 GHz). Figure 3.4A shows the parameters \mathcal{P} and \mathcal{T} as functions of the distance to the wall d . One can see that the parameter \mathcal{T} is reasonably high throughout the range, whereas the value of \mathcal{P} is relatively small. Let us pick and fix the value $d = 0.2$ m where \mathcal{P} has a relative maximum and vary the monopole length l . Figure 3.4B shows the parameters \mathcal{P} and \mathcal{T} as functions of the monopole length l . One can see a broad peak at $l \approx 0.1$ m with relatively good impedance match ($\mathcal{T} \approx 0.5$).

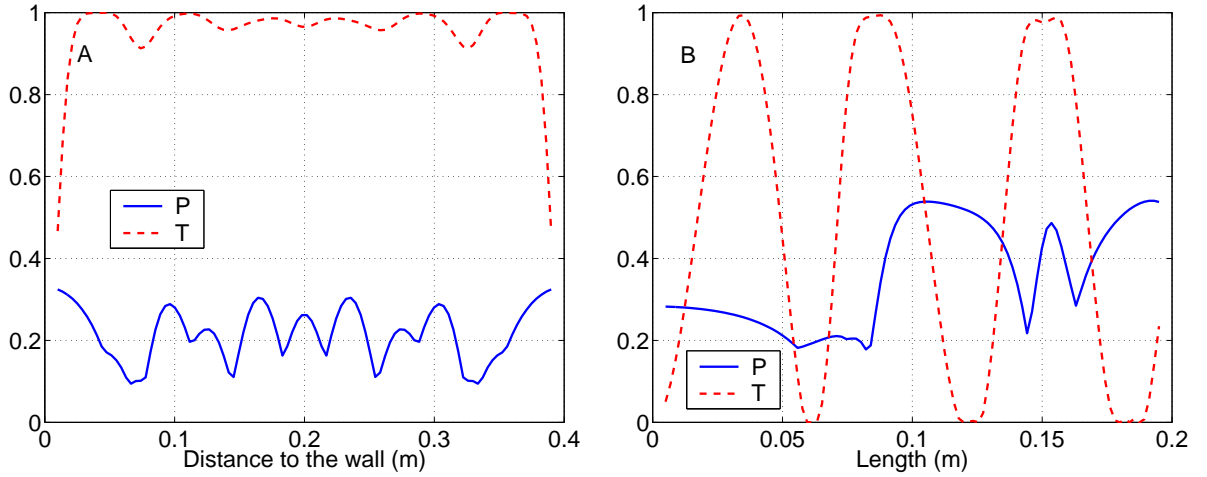


Figure 3.4: Parameters \mathcal{P} and \mathcal{T} as functions of the distance to the wall d ($l = 3.06$ cm) (A) and monopole length l ($d = 0.2$ m) (B) for a monopole antenna in a rectangular 0.4 m x 0.2 m duct at 2.45 GHz.

Mode distributions excited by monopole antennas with $l = 3.06$ cm, $d = 0.2$ m and $l = 10$ cm, $d = 0.2$ m are shown in Figure 3.5A and Figure 3.5B, respectively. One can see that an optimized antenna has better mode excitation characteristics. Namely, more than 50 percent of total power is now transmitted into mode TE_{52} .

Consider now a monopole antenna inserted in a cylindrical waveguide as shown in Figure 3.6.

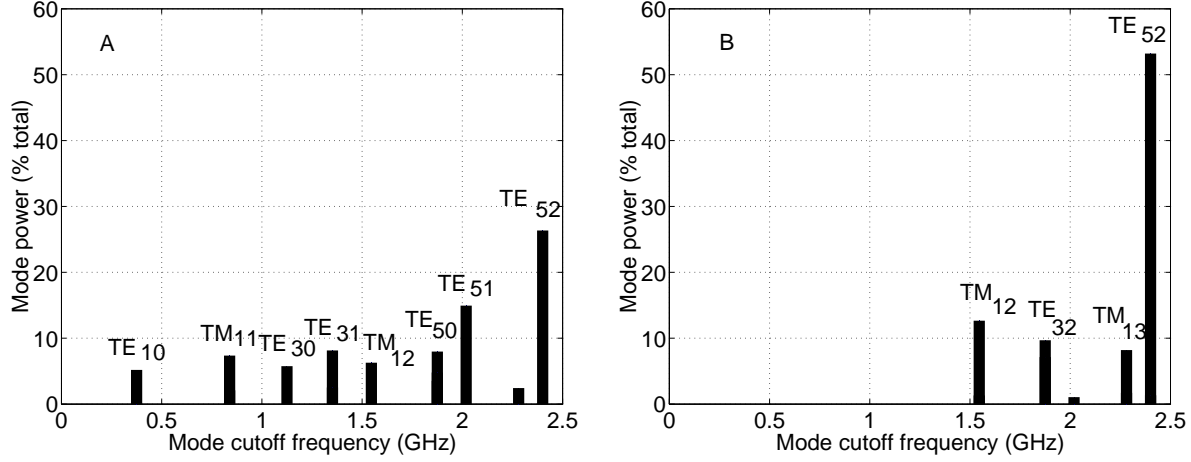


Figure 3.5: Mode distributions excited by monopole antennas with $l = 3.06$ cm, $d = 0.2$ m (A) and $l = 10$ cm, $d = 0.2$ m (B) in a rectangular duct 0.4 m x 0.2 m at 2.45 GHz.

The coordinate ξ along the antenna is

$$\xi = \begin{cases} a - r & \text{if } l \leq a \\ a + r & \text{if } l > a \end{cases} . \quad (3.18)$$

The interaction integral that needs to be found is

$$\mathcal{I} = \begin{cases} - \int_{a-l}^a \frac{\sin k(l-a+r)}{\sin kl} \epsilon_r(r)|_{\phi=0} dr & \text{if } l \leq a \\ - \int_0^a \frac{\sin k(l-a+r)}{\sin kl} \epsilon_r(r)|_{\phi=0} dr + \int_0^{l-a} \frac{\sin k(l-a-r)}{\sin kl} \epsilon_r(r)|_{\phi=\pi} dr & \text{if } l > a \end{cases} \quad (3.19)$$

Using the normalized field expressions given by Equations A.28 and A.33, and performing the change of variables $\zeta = r/a$, we can find that the interaction integral \mathcal{I} is

$$\mathcal{I} = \begin{cases} \frac{jkn}{g^2 \sin kl} \int_{1-l/a}^1 \frac{J_n(ga\zeta) \sin ka(l/a - 1 + \zeta)}{\zeta} d\zeta & \text{if } l \leq a \\ \frac{jkn}{g^2 \sin kl} \int_0^1 \frac{J_n(ga\zeta) \sin ka\zeta}{\zeta} d\zeta - \left[\frac{jkn(-1)^n}{g^2 \sin kl} \right. \\ \left. \times \int_0^{l/a-1} \frac{J_n(ga\zeta) \sin ka(l/a - 1 - \zeta)}{\zeta} d\zeta \right] & \text{if } l > a \end{cases} \quad (3.20)$$

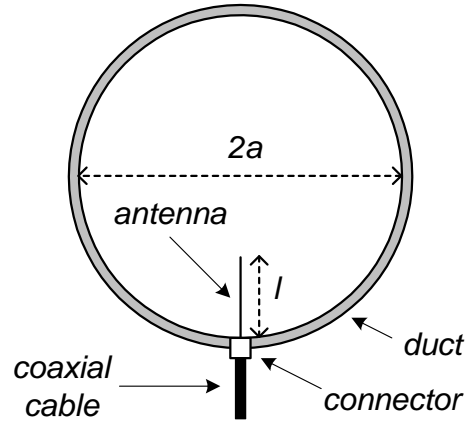


Figure 3.6: Monopole antenna in a cylindrical duct.

for TE modes and

$$\mathcal{I} = \begin{cases} \frac{j\beta a}{g \sin kl} \int_{1-l/a}^1 J'_n(ga\zeta) \sin ka(l/a - 1 + \zeta) d\zeta & \text{if } l \leq a \\ \frac{j\beta a}{g \sin kl} \int_0^1 J'_n(ga\zeta) \sin ka\zeta d\zeta - \left[\frac{j\beta a(-1)^n}{g \sin kl} \right. \\ \left. \times \int_0^{l/a-1} J'_n(ga\zeta) \sin ka(l/a - 1 + \zeta) d\zeta \right] & \text{if } l > a \end{cases} \quad (3.21)$$

for TM modes.

The mode radiation resistance can be found to be

$$R = \frac{\eta}{\pi \sin^2 kl} \times \left\{ \begin{array}{ll} \frac{kn^2}{\beta} \left[\int_{1-l/a}^1 \frac{J_n(ga\zeta) \sin ka(l/a - 1 + \zeta)}{J_n^2(ga)(g^2a^2 - n^2)\zeta} d\zeta \right]^2 & \text{if } TE \text{ and } l \leq a \\ \frac{kn^2}{\beta J_n^2(ga)(g^2a^2 - n^2)} \left[\int_0^1 \frac{J_n(ga\zeta) \sin ka\zeta}{\zeta} d\zeta \right. \\ \left. - (-1)^n \int_0^{l/a-1} \frac{J_n(ga\zeta) \sin ka(l/a - 1 - \zeta)}{\zeta} d\zeta \right]^2 & \text{if } TE \text{ and } l > a \\ \frac{\beta}{kJ_n'^2(ga)} \left[\int_{1-l/a}^1 J_n'(ga\zeta) \sin ka(l/a - 1 + \zeta) d\zeta \right]^2 & \text{if } TM \text{ and } l \leq a \\ \frac{\beta}{kJ_n'^2(ga)} \left[\int_0^1 J_n'(ga\zeta) \sin ka\zeta d\zeta \right. \\ \left. - (-1)^n \int_0^{l/a-1} J_n'(ga\zeta) \sin ka(l/a - 1 - \zeta) d\zeta \right]^2 & \text{if } TM \text{ and } l > a \end{array} \right. \quad (3.22)$$

The Equation 3.22 reduces to the one derived by [95] for the TE_{11} mode case for $l \leq a$.

A monopole antenna in a cylindrical duct has only one variable parameter – antenna length l . Let us set the diameter of a cylindrical duct to be 0.305 m. Figure 3.7 shows the parameters \mathcal{P} and \mathcal{T} at 2.45 GHz for a monopole antenna as a function of the monopole length l . One can see that for $l \approx 0.15$ - 0.16 m, the parameter \mathcal{P} is high and the impedance match is good ($\mathcal{T} > 0.8$).

Mode distributions excited by a monopole antenna with $l = 3.06$ cm and $l = 15.6$ cm are shown in Figure 3.8A and Figure 3.8B, respectively.

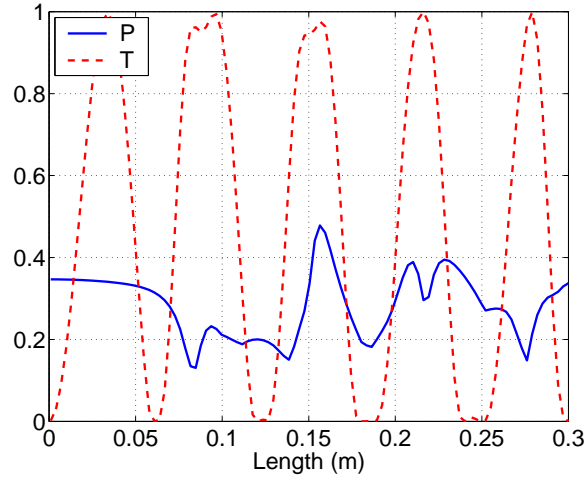


Figure 3.7: Parameters \mathcal{P} and \mathcal{T} as functions of monopole length in a 30.5 cm cylindrical duct at 2.45 GHz .

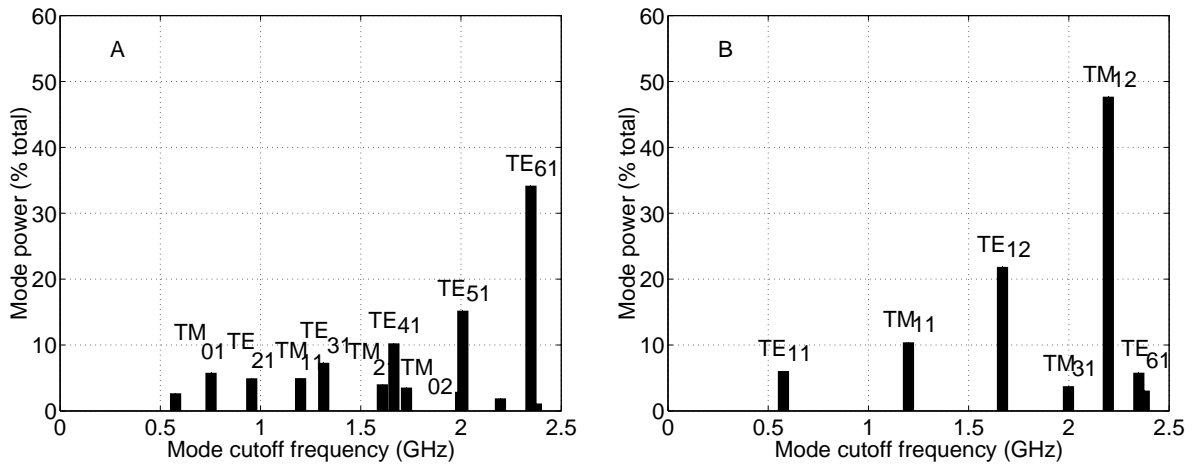


Figure 3.8: Mode distributions excited by monopole antennas with $l = 3.06$ cm (A) and $l = 15.6$ cm (B) in a 30.5 cm cylindrical duct at 2.45 GHz.

3.5 Dipole antenna

A dipole antenna allows one to achieve greater mode selectivity compared to a monopole antenna. We will assume that there is no current flowing on the outside of a coaxial cable feeding the dipole antenna in the duct. From a theoretical point of view, this simplifies calculations. From a practical point of view, it allows one to eliminate unwanted currents which can excite additional waveguide modes. To implement such an antenna, a balun needs to be designed to feed the dipole. Balun design is a well known procedure in antenna engineering [111, 112].

Consider a dipole antenna inserted in a rectangular waveguide as shown in Figure 3.9. Such an antenna has three variable parameters: the height h , the arm length l , and the position d . In addition, the angular orientation of antenna arms with respect to the waveguide axis can be varied.

To eliminate currents flowing on the outside of the coaxial cable inside a duct, a balun is used on the last portion of the coax that feeds the dipole. The coordinate ξ along the antenna is $\xi = |x - d|$.

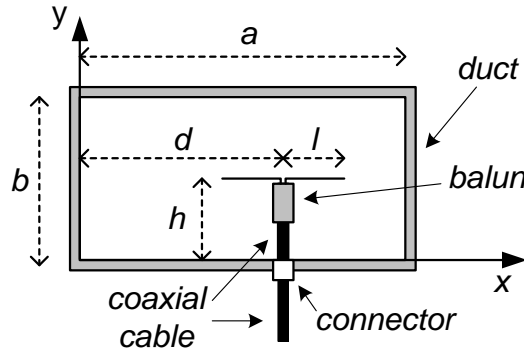


Figure 3.9: Dipole antenna in a rectangular duct.

The interaction integral \mathcal{I} that needs to be found is

$$\mathcal{I} = \int_{d-l}^d \epsilon_x(x)|_{y=h} \frac{\sin k(l+x-d)}{\sin kl} dx + \int_d^{d+l} \epsilon_x(x)|_{y=h} \frac{\sin k(l-x+d)}{\sin kl} dx. \quad (3.23)$$

An intermediate result needed for further computations is

$$\mathcal{D} = \int_{d-l}^d \cos \frac{n\pi x}{a} \sin k(l+x-d) dx + \int_d^{d+l} \cos \frac{n\pi x}{a} \sin k(l-x+d) dx. \quad (3.24)$$

This definite integral can easily be computed in a closed form, but the resulting expression is rather bulky. For brevity, we will omit this intermediate result. We refer the interested reader to a website [113], which contains a good collection of direct links to mathematical tools, including Mathematica tools for calculating definite integrals.

Using \mathcal{D} and the normalized field expressions given by Equations A.13 and A.18, we can find that the parameter \mathcal{I} is

$$\mathcal{I} = \frac{j\pi\mathcal{D}}{g^2 \sin kl} \sin \frac{m\pi h}{b} \times \begin{cases} \frac{km}{b} & \text{if } TE \\ -\frac{\beta n}{a} & \text{if } TM \end{cases}. \quad (3.25)$$

The mode radiation resistance can be found to be

$$R = \eta \frac{\chi_n \chi_m \mathcal{D}}{2k^2 \beta ab} \frac{\pi^2 \sin^2 \left(\frac{m\pi h}{b} \right)}{g^2 \sin^2 kl} \times \begin{cases} \frac{km^2}{b^2} & \text{if } TE \\ \frac{\beta n^2}{a^2} & \text{if } TM \end{cases}. \quad (3.26)$$

A dipole antenna in a rectangular waveguide can also be optimized using parameters \mathcal{P} and \mathcal{T} , obtained via an interaction integral \mathcal{I} , in exactly the same fashion as was done for the monopole antenna. From a practical point of view, we are mostly interested in propagation in cylindrical ducts and hence proceed directly to the next case of interest – a dipole antenna in a cylindrical waveguide.

Consider a dipole antenna with circumferential arms inserted in a cylindrical waveguide as shown in Figure 3.10. Circumferential arc arms in a cylindrical waveguide simplify modelling compared to straight dipole arms because no radial field variation needs to be considered. Such an antenna has two variable parameters: the height h and the arm length l . Alternative equivalent parameters are the radius of the circumferential dipole (arc radius) $r_d = a - h$ and the arm angle $\phi_l = l/(a - h)$. In addition, the angular orientation of antenna arms with respect to the waveguide axis can be varied.

The coordinate ξ along the antenna is $\xi = r_d |\phi|$. The interaction integral that needs to be found

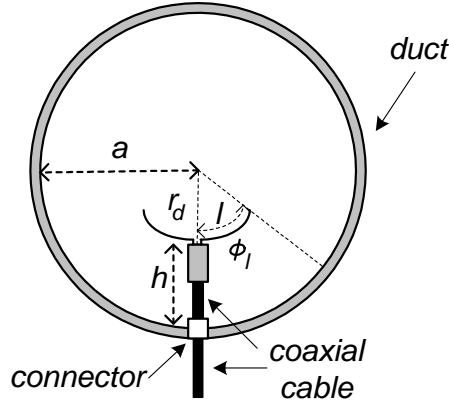


Figure 3.10: Dipole antenna in a cylindrical duct.

is

$$\mathcal{I} = \int_{-\phi_l}^{\phi_l} \frac{\sin k(l - r_d|\phi|)}{\sin kl} \epsilon_\phi(\phi)|_{r=r_d} r_d d\phi. \quad (3.27)$$

An intermediate result needed for further computations is:

$$\begin{aligned} \mathcal{D} = \int_0^{\phi_l} \sin k(l - r_d\phi) \cos(n\phi) d\phi &= \frac{kr_d \cos kl}{n^2 - k^2 r_d^2} + \frac{1}{2} \left[\frac{\cos kl \cos(n - kr_d)\phi_l}{n - kr_d} \right. \\ &+ \left. \frac{\sin kl \sin(n - kr_d)\phi_l}{n - kr_d} \right] + \frac{1}{2} \left[\frac{\cos kl \cos(n + kr_d)\phi_l}{n + kr_d} + \frac{\sin kl \sin(n + kr_d)\phi_l}{n + kr_d} \right]. \end{aligned} \quad (3.28)$$

Using the normalized field expressions given by Equations A.29 and A.34, we can find that the parameter \mathcal{I} is

$$\mathcal{I} = \frac{j2\mathcal{D}r_d}{g \sin kl} \times \begin{cases} kJ'_n(gr_d) & \text{if } TE \\ -\frac{\beta n}{gr_d} J_n(gr_d) & \text{if } TM \end{cases}. \quad (3.29)$$

The mode radiation resistance can be found to be

$$R = \eta \frac{\mathcal{D}^2}{\pi \sin^2 kl} \times \begin{cases} \frac{k}{\beta} \frac{g^2 r_d^2 J_n'^2(gr_d)}{J_n^2(ga) [(ga)^2 - n^2]} & \text{if } TE \\ \frac{\beta}{k} \frac{n^2 J_n^2(gr_d)}{g^2 a^2 J_n'^2(ga)} & \text{if } TM \end{cases}. \quad (3.30)$$

Let us choose two antenna parameters to be varied: arm length l and arc radius r_d . Each of the parameters \mathcal{P} and \mathcal{T} is a function of l and r_d and can be plotted as a two-dimensional surface. For simplicity, we will explore the behavior of \mathcal{P} and \mathcal{T} as a function of one parameter, with the other parameter value fixed.

Let us set the diameter of a cylindrical duct to be 30.5 cm and the arm length to be quarter-wavelength at 2.45 GHz: $l = 3.06$ cm. Figure 3.11A shows the parameters \mathcal{P} and \mathcal{T} for a dipole antenna with $l = 3.06$ cm as functions of the radius r_d . One can see that there is a wide peak of parameter \mathcal{P} around $r_d \approx 4$ cm.

Let us now set $r_d = 4$ cm and vary the arm length l , which can change between 0 and $\pi r_d \approx 12.5$ cm. Figure 3.11B shows the parameters \mathcal{P} and \mathcal{T} for a dipole antenna with $r_d = 4$ cm as functions of the arm length l . One can see a broad peak of \mathcal{P} at $l = 7$ cm but the impedance match is poor (\mathcal{T} is small).

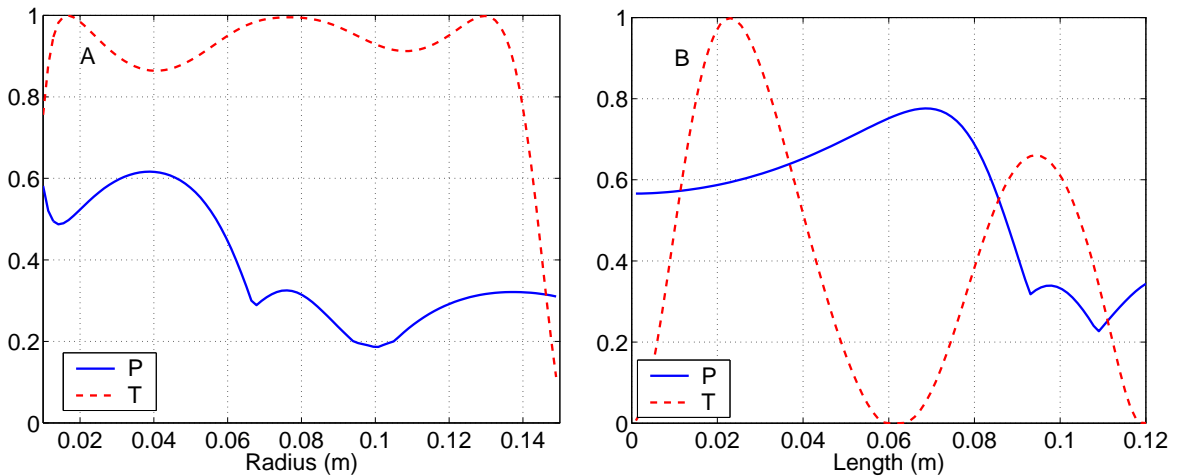


Figure 3.11: Parameters \mathcal{P} and \mathcal{T} for a dipole antenna as functions of the arc radius for $l = 3.06$ cm (A) and arm length for $r_d = 4$ cm (B) in a 30.5 cm cylindrical duct at 2.45 GHz.

$l = 7$ cm are shown in Figure 3.12A and Figure 3.12B. The strongest mode TE_{02} is excited much stronger by the second antenna (Figure 3.12B), but the first antenna (Figure 3.11A) delivers a better impedance match with the transmitter due to different arm length.

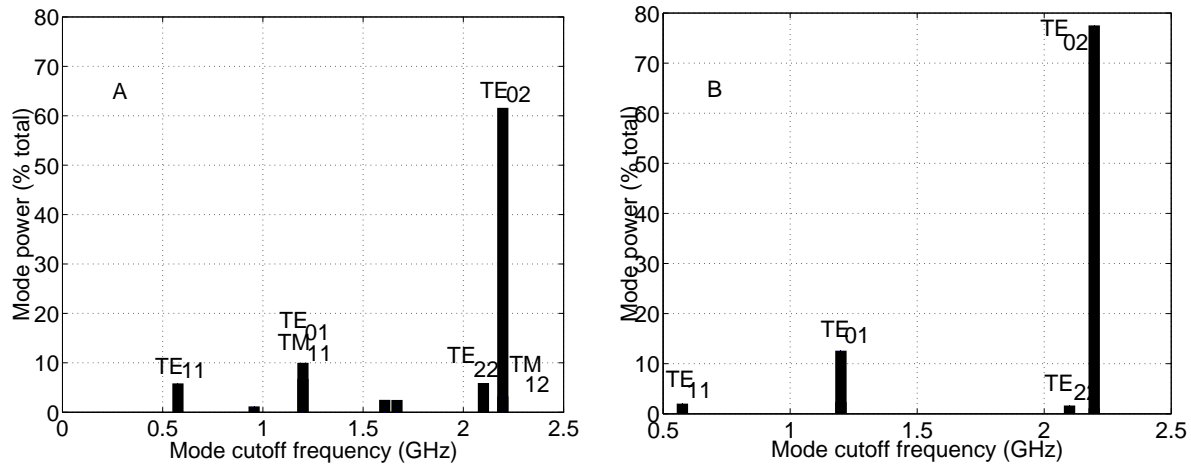


Figure 3.12: Mode distributions excited by dipole antennas with $l = 3.06$ cm, $r_d = 4$ cm (A) and $l = 7$ cm, $r_d = 4$ cm (B) in a 30.5 cm cylindrical duct at 2.45 GHz.

3.6 Antenna array

One other type of antenna structure that can be used for selective mode excitation is an antenna array. In a multimode waveguide, a single antenna (e.g., monopole or dipole) is likely to excite a multitude of modes. The number of elements in an array then must generally be equal to or greater than the number of modes that can propagate if a single, arbitrary mode is to be excited. Antennas may be located anywhere on the walls of a waveguide. Antenna array elements can be of any type (e.g., monopoles and dipoles).

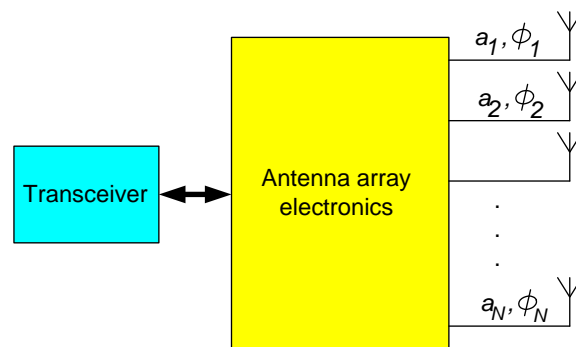


Figure 3.13: Block diagram of a general transmitting antenna array.

To selectively excite a desired mode, each individual element of an antenna array needs to be

driven with a current of an appropriate amplitude and phase as shown in Figure 3.13. In addition to that, to achieve the best results, antenna positions in a duct must be optimized.

An antenna array can also be used for reception. Combining signals from array elements with variable complex coefficients allows one to obtain a good overall channel response under a variety of conditions.

As an example, consider an array antenna in a duct with matched ends, shown in Figure 3.14. This antenna array consists of N identical elements located in a straight duct along the direction of propagation with equal spacing between the elements. Spacing between the antennas in an array must be such that the signals excited by different antennas are sufficiently independent. The minimum spacing distance can be estimated from the spatial autocorrelation function of the frequency response, measured between the transmitting and the receiving antennas as a function of separation distance.

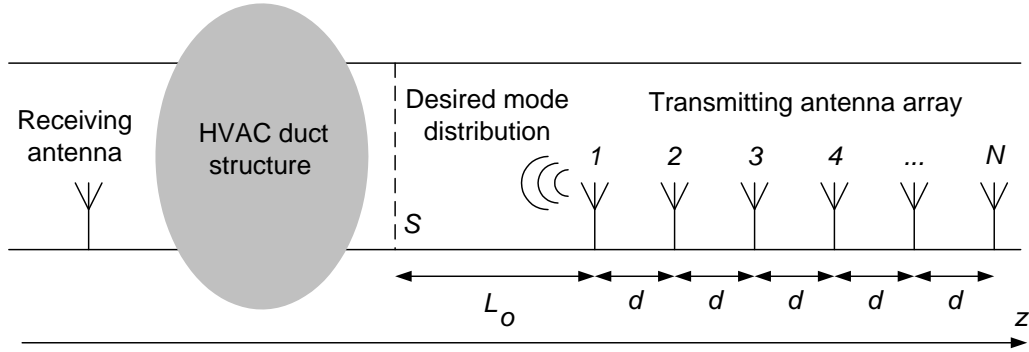


Figure 3.14: Antenna array for selective mode excitation.

The band-limited frequency response $H(\omega, z)$ between the transmitting and the receiving antennas inserted into a duct system can be calculated from Equation 2.19, where z denotes the position of the receiving antenna in the duct. The spatial autocorrelation function of a frequency response between two antennas, located z_o apart in an HVAC duct system, computed over the distance span of d_o is

$$S(\omega, z) = \int_{z_o-d_o/2}^{z_o+d_o/2} H(\omega, z+z')H^*(\omega, z') dz'. \quad (3.31)$$

Figure 3.15A shows the calculated channel attenuation as a function of distance z at 2.45 GHz for two 3.06 cm monopole probes in a straight 30.5 cm cylindrical duct with matched ends. Figure 3.15B shows the frequency autocorrelation function computed over the distance of 2 m for antenna separation of 15 m. The dashed line shows the 3 dB power level of the autocorrelation function (50% correlation). The periodic structure of the autocorrelation function contains highly correlated maxima and minima, resulting from the mutual interference of multiple modes. This demonstrates that channel attenuation is not a statistically uncorrelated function of distance.

The 3 dB width of the central peak can serve as an estimate for the coherence distance which gives a minimum antenna spacing in the array. One can see from Figure 3.15B that the first distance at which the autocorrelation function goes below -3 dB level is approximately 0.15 m. This allows the coherence distance to be estimated to be approximately 0.15 m, which means that 20 antennas can fit on a 3 meter long duct section to form an array. The last point at which the autocorrelation function goes below -3 dB level is a function of the distance span and cannot serve as an estimate for the coherence distance.

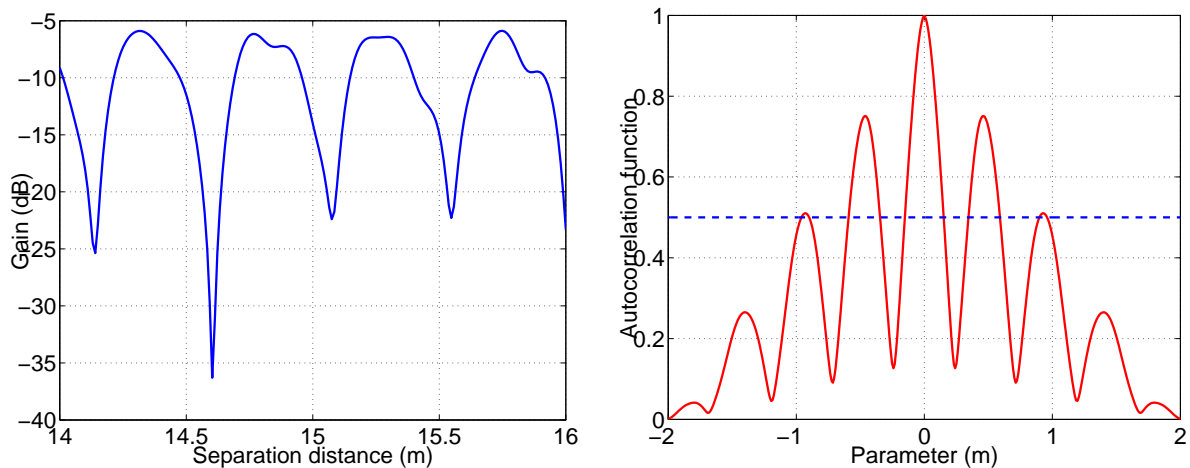


Figure 3.15: Attenuation (dB) as a function of distance between monopole antennas in a straight matched duct (A) and its spatial autocorrelation function (B) for two 3.06 cm monopole antennas in a 30.5 cm cylindrical duct at 2.45 GHz separated by 15 m.

Assume that we have electronics available that can excite antenna array elements with any specified amplitudes and phases. Let us demonstrate how to find amplitudes and phases on array elements

needed to excite a specific mode distribution, travelling towards the receiving antenna and having a desired mode coefficient vector \vec{C} at the cross-section S .

The electric field of mode u measured at the cross-section S is a superposition of fields excited by each probe and propagated to S :

$$C_u(\omega) = \sum_{n=1}^N B_{un}(\omega) I_n(\omega), \quad (3.32)$$

where I_n is the complex current on antenna element n and B_{un} describes the coupling of antenna n into mode u and can be found from Equation 2.6:

$$B_{un} = -\frac{\mathcal{I}_u}{4p_u} e^{\gamma_u[L_o+d(n-1)]}. \quad (3.33)$$

The sought vector of current amplitudes and phases on antenna array elements can be found by solving the linear system given by Equation 3.32. The number of probes in an array can be smaller or larger than the number of waveguide modes, which makes the linear system given by Equation 3.32 under-determined or over-determined. The approximate solution to the system

$$\vec{C} = \hat{B} \vec{I} \quad (3.34)$$

allows one to find the vector \vec{I} necessary for excitation of the mode distribution \vec{C} .

There are a few ways to find an approximate solution to the Equation 3.34. In Matlab*, the vector \vec{I} can be found using the pseudo-inverse function (`pinv`), the backslash operation (`\`), or the nonlinear minimization (`fminsearch`).

Active antenna array electronics and additional computations required to compute weight coefficients increase the antenna cost. An alternative approach is to use an antenna array where signals from all elements are combined in phase using a simple passive RF power combiner, and to vary the position and spacing of the array elements to obtain a good channel response. Once optimal position and spacing are found, a receiving antenna can be attached to the duct system. Such an antenna is relatively cheap.

*Matlab is a registered trademark of The Mathworks, Inc.

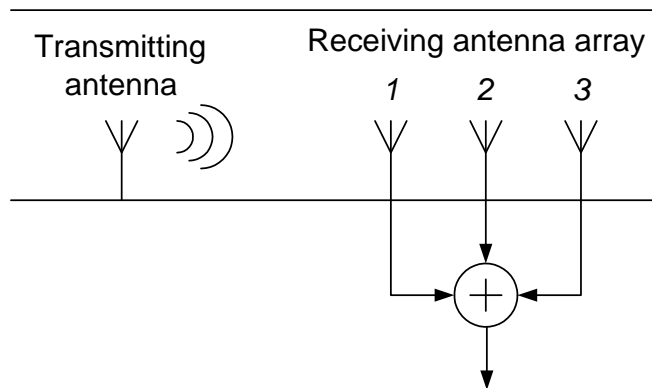


Figure 3.16: A receiving 3-element antenna array.

As an example, consider a 3-probe antenna array schematically shown in Figure 3.16. A practical implementation of this antenna is shown in Figure 3.17. Each element is a quarter-wavelength monopole probe (3.1 cm at 2.45 GHz), which delivers a good impedance match. Signals from the probes are combined using a 0-degree 3-way RF combiner.

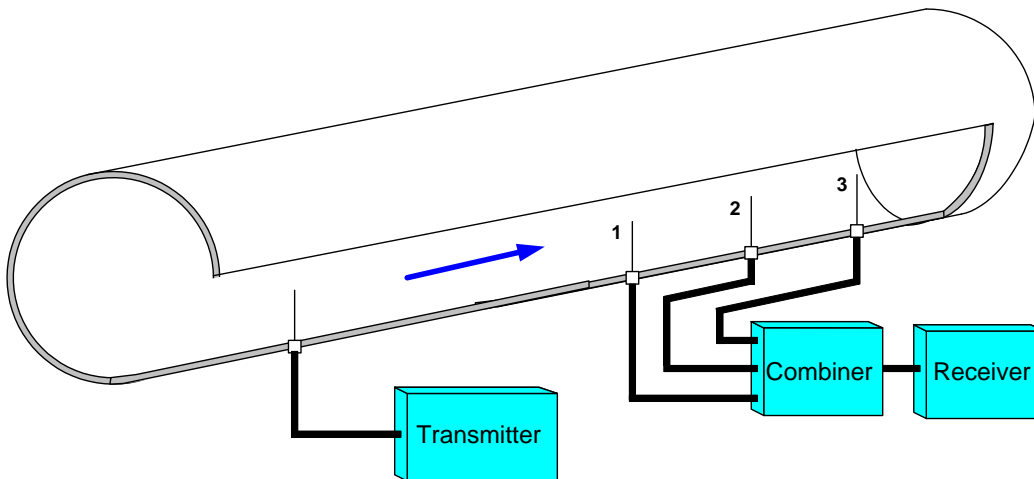


Figure 3.17: Practical implementation of a passive receiving 3-element antenna array.

The frequency responses between the transmitting antenna and the receiving probes will be shifted in the frequency domain with respect to each other because of the different spatial position of each probe. Adding the responses together and choosing an optimal probe separation allows

one to mutually compensate for nulls in the response of one probe with peaks in the response of another probe. Figure 3.18 shows the responses of each individual probe and their complex sum as would be obtained via the RF power combiner. It should be noted that this calculation neglects mutual coupling between the three antennas in the array. Thus although this example illustrates the concept, close agreement with measurements would likely require the mutual coupling to be taken into account. Also, a physical RF power splitter/combiner would introduce approximately 4.8 dB additional loss due to power splitting. This would shift down the solid curve shown in Figure 3.18.

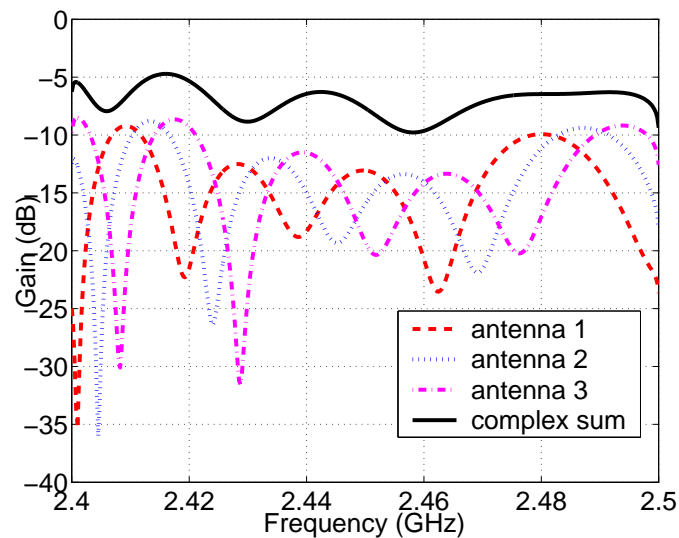


Figure 3.18: Frequency responses of the channel between a single transmitting antenna and each antenna in an array located 5 m away in a straight 30.5 cm cylindrical duct. Each probe is a 3.1 cm monopole probe. Spacing between array probes is 5 cm.

3.7 Mode content analysis with a frequency-swept antenna

Knowing the multimode content at various locations in a HVAC duct system is important for characterizing channel properties and understanding the behavior of complicated HVAC elements. An overview of various mode content measurement methods can be found in Chapter 4. An excellent demonstration of using an antenna array for mode measurement is described by Baird [106], which

allows one to extract frequency-dependent mode coefficients.

Often, we are interested in an average mode content in the band of interest rather than in the specific frequency-domain behavior of mode coefficients. If we make an assumption that mode coefficients do not strongly depend on frequency, then measurements performed at different frequencies using the same antenna can be considered as independent sources of information. This gives one a linear system of equations which allows one to extract the average values of mode coefficients in the band of measurement. In other words, for any measured frequency response, we should be able to find such a set of mode coefficients at the receiver that approximate well the measured response. This gives an extremely simple way of measuring the mode content in a multimode duct using just one antenna.

As an example, consider an antenna in a duct with matched ends, shown in Figure 3.19. This antenna can be used to measure the frequency response at N frequencies. The spacing between the frequencies must be such that the responses measured at different frequencies are sufficiently independent. The minimum spacing distance between frequencies can be estimated from the auto-correlation function of the frequency response, measured between the transmitting and the receiving antennas. The band-limited frequency response $H(\omega)$ between two antennas inserted in a duct can

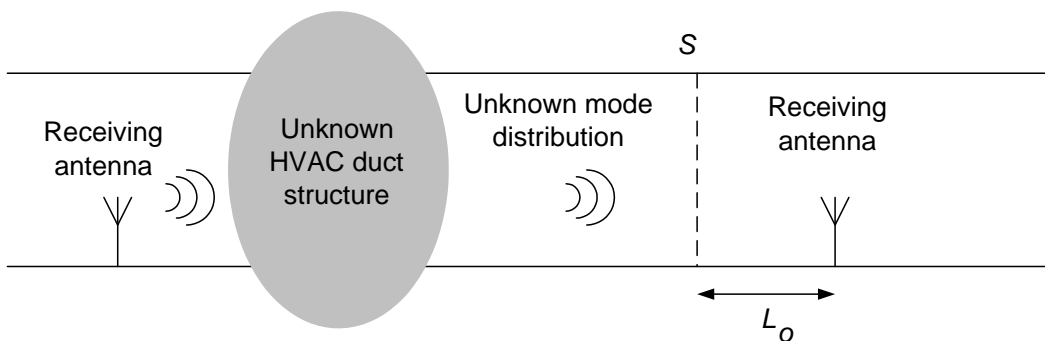


Figure 3.19: Swept-frequency mode content measurement with a single antenna.

be calculated from Equation 2.19. The frequency autocorrelation function of a frequency response

between two antennas in the band $(\omega_1 \dots \omega_2)$ is

$$S(\omega) = \int_{\omega_1}^{\omega_2} H(\omega + y)H^*(y) dy. \quad (3.35)$$

Figure 3.20A shows the calculated frequency response in 2.4-2.5 GHz band for two 3.06 cm monopole probes located 15 m apart in a straight 30.5 cm cylindrical duct with matched ends. Figure 3.20B shows the normalized autocorrelation function computed over the same frequency band (right). The dashed line shows the 3 dB power level of the autocorrelation function. The 3 dB width of central peak can serve as an estimate for the coherence bandwidth which gives a minimum frequency spacing for measurements. One can estimate from Figure 3.20 that the coherence bandwidth is about 3.3 MHz, which means that thirty independent frequency measurements can fit into a 100 MHz band.

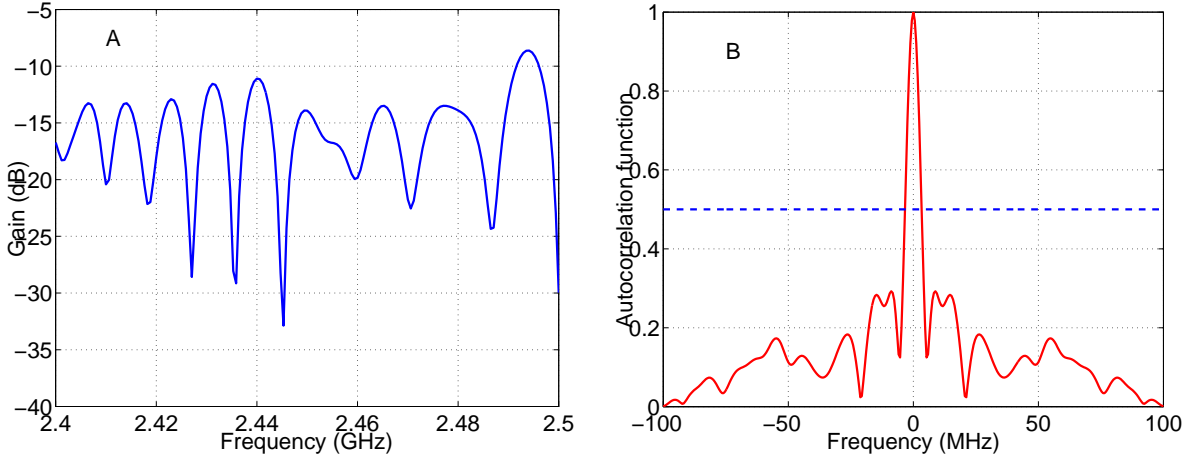


Figure 3.20: Attenuation as a function of frequency (A) and its normalized frequency autocorrelation function (B) for two 3.06 cm monopole antennas located 15 m apart in a 30.5 cm straight cylindrical duct with matched ends.

Assume that an unknown mode content vector \vec{C} is to be measured at the cross-section S . The frequency response between the transmitting and the receiving antenna can be measured at N frequency points:

$$H(\omega_i) = \sum_{v=1}^V A_{iv} C_v(\omega_i), \quad (3.36)$$

where A_{iv} describes the influence of mode v on the frequency response measured at frequency ω_i and can be found from Equation 2.6:

$$A_{iv} = \frac{Z_o + Z_L}{(Z_o + Z_a)(Z'_a + Z_L)} \frac{Z'_v p'_v}{\mathcal{I}'_v} e^{-\gamma_v L_o}. \quad (3.37)$$

Assume that mode coefficients are weak functions of frequency and can be approximated as constants:

$$C_v(\omega) \approx \text{const}_v. \quad (3.38)$$

This assumption strongly depends on the mode cutoff frequencies and operating frequency band. Figure 3.21 shows the magnitude of normalized mode coefficients excited in a 30.5 cm cylindrical duct by a 3.06 cm monopole antenna as functions of frequency in the 2.4-2.5 GHz band. In this band, no cutoff frequencies are located. One can see that only the mode coefficient of TE_{61} is notably frequency dependent (TE_{61} is a higher order mode, whose cutoff frequency is close to 2.4 GHz).

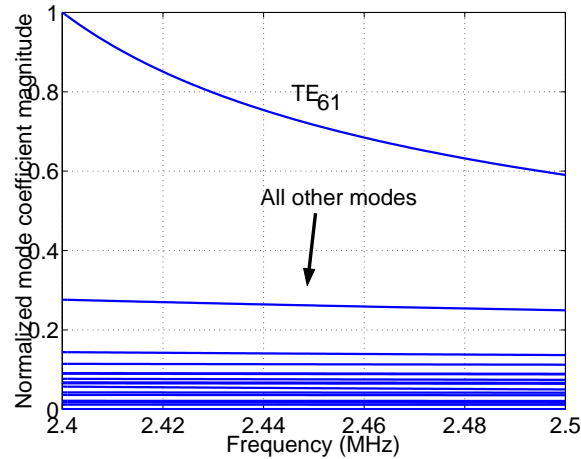


Figure 3.21: Magnitude of normalized mode coefficients excited in a 30.5 cm cylindrical duct by a 3.06 cm monopole antenna as functions of frequency in 2.4-2.5 GHz band.

This result demonstrates that this method is applicable for mode content extraction as long as no modes are present whose cutoff is very near or within the operating frequency band. The sought mode content vector can be found by solving the linear system given by Equation 3.36. The number

of measurement frequencies can be larger than the number of waveguide modes to be measured, which means that the linear system given by Equation 3.36 is over-determined.

The approximate solution to the system

$$\vec{H} = \hat{A} \vec{C} \quad (3.39)$$

can be found in Matlab using the pseudo-inverse function (`pinv`), the backslash operation (`\`), or the nonlinear minimization (`fminsearch`).

Figure 3.22 shows theoretically generated and extracted coefficients of the 5 modes for which a quarter-wavelength monopole antenna is the most sensitive. The separation between the two 3.1 cm monopole probes in a 30.5 cm cylindrical duct is 14.6 cm, and 11 equally spaced frequency points in the 2.4-2.5 GHz band were used to extract the mode coefficients using the pseudo-inverse function. One can see that theoretically generated mode coefficients excited in a straight duct by a 3.1 cm monopole antenna and the coefficients extracted from the frequency response generated based on the excited mode coefficients are very close. The accuracy of mode extraction depends on how well

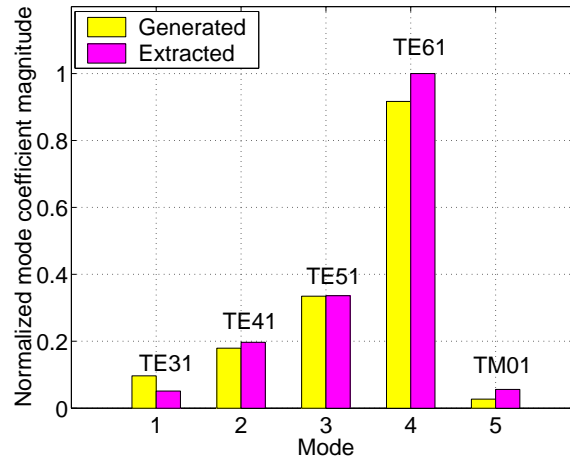


Figure 3.22: Normalized magnitude of theoretically generated mode coefficients excited in a 30.5 cm cylindrical duct by a 3.1 cm monopole antenna and their values extracted via the mode extraction technique.

the matrix \hat{A} is conditioned. The matrix condition number can be defined as the ratio of the largest singular value to the smallest one. The condition number can be found in Matlab using the condition

function (cond). Large condition number means that matrix is nearly singular. There should be a sufficient distance between the measuring receiving antenna and the plane where the mode content is analyzed to allow multiple modes to acquire enough phase difference. The modes to be extracted must be the ones sensed well by the antenna to prevent an ill-conditioned matrix.

Using the frequency response to extract the mode coefficients leads to another interesting application. From reciprocity, a selective mode excitation is possible with a single antenna if it is fed by an RF signal, shaped in a frequency domain in a special way so that the antenna excites only selected modes. This technique would involve building a special RF post-processor inserted between the transmitter and the antenna. This additional signal shaping in the frequency domain would have to be strictly coordinated with the modulation scheme used by the transmitter to ensure mutual coexistence.

3.8 Summary

In this Chapter, the characteristics of monopole and dipole antennas in rectangular and cylindrical ducts were derived. We demonstrated how to find antenna parameters which maximizes selective mode excitation. A general antenna array in an arbitrary duct was analyzed, for which we have shown how to find the current vector which excites a desired mode distribution. We also described a novel technique of mode content measurement using a single frequency-swept antenna.

Chapter 4

Transfer matrices

4.1 Introduction

Consider a microwave device with multiple ports. We are interested in a propagation path from one port to another and thus can consider the device as a two-port network.

A number of equivalent parameters can be used to describe an arbitrary two-port network. Frickey [114] and Marks and Williams [115] provide an excellent overview of various parameters and relationships between them: impedance matrix Z , admittance matrix Y , hybrid matrix h , chain matrix $ABCD$, scattering matrix S , and chain transfer matrix T . For a multimode device, the elements of the aforementioned matrices are sub-matrices [116, 117].

We need to find the frequency response of a complex waveguide system with multiple modes travelling in it. A transfer matrix method provides a good frequency-domain description of wave propagation in such a system, which may contain multiple elements. This method, also known as a transmission matrix method, has been widely used for beam propagation modelling in optics [118, 119] and for modelling of power distribution networks in VLSI design [120]. Recently, the transfer matrix method was applied to modelling propagation in arbitrary dielectric waveguides at microwave frequencies [121]. We will use this method to model propagation in an arbitrary network of metal hollow multimode waveguides.

In our approach, the transfer matrix of an HVAC duct element needs to be found only once for subsequent use in propagation computations. The transfer matrix of an arbitrary waveguide element can be found in three different ways: numerically, analytically, or experimentally.

General waveguide structures can be modelled with numerical techniques [122]. A number of powerful software packages for analyzing arbitrary electromagnetic structures is available. One of the products is High Frequency System Simulator (HFSS) by Ansoft, which is based on the finite element method. Solving the problem using HFSS involves building a geometrical model of the structure, setting the parameters of the material and the boundary conditions, specifying the excitation sources, setting the parameters of solution, and solving.

Some geometries allow analytical solutions, e.g., using the mode-matching technique [123, 124]. Most of these solutions are quite complex and may involve multiple integrals and summations as well as some amount of numerical modelling [125].

The transfer matrix of an element can also be measured experimentally. To measure the transfer matrix of an element, the capability to analyze the mode content in a waveguide is needed [126]. Most of the mode content measurement approaches can be divided into four groups: scanning the field pattern, using mode-selective couplers, open-end radiation measurement, and array processing.

The scanning field pattern technique has been used by many authors. Forrer and Tomiyasu [127] used a moving probe to measure the electric field magnitude and phase at the walls of a waveguide and used a Fourier analysis to compute the power flow in each mode. Fixed multiple-probe arrays were used by Price [128], Taub [129], Levinson and Rubinstein [130], and Baird and Roper [105, 106]. Klinger [131] used a fixed probe and a moving short termination to measure the multimode content. Glock [116] used a fixed probe, a fixed termination, but moving (adjustable length) waveguide to perform necessary measurements.

The mode-selective coupling has been used by many authors as well. Both Lewis [132] and Beck [126] used a series of specially designed mode couplers to couple a mode to its own output port. Mode coupling was also used by Seguinot [133] in application to multimode microstrip lines.

In high-power microwave engineering, measuring the radiation pattern of an open-ended wave-

guide is typically used to extract the mode content of the high-power source (magnetron, gyrotron, etc.) [134].

Array processing involves measuring the signal at the elements of an antenna array mounted on the waveguide and using those measurements for mode content extraction. To achieve good results, antenna locations must be carefully chosen (perhaps, even optimized in the process of measurement). An excellent example of using an antenna array for mode measurement is described by Roper [105]. Other related work is presented in [106, 135].

For experimentally determining transfer matrices, preference should be given to measurement techniques which are simplest and most efficient to implement, since mode content will need to be measured multiple times for various excitation vectors to determine all elements of the transfer matrix.

In this Chapter, we will analyze the most common HVAC duct components: straight sections, bends, tapers, and T-junctions, all of them made of cylindrical ducts. We will analytically derive transfer matrices for straight sections, bends, and tapers. We will present experimental results on mode transformation by T-junctions. Rectangular components can be analyzed in a similar fashion.

4.2 Definitions

Consider an arbitrary multiple port HVAC element, shown in Figure 4.1. Assume that N is the largest number of modes that can travel on any port of this element. The propagating electromagnetic field at each port can be completely characterized by the N -dimensional vector which defines the complex amplitudes of the electric field of each mode. The magnetic field is uniquely related to the electric field.

From an RF waves point of view, the wave propagation between the two ports of an element can be completely characterized by the frequency-dependent transfer matrix \hat{T} . The matrix \hat{T} is a function of the element geometry. A wave incident onto port 1 is uniquely characterized by the

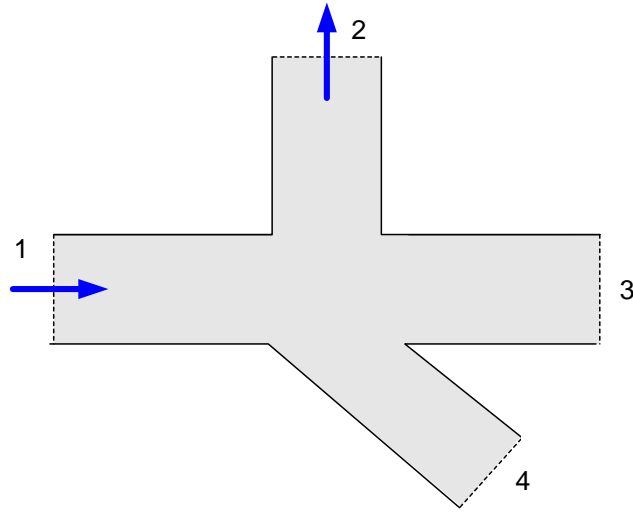


Figure 4.1: A general HVAC element with multiple ports.

mode coefficient vector \vec{C} :

$$\vec{C} = [C_1, C_2, \dots, C_U]^T. \quad (4.1)$$

A wave exiting from port 2 is uniquely characterized by the mode coefficient vector \vec{C}' :

$$\vec{C}' = [C'_1, C'_2, \dots, C'_V]^T. \quad (4.2)$$

The relationship between those vectors is given by the transfer matrix \hat{T} :

$$\vec{C}' = \hat{T}\vec{C}. \quad (4.3)$$

The matrix \hat{T} can be written as

$$\hat{T} = \begin{bmatrix} T_{11} & T_{12} & \dots & \dots & T_{1U} \\ T_{21} & T_{22} & \dots & \dots & T_{2U} \\ \cdot & \cdot & & & \cdot \\ \cdot & \cdot & & & \cdot \\ \cdot & \cdot & & & \cdot \\ T_{V1} & T_{V2} & \dots & \dots & T_{VU} \end{bmatrix}, \quad (4.4)$$

where U is the number of modes entering port 1 and V is the number of modes exiting from port 2. Equation 4.3 shows that the HVAC duct structure is a linear system. The response to a linear combination of excitations can be found as a linear combination of responses to each individual excitation.

4.3 Matrix properties

The transfer matrices of HVAC elements possess some properties similar to the properties of scattering matrices of waveguide components [136]. Transfer matrices that we will use are square, with the size determined by the maximum possible number of modes. If the number of modes in the input and in the output is different, some elements of the transfer matrix are zero.

- A transfer matrix is symmetric ($\hat{T} = \hat{T}^T$) if the element is reciprocal. This property follows from reciprocity, which says that the transfer matrix \hat{T}_{12} from port 1 to port 2 must be the same as the transfer matrix \hat{T}_{21} from port 2 to port 1: $\hat{T}_{12} = \hat{T}_{21} = \hat{T}$. An element is reciprocal if it does not contain active devices, ferrites, or magnetized plasmas. The number of unknown elements in a symmetric matrix $N \times N$ is $N(N + 1)/2$ (the number of non-diagonal terms above the principle diagonal plus the number of terms in the principle diagonal).
- A transfer matrix \hat{T} is diagonal if the element does not cause any mode coupling. Non-diagonal elements of the matrix \hat{T} represent coupling between modes.
- A transfer matrix between two ports is orthogonal ($\hat{T}^{-1} = \hat{T}^T$) if the ports are indistinguishable from the point of view of geometrical symmetry. This property follows from the fact that if $\vec{C}' = \hat{T}\vec{C}$ then $\vec{C} = \hat{T}^{-1}\vec{C}'$ while at the same time $\vec{C} = \hat{T}\vec{C}'$ from symmetry.

All HVAC elements presently in use are reciprocal, owing to the materials used in their construction. Some HVAC elements, such as the Y-junction shown in Figure 4.2, are also symmetric.

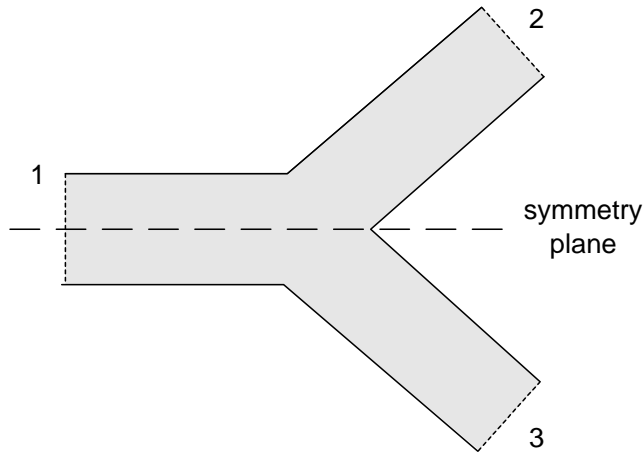


Figure 4.2: A symmetrical HVAC element: Y-junction.

4.4 Cascaded system

A transfer matrix method allows one not only to describe the behavior of a single element but also to characterize any sequence of cascaded elements, provided that their transfer matrices are known.

Transfer matrices satisfy the condition that if \hat{T}_A is the transfer matrix of an element A and \hat{T}_B is the transfer matrix of an element B , then the transfer matrix of elements A and B , cascaded in series, is $\hat{T}_{AB} = \hat{T}_B \hat{T}_A$.

Consider the system shown in Figure 4.3, which contains six cascaded elements: straight, taper, straight, bend, T-junction, and straight. Since we use column vectors, the transfer matrix of a cas-

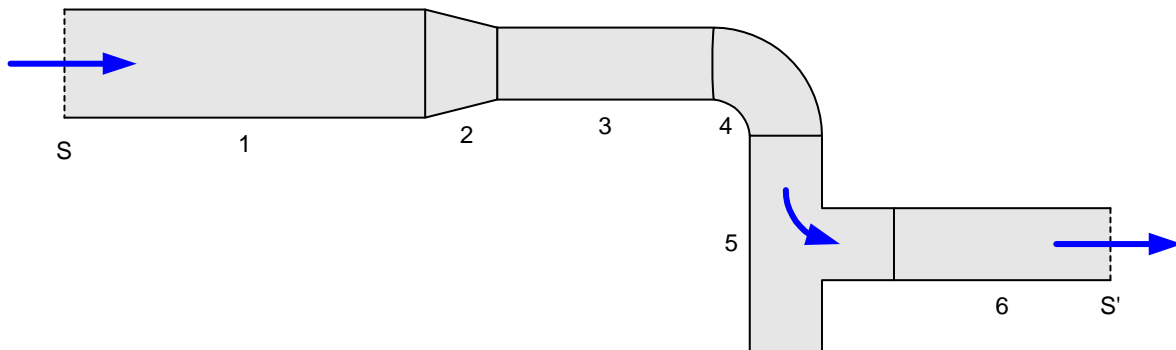


Figure 4.3: Cascaded system of HVAC elements.

caded system that describes propagation from cross-section S to cross-section S' can be represented as

$$\hat{T} = \hat{T}_K \hat{T}_{K-1} \dots \hat{T}_1. \quad (4.5)$$

where K is the total number of elements ($K = 6$ in this case) and \hat{T}_k is the transfer matrix between the ports of the k -th element that lies on the shortest path connecting cross-sections S and S' . The order of cascading HVAC system elements is important, unless their transfer matrices commute.

4.5 Straight sections

Figure 4.4 shows an HVAC element in the form of a straight cylindrical section. The parameters of the straight are the length L_S and the radius a .

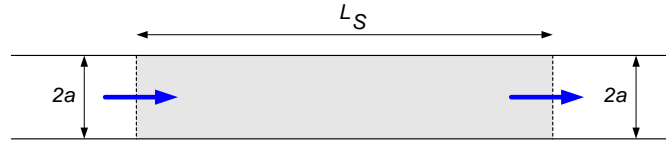


Figure 4.4: HVAC element in the form of a straight section.

Modes propagating in a straight section do not interact. The transfer matrix that describes a straight section is

$$\hat{T}_S = \begin{bmatrix} e^{-\gamma_1 L_S} & 0 & \dots & 0 \\ 0 & e^{-\gamma_2 L_S} & \dots & 0 \\ \cdot & \cdot & & \cdot \\ \cdot & \cdot & & \cdot \\ \cdot & \cdot & & \cdot \\ 0 & 0 & \dots & e^{-\gamma_U L_S} \end{bmatrix}. \quad (4.6)$$

where γ_u is the complex propagation constant of mode u and U is the maximum number of propagating modes.

4.6 Bends

Figure 4.5 shows an HVAC element in the form of a cylindrical bend. The parameters of the bend are the curvature radius R , the inner radius a , and the angle of the bend ϕ_B .

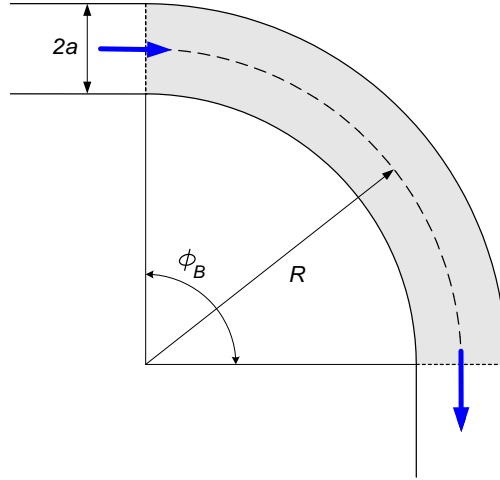


Figure 4.5: HVAC element in the form of a bend.

Waveguide bends are well known in microwave and optical engineering [137, 138, 139, 140]. Propagation in bends can be modelled using the method of moments [141], dyadic Green's functions [142], or numerical techniques [143]. A simple way to model a circular bend is to treat it as a section of toroid. The problem of electromagnetic field solution and eigenmodes in a toroid has been analyzed by many authors [144, 145, 146, 147].

Fields of TE and TM modes of a cylindrical waveguide become distorted once they enter the bend [148]. In the first order approximation, the cutoff wave number for each mode in a gentle bend ($a/R < 1$) is only slightly different from the wave number in a straight duct.

The cutoff wave number g^B of a toroidal mode in a bend is given by [36, 144, 145]:

$$g^B = g \sqrt{1 + \frac{3}{4g^2 R^2}}, \quad (4.7)$$

where g is the cutoff wave number of an equivalent TE or TM mode in a cylindrical waveguide.

The mode propagation constant γ^B in a bend is a function of the cutoff wave number and can be computed directly from Equations A.7 and A.38 with the values of the wave cutoff number substituted from Equation 4.7. It follows that the approximate transfer matrix of a bend is:

$$\hat{T}_B = \begin{bmatrix} e^{-\gamma_1^B R \phi_B} & 0 & \dots & 0 \\ 0 & e^{-\gamma_2^B R \phi_B} & \dots & 0 \\ \cdot & \cdot & \cdot & \cdot \\ \cdot & \cdot & \cdot & \cdot \\ \cdot & \cdot & \cdot & \cdot \\ 0 & 0 & \dots & e^{-\gamma_U^B R \phi_B} \end{bmatrix}, \quad (4.8)$$

where U is the maximum number of propagating modes. The reflection from the bend can be estimated from the change in characteristic impedance of each mode, which can be found from the propagation constant.

4.7 Tapers

Figure 4.6 shows an HVAC element in the form of a cylindrical taper. The parameters of the taper are the length L_{Tp} and the two end radii: radius a and radius b .

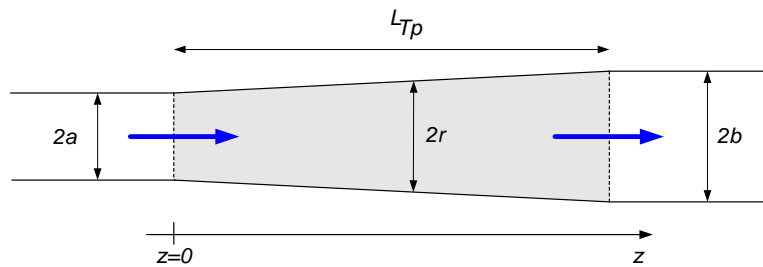


Figure 4.6: HVAC element in the form of a taper.

The problem of modelling waveguide tapers has been explored in [38, 149, 150]. A simple way to model a gentle taper is to treat it as a cylindrical waveguide with a changing radius. The fields of TE and TM modes gradually change from those in a cylindrical waveguide with radius a to those

in a cylindrical waveguide with radius b . If the taper is gentle, no mode coupling takes place and back-scattering can be neglected for input modes that also propagate in the output. A gentle taper is one for which the change in diameter takes place over a distance that is long compared to λ_g – the mode wavelength in the duct waveguide.

Consider a wave arriving from the left (from the duct with a smaller radius a). The number of modes continuing to travel in the duct with the larger radius b is the same as the number of arriving modes. From power conservation, the total power flowing into the left end must be equal to the total power flowing out from the right end (neglecting losses in the taper and back-scattering). In terms of mode coefficients C_u and normalized power densities p_u , we can write that

$$p_u^a |C_u^a|^2 = p_u^b |C_u^b|^2, \quad (4.9)$$

where p_u for a waveguide of a certain radius is given by Equation A.39. It follows that

$$a^4 \beta_u^a |C_u^a|^2 = b^4 \beta_u^b |C_u^b|^2, \quad (4.10)$$

where β_u^a and β_u^b are the propagation constants of mode u in the waveguides with radii a and b , respectively. This allows one to find the change in mode amplitude when going through the taper:

$$|C_u^b| = \frac{a^2}{b^2} \sqrt{\frac{\beta_u^a}{\beta_u^b}} |C_u^a|. \quad (4.11)$$

In addition to this change in amplitude, each mode experiences the usual attenuation and phase lag present in any waveguide. One can see from Equation A.7 that the propagation constant β_u of mode u depends on the radius r of a cylindrical waveguide as

$$\beta_u(r) = k \sqrt{1 - \frac{g^2 a^2}{k^2 r^2}}, \quad (4.12)$$

where g is the mode cutoff wave number in a waveguide with radius a and ga is the root of the Bessel function. Equation A.38 shows that the attenuation constant α_u of mode u depends on the radius r of a cylindrical waveguide as

$$\alpha_u(r) = \frac{R_s}{\eta a} \frac{k}{\beta_u(r)} \times \begin{cases} \frac{c^2 g^2 a^2}{\omega^2 r^2} + \frac{n^2}{g^2 a^2 - n^2} & \text{if } TE \\ 1 & \text{if } TM \end{cases}. \quad (4.13)$$

The radius of the taper shown in Figure 4.6 is a linear function of the position z ($0 \leq z \leq L_{Tp}$):

$$r(z) = a + (b - a) \frac{z}{L_{Tp}}. \quad (4.14)$$

The total attenuation and phase lag for each mode u can be found from the average propagation constant in the taper obtained as:

$$\gamma_u^T = \frac{1}{L_{Tp}} \int_0^{L_{Tp}} \gamma_u(z) dz = \frac{1}{b - a} \int_a^b \gamma_u(r) dr, \quad (4.15)$$

where $\gamma_u = \alpha_u + j\beta_u$, with α_u given by Equation 4.13 and β_u given by Equation 4.12. This allows one to finally write the transfer matrix of a taper as

$$\hat{T} = \frac{a^2}{b^2} \begin{bmatrix} \sqrt{\frac{\beta_1^a}{\beta_1^b}} e^{-\gamma_1^T L_{Tp}} & 0 & \dots & 0 \\ 0 & \sqrt{\frac{\beta_2^a}{\beta_2^b}} e^{-\gamma_2^T L_{Tp}} & \dots & 0 \\ \cdot & \cdot & \cdot & \cdot \\ \cdot & \cdot & \cdot & \cdot \\ 0 & 0 & \dots & \sqrt{\frac{\beta_U^a}{\beta_U^b}} e^{-\gamma_U^T L_{Tp}} \end{bmatrix}, \quad (4.16)$$

where U is the maximum number of propagating modes.

We considered only propagation from left to right, when an increase in diameter does not change the number of propagating modes. Propagation in the opposite direction may appear more complicated since some modes may not be admitted into the cylindrical waveguide of smaller diameter. However, reciprocity states that the channel response between two antennas coupled into a passive waveguide system is the same, independently of which antenna is transmitting. Thus it is sufficient to analyze propagation only in one direction.

4.8 T-junction

Consider a T-junction formed by two perpendicularly joined straight cylindrical duct sections. The two sections may or may not have the same diameter. The T-junction is symmetrical if the second duct section is joined to the middle of the first duct section.

A common HVAC element is a symmetrical T-junction, formed by two perpendicularly joined cylindrical ducts of the same diameter, as shown in Figure 4.7. The parameters of this symmetrical T-junction are the length L_{Tn} , the length L_p , and the radius a .

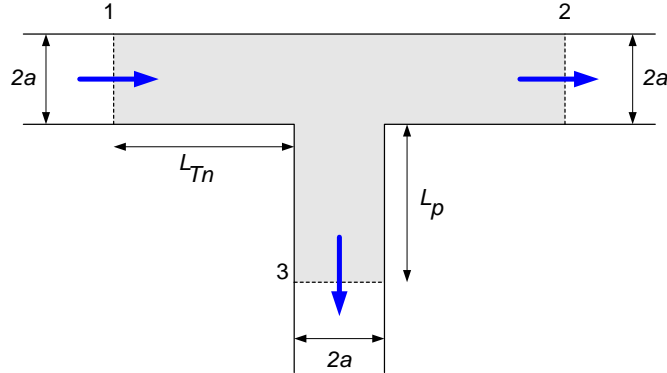


Figure 4.7: HVAC element in the form of a symmetrical T-junction.

T-junction power dividers are well known in microwave engineering [32, 151]. In the literature, mostly rectangular T-junctions have been analyzed [152, 153, 124]. Recently, works on rectangular-to-cylindrical T-junctions have appeared [123, 154]. To the best of our knowledge, the analysis of a cylindrical-to-cylindrical T-junction has not appeared in literature yet. This complex geometry does not allow an analytical solution.

One approach to modelling a cylindrical T-junction is to use HFSS. To extract a transfer matrix, an excitation source that excites only one mode at the input port needs to be specified. The vector of mode amplitudes at the output port gives one row of the transfer matrix between the ports. This process needs to be repeated N times to reconstruct the whole matrix, where N is the maximum number of propagating modes. Specifying a selective mode excitation source and resolving mode coefficients from the computed field distribution may be a complex task. Also, a multimode waveguide structure may require a large computation time when analyzed using a finite-element method.

Another approach is to determine the transfer matrix of a cylindrical T-junction experimentally. Preference should be given to the experimental mode content measurement technique that is the

simplest and most efficient to implement since mode content will need to be measured multiple times for various excitation vectors. In this regard, the frequency-swept antenna technique proposed in Chapter 3 is an attractive candidate.

To find the response of the specific channel containing T-junctions, only the response of a T-junction to an incoming mode distribution needs to be found rather than all elements of the transfer matrix. With the frequency-swept antenna, this response can potentially be determined using only one measurement.

Since the T-junction in question is symmetrical, two transfer matrices (\hat{T}_{12} and \hat{T}_{13}) are sufficient to characterize all possible port combinations. Each of those matrices is symmetric from reciprocity and thus has only $N(N + 1)/2$ unknowns. In addition to that, the matrix \hat{T}_{13} is orthogonal, which imposes an additional condition:

$$\hat{T}_{13}\hat{T}_{13} = \hat{I}. \quad (4.17)$$

System 4.17 gives $N(N + 1)/2$ additional equations, but not all of them are linearly independent.

As an example, consider a 3-mode case. The matrix \hat{T}_{13} is a symmetric 3×3 matrix:

$$\hat{T}_{13} = \begin{bmatrix} a & b & c \\ b & d & e \\ c & e & f \end{bmatrix}. \quad (4.18)$$

This matrix contains 6 unknowns: $a, b, c, d, e,$ and f . System 4.17 can be rewritten as

$$\begin{bmatrix} a & b & c \\ b & d & e \\ c & e & f \end{bmatrix} \begin{bmatrix} a & b & c \\ b & d & e \\ c & e & f \end{bmatrix} = \begin{bmatrix} 1 & 0 & 0 \\ 0 & 1 & 0 \\ 0 & 0 & 1 \end{bmatrix}, \quad (4.19)$$

which leads to the following system of equations:

$$\left\{ \begin{array}{l} a^2 + b^2 + c^2 = 1 \\ ab + bd + ce = 0 \\ ac + be + cf = 0 \\ b^2 + d^2 + e^2 = 1 \\ bc + de + ef = 0 \\ c^2 + e^2 + f^2 = 1 \end{array} \right. \quad (4.20)$$

This system of nonlinear equations is under-determined (otherwise only one 3×3 symmetric orthogonal matrix would exist). Some of the coefficients a , b , c , d , e , and f must be measured to obtain a unique solution to System 4.20.

Figure 4.8 shows the measured normalized mode coefficients of modes coming in and out of the T-junction. These results were obtained experimentally using a single swept antenna mode extraction technique for a T-junction made of 30.5 cm cylindrical ducts. Five most significantly excited modes were extracted via the pseudo-inverse function using 27 equally spaced frequency points in the 2.4-2.5 GHz band. The details of the experimental setup are described in Chapter 6. One can see that the strongest mode (TE_{61}) is attenuated the most when going through the T-junction.

4.9 Summary

This Chapter described the transfer matrix method, the properties of transfer matrices, and the various approaches to determining the transfer matrix of an HVAC element. Simple expressions were derived for the approximate transfer matrices of most common HVAC elements: straight, bend, and taper. Mode transforming properties of the T-junction were analyzed experimentally.

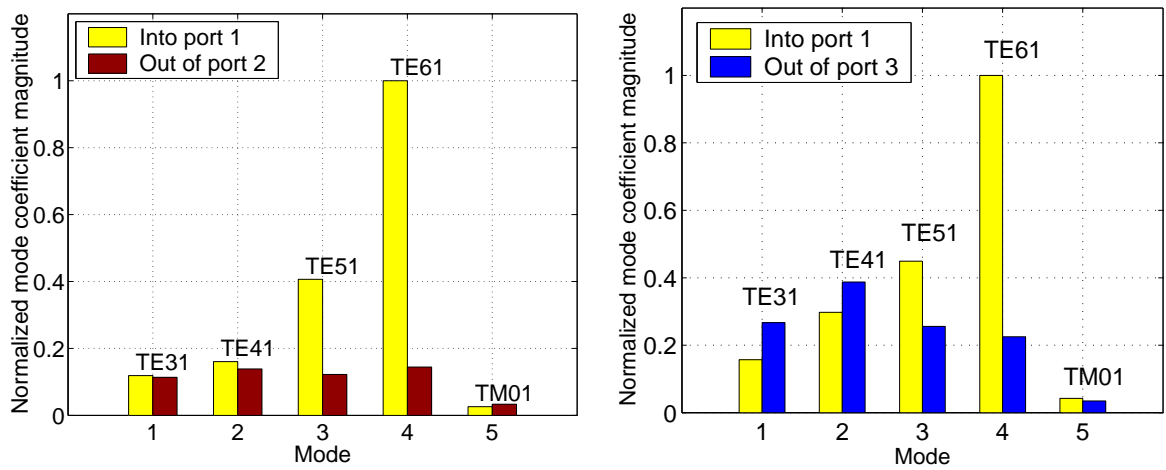


Figure 4.8: Mode distribution coming into port 1 and mode distributions coming out of ports 2 and 3 of the T-junction made of 30.5 cm cylindrical ducts in the 2.4-2.5 GHz band.

Chapter 5

Impulse response

5.1 Introduction

There are several physical mechanisms that affect both the HVAC duct channel's transfer function and impulse response [155]. Namely, they are probe coupling, attenuation, and dispersion. These mechanisms are well known both in microwave and optical engineering [156, 157, 158].

Probe coupling is due to the fact that the transmitting antenna excites various modes differently and the receiving antenna responds differently to the various modes as well.

Attenuation is due to the finite conductivity of the duct walls and losses at each reflection from non-uniformities in the duct system.

Dispersion is due to the fact that different components of a signal arrive at the receiver at different times. There are three different types of dispersion in the duct system: intramodal dispersion (also known as chromatic waveguide dispersion) is due to the fact that different spectral components of each mode travel with different velocities, intermodal dispersion is due to the fact that different modes travel with different velocities, and multipath dispersion is due to multiple echoes caused by reflections from non-uniformities and terminations.

The impulse response characteristics of a traditional ("free-space") indoor radio propagation channel have been studied extensively by several researchers [18, 19, 20, 21, 159]. Impulse re-

sponses of some wave-guiding structures have been studied, e.g., in application to ultrasonic transducer design [160, 161] and to propagation in road tunnels [162]. Also, in the early 50's, Bell labs researchers experimentally explored the time domain response of an excited straight multimode waveguide used for long distance communications [35]. Aside from that, impulse response characteristics of a general multimode waveguide system, such as HVAC ducts, have not yet been explored from a wireless communications perspective.

We concentrate on the properties of an HVAC system in the form of a straight duct terminated on both ends. All physical mechanisms affecting the impulse response of an arbitrary HVAC duct system can be explored with this simple system.

5.2 Definitions

In wireless communications, the transceiver bandwidth is usually limited [163], and the quantity typically analyzed is the power delay profile $p(t)$ related to a narrow-band impulse response $h(t)$ as

$$p(t) = |h(t)|^2 = \left| \int_{\omega_1}^{\omega_2} H(\omega) e^{j\omega t} d\omega + c.c. \right|^2, \quad (5.1)$$

where ω_1 and ω_2 are the lower and the upper frequencies of the transceiver band. Often, $H(\omega)$ is measured or computed for a discrete set of frequencies. In this case, a discrete Fourier transform (DFT) must be used to compute the impulse response and the power delay profile.

Assume that the frequency response $H(f)$ is measured at N discrete frequencies f_1, \dots, f_N :

$$H(f_k) = H_k = a_k e^{j\phi_k}, \quad k = 1 \dots N \quad (5.2)$$

The discrete impulse response can be computed as

$$h_n = \sum_{k=1}^{2N} H_k^* e^{j \frac{2\pi(k-1)(n-1)}{2N}}, \quad (5.3)$$

where

$$H_k^* = \begin{cases} H_k, & k = 1 \dots N \\ H_{2N-k}, & k = N + 1 \dots 2N \end{cases}. \quad (5.4)$$

One of the important characteristics of the channel is the RMS delay spread of the power delay profile which defines the coherence bandwidth of the channel, and hence the maximum data rate without inter-symbol interference (ISI). The RMS delay spread σ_τ is computed from the power delay profile as [18, 164]

$$\sigma_\tau = \sqrt{\frac{\int_0^\infty (t - \bar{\tau})^2 p(t) dt}{\int_0^\infty p(t) dt}}, \quad (5.5)$$

where $\bar{\tau}$ is the mean excess delay defined as

$$\bar{\tau} = \frac{\int_0^\infty t p(t) dt}{\int_0^\infty p(t) dt}. \quad (5.6)$$

The RMS delay spread can also be found as

$$\sigma_\tau = \sqrt{\bar{\tau}^2 - \bar{\tau}^2}, \quad (5.7)$$

where $\bar{\tau}^2$ is the mean squared delay defined as

$$\bar{\tau}^2 = \frac{\int_0^\infty t^2 p(t) dt}{\int_0^\infty p(t) dt}. \quad (5.8)$$

The RMS delay spread is typically computed using power delay profile values above a certain threshold with respect to the maximum signal level. In the analysis presented in this Chapter, we use a threshold of -20 dB.

5.3 Physical mechanisms

Consider a straight terminated duct with two antennas as shown in Figure 5.1, where L is the distance between the transmitter and the receiver, L_1 and L_2 are the distances from the antennas to the respective terminated ends with reflection coefficient G , which, for simplicity, is assumed to be constant. Figure 5.1 shows qualitatively all three types of dispersion in the straight duct system (only two propagating modes are kept for illustration). Drawing a vertical line allows one to approximately determine the arrival times of the power delay profile components at any given position along the duct.

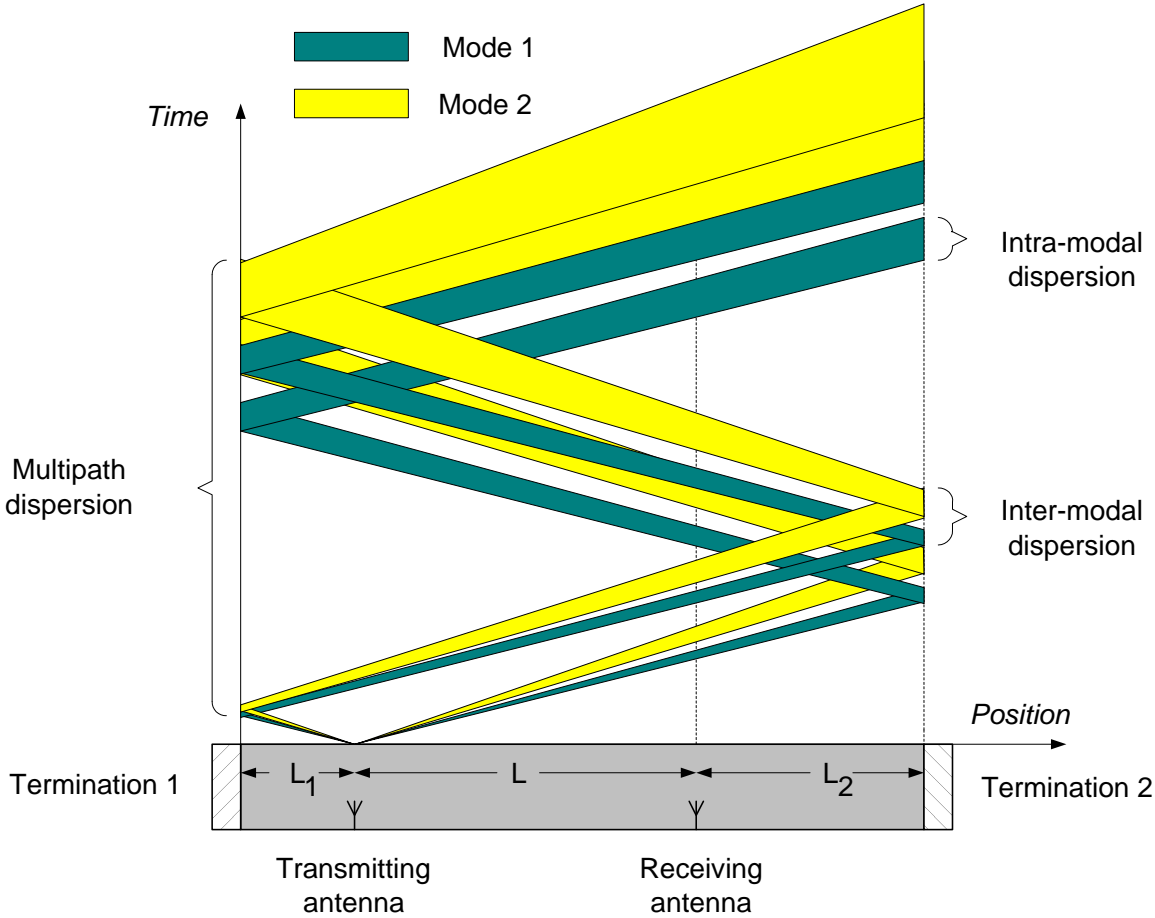


Figure 5.1: Propagation of two modes in a straight terminated duct with three types of dispersion present.

Different physical mechanisms have different influence on the power delay profile. The probe coupling process can be characterized by the frequency-dependent radiation resistance of each mode which determines how much of the transmitted power is carried by a given mode. The effects of both intermodal dispersion and intramodal dispersion on the RMS delay spread depend on probe coupling characteristics. Radiation resistances define the initial mode power distribution as well as the weights of the different spectral components of each mode.

Mode attenuation constants, which characterize attenuation in the duct walls, depend on the mode type (TE or TM), mode indices (n and m), and frequency. Similar to probe coupling, attenuation also affects both intermodal dispersion and intramodal dispersion effects. Attenuation defines the decay rate of different modes in a propagating mode distribution as well as the decay rate of individual frequency components.

In a straight duct, the power in each mode drops exponentially with the path length that a mode traverses before reaching the receiver. One can relate the path length to time via mode velocity and obtain an upper bound of the power delay profile shape for mode n as

$$p_n(t) = p_n(t_o) e^{-2\alpha_n v_n(t-t_o)}, \quad (5.9)$$

where t_o is the time of the first arrival and v_n is the group velocity of mode n in the duct.

Dispersion is the most significant mechanism affecting the impulse response and is analyzed in the next Section.

5.4 Dispersion

Signal dispersion is due to the fact that different components of a signal arrive at the receiver at different times. There are three different types of dispersion observed in the duct system: intramodal dispersion, intermodal dispersion, and multipath dispersion. Below we look more closely at the power delay profiles in the situations when each of the dispersion types mentioned above is predominant.

Let us assume the following geometrical parameters for the system shown in Figure 5.1: $L = 25$ m, $L_1 = 1$ m, and $L_2 = 1$ m. We consider straight cylindrical ducts, 30.5 cm in diameter, made of galvanized steel (conductivity $\sigma = 10^6$ S/m), and excited in the 2.4-2.5 GHz ISM band by 3.5 cm long coaxially fed monopole probes. These are the specific characteristics of the ducts used in our experiments.

Intramodal dispersion is due to the fact that velocities of spectral components of each mode are frequency-dependent. To see the effect of the intramodal dispersion, assume that there are no multipath reflections from the terminated ends ($\Gamma = 0$) and only mode TE_{61} propagates, which excludes intermodal dispersion. Mode TE_{61} is chosen because it is excited the most by quarter-wavelength monopole probe antennas used in our experiments. The normalized calculated power delay profile in this case is shown in Figure 5.2A.

The intramodal dispersion manifests itself as broadening of the original transmitted pulse. Due to the band limitation, the 3 dB width of the narrowest pulse that can be transmitted is finite and is on the order of 10 ns with 100 MHz of bandwidth for a rectangular frequency window. The intramodal time spread per unit distance, Δt_s , can be found by differentiating the inverse of group velocity v_n as

$$\Delta t_s = \Delta \left[\frac{1}{v_n} \right] = \frac{\omega_c^2 \Delta \omega}{c [1 - (\omega_c/\omega)^2]^{\frac{3}{2}} \omega^3}, \quad (5.10)$$

where $\Delta \omega$ is the width of the frequency window. The significance of the intramodal time spread can be understood in comparison with the arrival time delay per unit distance, Δt_a , given as

$$\Delta t_a = \frac{1}{c [1 - (\omega_c/\omega)^2]}. \quad (5.11)$$

For lower order excited modes, the intramodal delay spread time is very small compared to the arrival delay time ($\Delta t_s/\Delta t_a = 0.002$ for TE_{11} mode). For higher order modes, these times are of comparable magnitude ($\Delta t_s/\Delta t_a = 0.567$ for TE_{61} mode).

Intermodal dispersion is due to the fact that different modes travel with different velocities. To analyze the intermodal dispersion, assume that there are no multipath reflections from the terminated

ends ($\Gamma = 0$). The normalized calculated power delay profile is shown in Figure 5.2B. Note that Figure 5.2B contains the intramodal dispersion effect as well due to the finite bandwidth used.

Multipath dispersion is due to multiple echoes caused by reflections from non-uniformities (bends, tapers, T-junctions, Y-junctions, terminations, etc.). To examine the multipath dispersion, assume that there are strong multipath reflections from the terminated ends ($\Gamma = -0.9$), but only the TE_{61} mode propagates. The normalized power delay profile is shown in Figure 5.2C, where one can clearly observe periodic peak structures. They correspond to reflections coming from the terminated ends, the distance between which is 27 m. Note that the intramodal dispersion effect is present as well which causes the spreading of these structures with time. The spacing between the same peaks in different structures is the round-trip time of the corresponding spectral component of mode TE_{61} between the ends of the duct.

Figure 5.2D shows the normalized power delay profile with all three types of dispersion present. The power delay profile is proportional to the absolute magnitude of the superposition of individual mode impulse responses, which may add constructively or destructively. Table 5.1 gives the RMS delay spread computed for each of the cases with different types of dispersion present. Note that the intramodal dispersion is always present due to the finite transceiver bandwidth. The RMS delay spread depends on the mode composition and exact amplitudes and phases of their impulse responses. One can see that the largest contribution to the RMS delay spread in relatively short straight ducts with short-terminated ends comes from multipath dispersion. Mitigating the reflections decreases the RMS delay spread and makes ducts “radio-friendly.” When reflections are minimized, or the duct is very long, the dominant contribution comes from intermodal dispersion. One can see from Table 5.1 that the delay spread for combined effects is slightly smaller compared to the delay spread caused by reflections and intramodal spreading of TE_{61} mode. The presence of multiple modes with different propagation velocities makes the power delay profile more dense which decreases the delay spread value.

Table 5.2 lists characteristics of the modes excited in a 30.5 cm cylindrical duct by a 3.5 cm monopole probe antenna operating at 2.5 GHz. The following notation is used: f_c is the cutoff

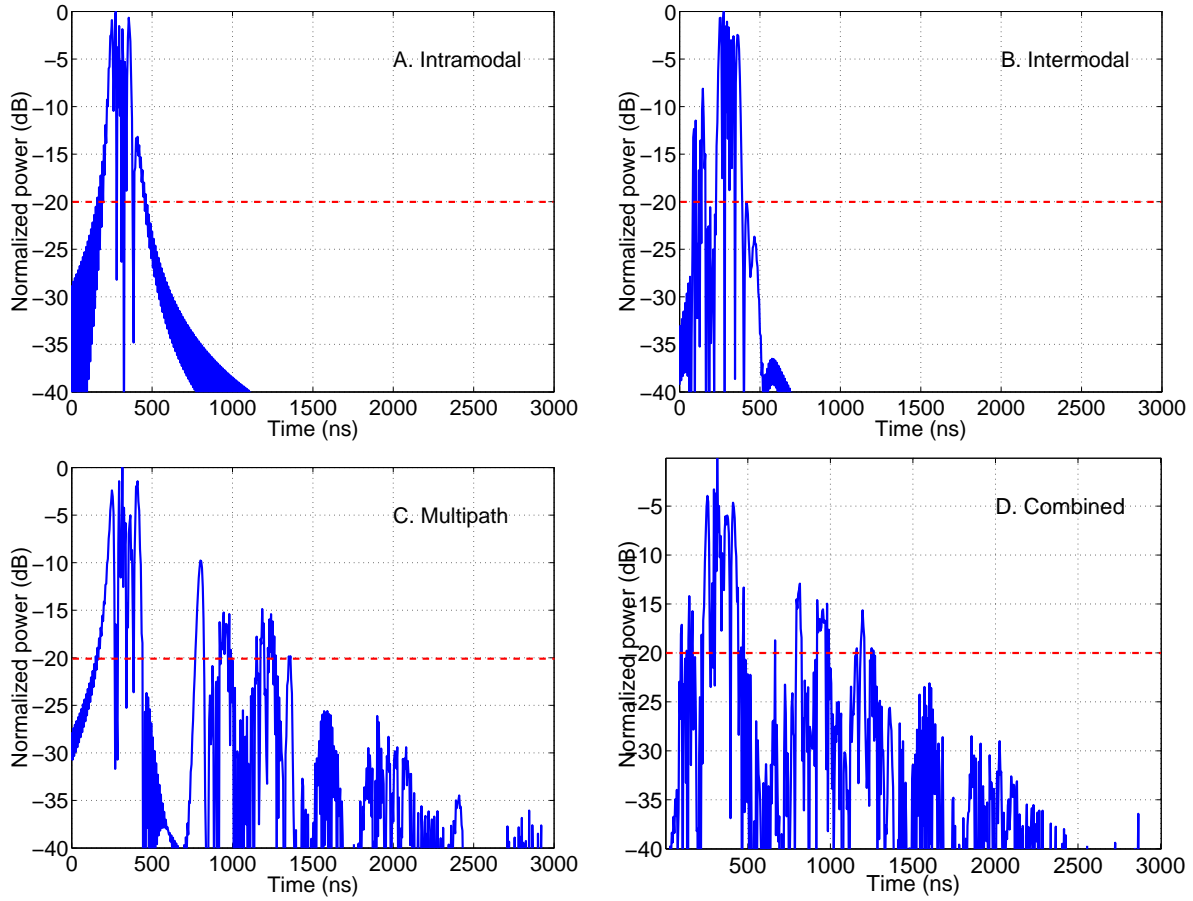


Figure 5.2: Different types of dispersion in the calculated power delay profiles: intramodal (A), intermodal and intramodal (B), multipath and intramodal (C), and combined (D).

Table 5.1: The RMS delay spread σ_τ due to different types of dispersion.

Dispersion type	Modes present	End reflection coefficient Γ	RMS delay spread σ_τ (ns)
Intramodal	TE_{61}	0	50.6
Intermodal + intramodal	all	0	55.9
Multipath + intramodal	TE_{61}	-0.9	197.8
Combined	all	-0.9	181.9

frequency, v/c is the normalized group velocity, α is the attenuation constant (assuming clean, smooth surfaces), R is the radiation resistance, P is the power carried by the mode (percent of total), Δt_a is the arrival time delay, Δt_s is the intramodal time spread in 2.4-2.5 GHz band.

Table 5.2: Parameters of the modes excited in a 30.5 cm cylindrical duct by a 3.5 cm monopole probe antenna at 2.5 GHz.

Mode type	f_c (GHz)	v/c	α (dB/100m)	R (Ohm)	P (%)	Δt_a (ns/100m)	Δt_s (ns/100m)
TE_{11}	0.577	0.973	0.73	1.62	2.95	342.6	0.8
TM_{01}	0.753	0.954	1.58	3.47	6.32	349.6	1.5
TE_{21}	0.957	0.924	1.46	2.97	5.41	360.8	2.7
TM_{11}	1.201	0.877	1.71	2.94	5.36	380.0	4.9
TE_{01}	1.201	0.877	0.39	0.00	0.00	380.0	4.9
TE_{31}	1.316	0.850	2.33	4.32	7.88	392.1	6.5
TM_{21}	1.609	0.765	1.96	2.35	4.28	435.5	13.7
TE_{41}	1.666	0.746	3.52	5.96	10.87	447.1	16.0
TE_{12}	1.670	0.744	0.97	0.14	0.25	448.0	16.1
TM_{02}	1.729	0.722	2.08	2.00	3.66	461.6	19.1
TM_{31}	1.999	0.601	2.50	1.68	3.07	555.0	46.8
TE_{51}	2.010	0.595	5.54	8.56	15.61	560.6	49.0
TE_{22}	2.101	0.542	2.23	0.42	0.77	615.0	73.5
TM_{12}	2.198	0.476	3.15	1.08	1.98	699.7	127.1
TE_{02}	2.198	0.476	2.44	0.00	0.00	699.7	127.1
TE_{61}	2.350	0.341	11.71	16.52	30.15	977.1	553.9
TM_{41}	2.377	0.309	4.85	0.79	1.44	1077.2	906.1

5.5 RMS delay spread

Having an ability to investigate the RMS delay spread dependence on the system parameters (L , L_1 , L_2 , Γ) could be very valuable for a system designer. From a system design point of view, the channel properties for long HVAC ducts (≥ 50 m) are of great interest. Obtaining experimental data for such distances is difficult due to the size of the experimental testbed that would have to be constructed. Our impulse response model allows prediction of the RMS delay spread behavior for *any distance*.

As an example, consider a straight “radio-friendly” duct (both ends are terminated with matched loads, with $\Gamma = 0$, and all other parameters are the same as before). In this situation, only intermodal and intramodal dispersions are present. In a typical indoor environment, RMS delay spread increases linearly with distance [19]. In the HVAC ducts, the behavior of the RMS delay spread is more complex. Figure 5.3 (see the upper curve with \circ symbols) shows the RMS delay spread as a function of the transmitter-receiver separation distance calculated with our model. At short distances, attenuation is small, and the delay spread increases linearly due to the intermodal dispersion. At longer distances, the mode attenuation decreases the number of modes with significant amplitudes, and the delay spread diminishes. At extremely long distances, the intermodal and intramodal dispersion of a few low order modes increases the RMS delay spread again.

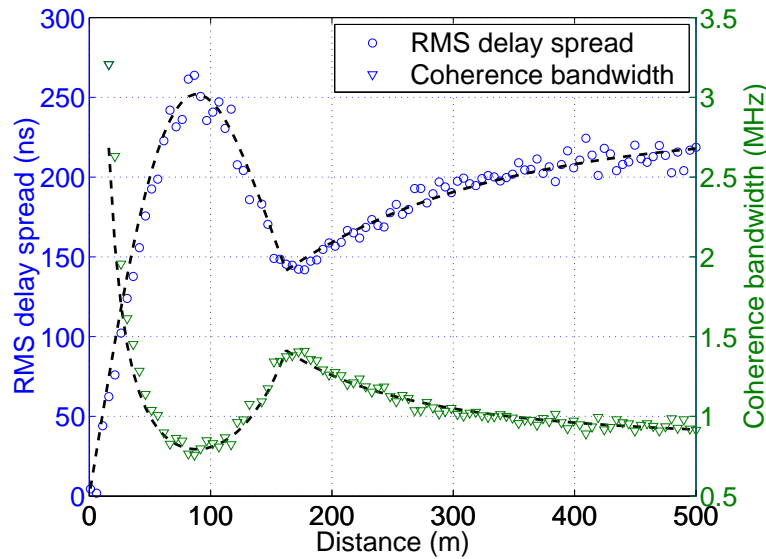


Figure 5.3: Calculated and analytically approximated RMS delay spread and coherence bandwidth as functions of transmitter-receiver separation distance for 30.5 cm diameter cylindrical ducts and 3.5 cm monopole antennas in the 2.4-2.5 GHz band.

The RMS delay spread dependence on distance for the geometry under consideration can be approximated with a simple piecewise analytical function as

$$\sigma_{\tau} = \begin{cases} A d e^{-(d/d_0)^2}, & d \leq 162 \text{ m} \\ B (1 - e^{-d/d_1}), & d > 162 \text{ m} \end{cases} \quad (5.12)$$

where $A = 4.7$ ns/m, $d_o = 125$ m, $B = 230$ ns, and $d_1 = 170$ m. The constant A defines the linear increase of the RMS delay spread for short distances (≤ 50 m), and the constant B defines the asymptotic limit of the RMS delay spread for long distances (≥ 400 m). A , B , d_o , and d_1 depend on antenna properties, duct material and geometry, and frequency band. This analytical approximation is plotted in Figure 5.3 (see the solid line in the upper curve).

The complex behavior of the RMS delay spread is due to the complexity of the multimode propagation problem. A mathematical example below demonstrates that the RMS delay spread behavior may be nontrivial even for a very simple impulse response structure.

Consider a normalized impulse response starting at $t = 0$, shaped by the exponential decay, and defined by the equations:

$$P(t) = \begin{cases} e^{-\frac{t}{T_0}}, & nT_0 \leq t < nT_0 + T_1, \quad \forall n \geq 0 \\ 0, & nT_0 + T_1 \leq t < (n+1)T_0, \quad \forall n \geq 0 \end{cases} \quad (5.13)$$

The impulse response described by the above equations is uniformly filled with stripes as shown in Figure 5.4. Assume that $T_0 \geq T_1$ (stripes do not overlap). For the impulse response shown in

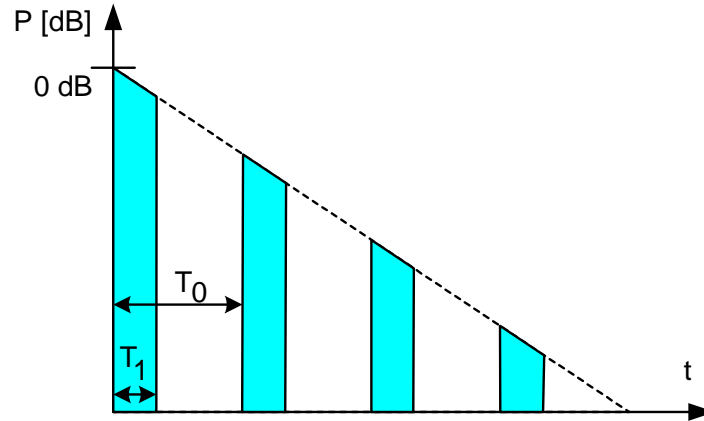


Figure 5.4: “Striped” impulse response profile.

Figure 5.4 the mean excess delay $\bar{\tau}$ and mean squared delay $\bar{\tau}^2$ can be analytically calculated. One

can show that

$$\bar{\tau} = T \left(1 - \frac{\xi_1 e^{-\xi_1}}{1 - e^{-\xi_1}} + \frac{\xi_0 e^{-\xi_0}}{1 - e^{-\xi_0}} \right), \quad (5.14)$$

$$\bar{\tau}^2 = 2T^2 \left[1 - \frac{\xi_1 e^{-\xi_1} (1 + \xi_1/2)}{1 - e^{-\xi_1}} + \frac{\xi_0 e^{-\xi_0}}{1 - e^{-\xi_0}} \left(1 - \frac{\xi_1 e^{-\xi_1}}{1 - e^{-\xi_1}} \right) + \frac{\xi_0^2 e^{-\xi_0} (1 + e^{-\xi_0})}{2(1 - e^{-\xi_0})^2} \right], \quad (5.15)$$

where $\xi_0 = T_0/T$, $\xi_1 = T_1/T$. One can easily see that

$$\lim_{T_0 \rightarrow 0, T_1 \rightarrow 0} \bar{\tau} = T, \quad (5.16)$$

as one would expect it for an exponentially decaying impulse response densely filled with discrete impulses. Similarly,

$$\lim_{T_0 \rightarrow \infty, T_1 \rightarrow \infty} \bar{\tau} = T, \quad (5.17)$$

as one would expect for an exponentially decaying impulse response filled up with one continuous stripe.

The RMS delay spread normalized by T is plotted in Figure 5.5 as a function of parameters ξ_0 and ξ_1 . Setting $T_0 = 2T_1$ makes the spacing between the stripes equal to the stripe width. The behavior of the RMS delay spread in this case is shown in Figure 5.6.

The impulse response in real HVAC ducts contains the effect of the mixture of different modes, where each mode has its own T . Parameters T_0 and T_1 depend on many factors and vary as functions of time. The RMS delay spread functional dependence cannot be derived analytically and must be extracted from the impulse responses obtained via an inverse Fourier transform from theoretically computed or experimentally measured frequency responses.

5.6 Coherence bandwidth

Figure 5.3 also shows the coherence bandwidth B_c (see the lower curve with \triangleright symbols) estimated from the RMS delay spread with 50% signal correlation as [164]

$$B_c = \frac{1}{5\sigma_\tau}. \quad (5.18)$$

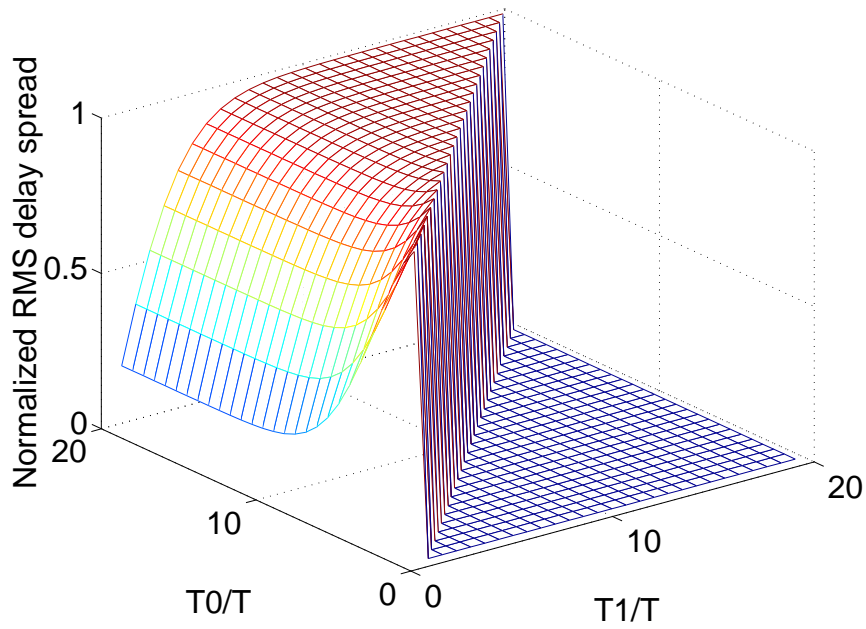


Figure 5.5: Normalized RMS delay spread of the “striped” impulse response as a function of $\xi_0 = T_0/T$ and $\xi_1 = T_1/T$, defined for $T_0 \geq T_1$.

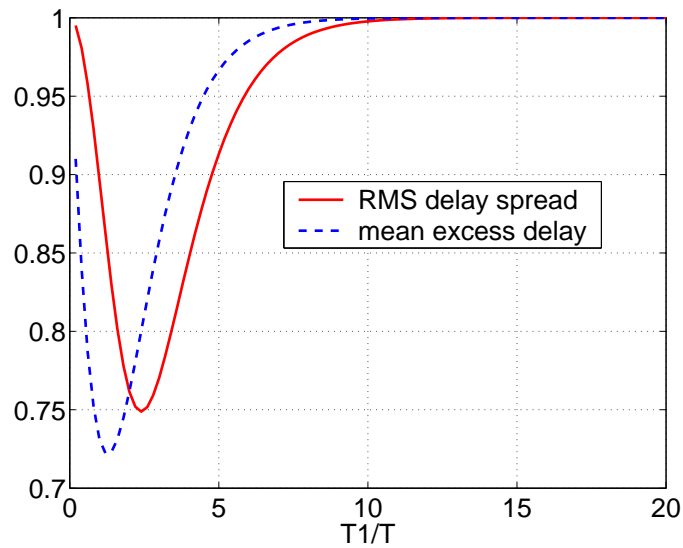


Figure 5.6: Normalized RMS delay spread and mean excess delay of the “striped” impulse response for $T_0 = 2T_1$.

A piecewise analytical approximation for the coherence bandwidth can be obtained directly from Equations (5.12) and (5.18) and is also plotted in Figure 5.3 (see the dashed line in the lower curve).

With no diversity, equalization, or coding, the maximum rate of data transmission in a given channel is strongly related to its coherence bandwidth. The coherence bandwidth metric is usually applied to the channels with statistically uncorrelated frequency response. The frequency response of the multimode waveguide typically contains highly correlated maxima and minima, resulting from the mutual interference of multiple modes. However, the coherence bandwidth is still a good measure of the maximum data rate attainable for a given channel. Given a specific coding and modulation scheme, the realistic channel capacity can be estimated from the coherence bandwidth [165].

5.7 Discussion

The dominant physical mechanism affecting RMS delay spread behavior is multipath reflections, even though intermodal and intramodal dispersions also play a non-negligible role.

When reflections are minimized to realize “radio-friendly” ducts, then the effects of intermodal dispersion dominate. Finally, both intermodal and intramodal dispersion can be minimized by selectively exciting a single (or small number) of preferred modes. We presented a model for the power delay profile in a straight terminated duct. We explored the parametric behavior of the RMS delay spread in “radio-friendly” ducts as a function of the transmitter-receiver distance and approximated it with a simple analytical formula.

The impulse response model that we presented provides insight into the parametric behavior of the RMS delay spread as a function of distance or any other system parameters. It allows the investigation of which system parameters must be adjusted to obtain the desired performance characteristics. Other parameters of the power delay profile (e.g., mean excess delay) can be analyzed with our model in a similar fashion.

While in this Chapter we considered an HVAC channel in the form of a straight duct, the real HVAC duct system is more complicated, as it may contain tapers, bends, T-junctions, etc. Efficient

modelling of the impulse response characteristics in such a system is a challenging task. Our measurements indicate that RMS delay spread behavior in the duct system with small non-uniformities, such as smooth circular bends, is almost identical to the RMS spread behavior in the straight ducts. Severe non-uniformities, such as T-junctions and Y-junctions, have more pronounced effects on the RMS delay spread.

5.8 Summary

This Chapter described different types of physical mechanisms which affect the impulse response. Those mechanisms include probe coupling, attenuation, and three types of dispersion. The influence of different types of dispersion on the RMS delay spread was analyzed. It was found that in short straight ducts terminated with metal caps, in the order of their importance, they are multipath reflections, intermodal dispersion, and intramodal dispersion. The behavior of the RMS delay spread as a function of transmitter-receiver separation distance in straight ducts was also explored.

Chapter 6

Comparison with experiment

6.1 Introduction

To validate the frequency and impulse responses predicted by the theoretical model for different antennas and duct cross-sections, experimental measurements on various configurations of real HVAC ducts were performed.

Figure 6.1 shows a typical duct used in the U.S. – a cylindrical pipe of 30.5 cm (12 in.) in diameter, made of galvanized steel. This type of duct is the most likely candidate to have an HVAC communication system implemented over it and thus was used in the majority of the experiments.

The frequency band used in all experiments was 2.4-2.5 GHz, which covers the ISM band (2.4-2.4835 GHz) employed by many popular wireless standards, such as IEEE 802.11b.

6.2 Experimental setup

Figure 6.2 shows the experimental setup. Depending on the nature of an experiment, a center piece was a single straight section or a combination of straight, bent, or tapered sections, joined together. Both antennas used were identical, either monopoles or dipoles, set on the line along the duct length. Table 6.1 lists the parameters of all ducts used in experiments. Figure 6.3 shows the Agilent



Figure 6.1: Cylindrical duct 30.5 cm (12 in.) in diameter, used in experiments.

Duct type	Cross-section	Size	Material	Conductivity
I	circular	diameter 30.05 cm	steel	10^6 S/m
II	circular	diameter 45.72 cm	steel	10^6 S/m
III	rectangular	20 cm x 10 cm	aluminum	3.5×10^7 S/m

Table 6.1: Parameters of ducts used in experiments.

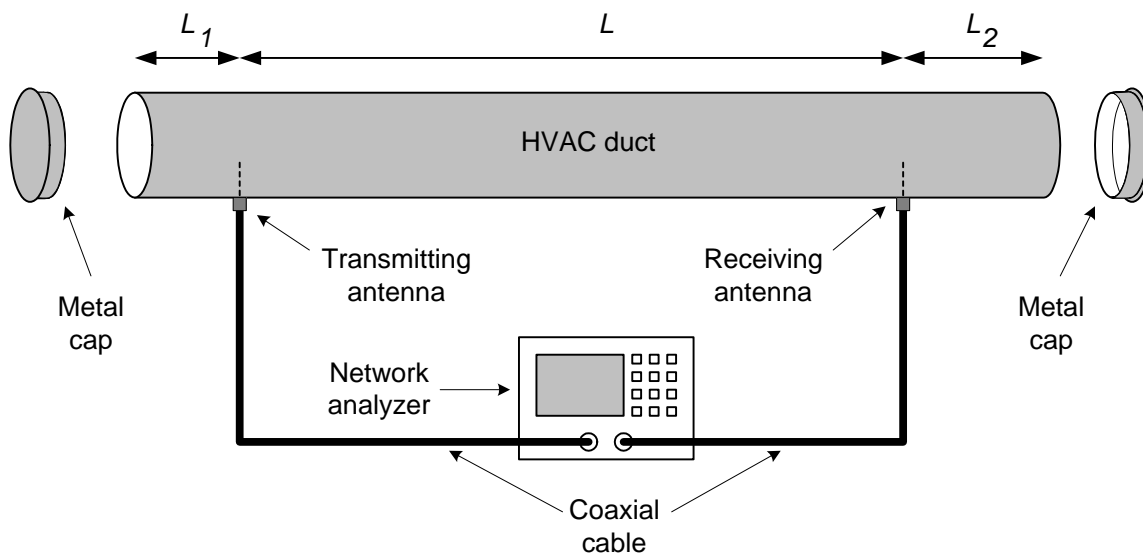


Figure 6.2: General experimental setup.

E8358A network analyzer with an internal port impedance of 50 ohms, which was used to measure the frequency response (S-parameter S_{21}) between the antennas in the 2.4-2.5 GHz band. Prior to each measurement, a calibration procedure was performed. The antenna cables were connected directly, and the cable response was measured and calibrated out. This procedure allowed one to measure purely the response of the channel contained between the terminals of two duct antennas, excluding the effect of the connecting cables.

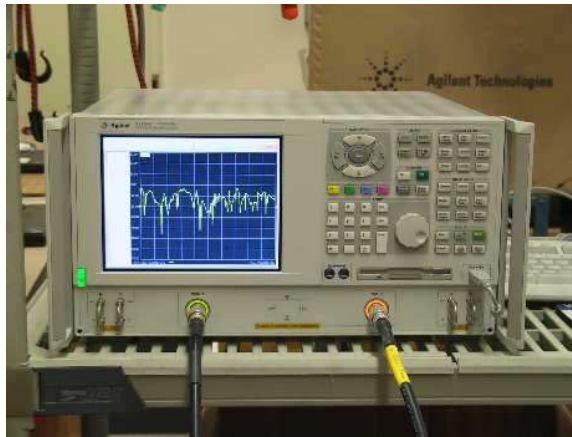


Figure 6.3: Agilent E8358A network analyzer used for measurements.

Four main elements were used in experiments: straight sections, bends, tapers, and T-junctions. In addition to that, metal caps were used to terminate the ends of the ducts in order to study the effect of reflections. Figures 6.4 and 6.5 show the setup for experiments involving bends and tapers, and T-junctions, respectively.

Table 6.2 lists the parameters of bends, tapers, and T-junctions used in experiments, using the same notation as in Chapter 4. Figure 6.6 shows a straight section, a metal end cap (which is a

Table 6.2: Parameters of bends, tapers, and T-junctions used in experiments.

Element	Duct type	Diameter in	Diameter out	Other parameters
Bend	I	30.05 cm	30.05 cm	$R = 0.45$ m, $\phi_B = 90$ deg.
Taper	I \rightarrow II	30.05 cm	45.72 cm	$L_T = 0.23$ m
T-junction	I	30.05 cm	30.05 cm	$L_{T_n} = 5.1$ cm, $L_p = 5.1$ cm

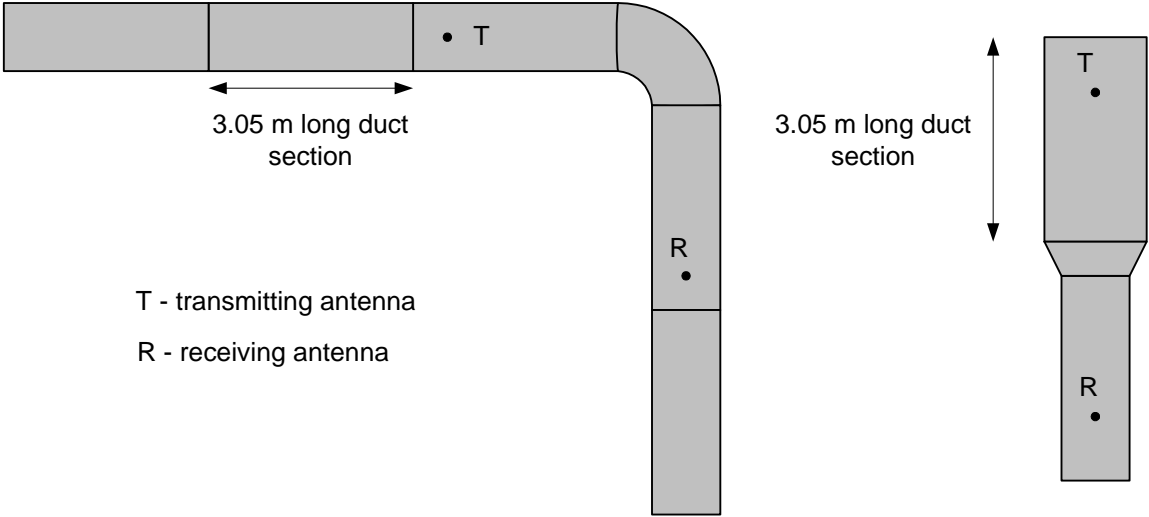


Figure 6.4: Experimental setup for bend and taper measurements.

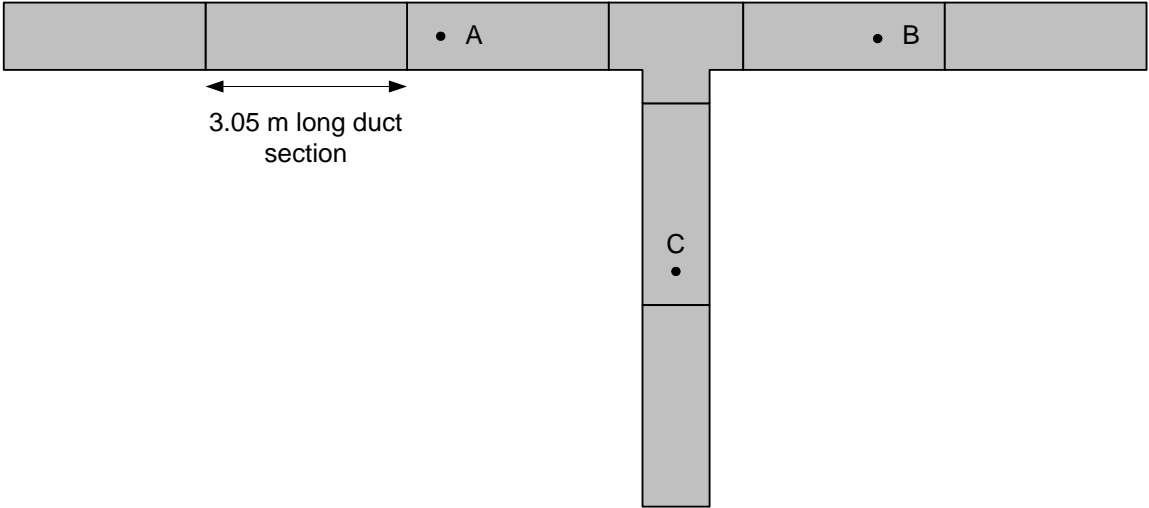


Figure 6.5: Experimental setup for T-junction measurements.

good approximation of a short termination), a bend, a taper, and a T-junction used in experiments.

Two types of antennas were used in experiments: monopole antennas of different length and dipole antennas. Both types of antennas are shown in Figure 6.7. Antennas were mounted on HVAC ducts as shown in Figure 6.8. Figure 6.9 shows the outside and inside view of the monopole probe antenna mounted on the duct.

6.3 Frequency response

The measured and predicted frequency responses were compared for various configurations involving straight, bent, and tapered ducts excited by various antennas. Three main parameters were varied during the experiments: transmitter-receiver separation distance, antenna parameters, and the duct end termination.

The parameters of all experiments are given in Table 6.3, which lists the antenna length l , the radial location r_d of the dipole antenna (which was not curved), the separation distance L , the distances L_1 and L_2 from the antennas to the respective duct ends, and the terminal reflection coefficients G_1 and G_2 used for theoretical calculations. For the experiments involving bends or tapers, the distance L includes the center path inside the bend or the taper.

Figure 6.10 shows experimental and theoretical frequency responses for two monopole antennas with separation distance varied, antenna length fixed, and other parameters given in Table 6.3. One can see that the agreement between the curves is within a few dB. Theoretical curves reproduce most major maxima and minima observed in the experiments.

Observed differences are due to mode reflections from the duct open ends and the fact that ducts and components are not precision cylindrical guides. If a duct was terminated with matched loads, no reflections from the ends would arise. However, a matched load for an arbitrary multimode waveguide is a non-trivial device. A good approximation to that is simply leaving the waveguide end open. In heavily overmoded waveguides, an open end reflection coefficient is mode-dependent but relatively small (see, e.g., [166, 167, 168, 169, 170, 171, 172, 173]). For modelling purposes,



Figure 6.6: Straight section, metal end cap, bend, taper, and T-junction used in experiments.

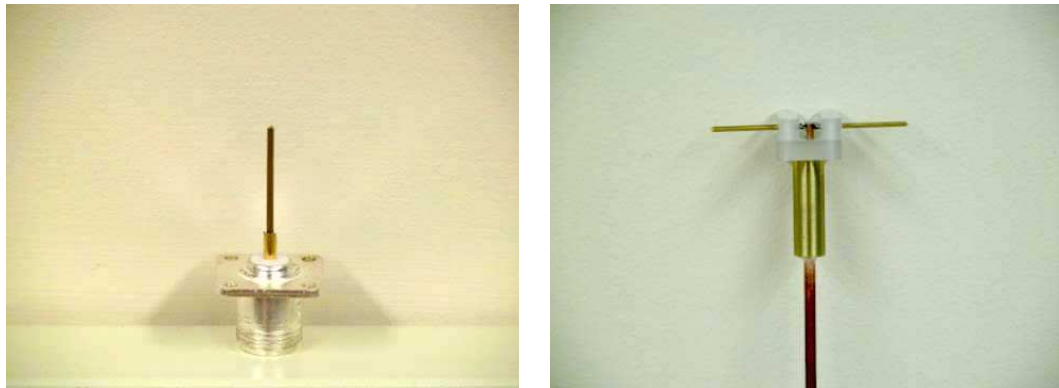


Figure 6.7: Monopole and dipole antennas used in experiments.

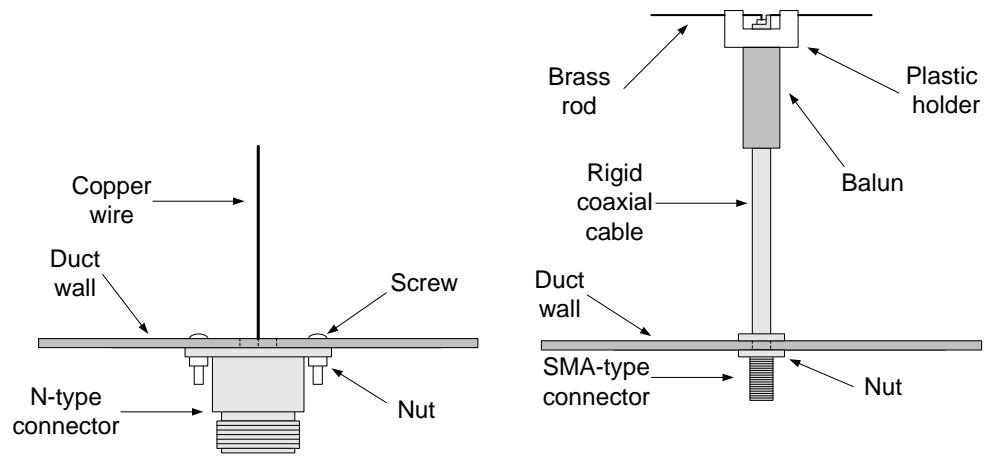


Figure 6.8: Mounting of monopole and dipole antennas on the duct.

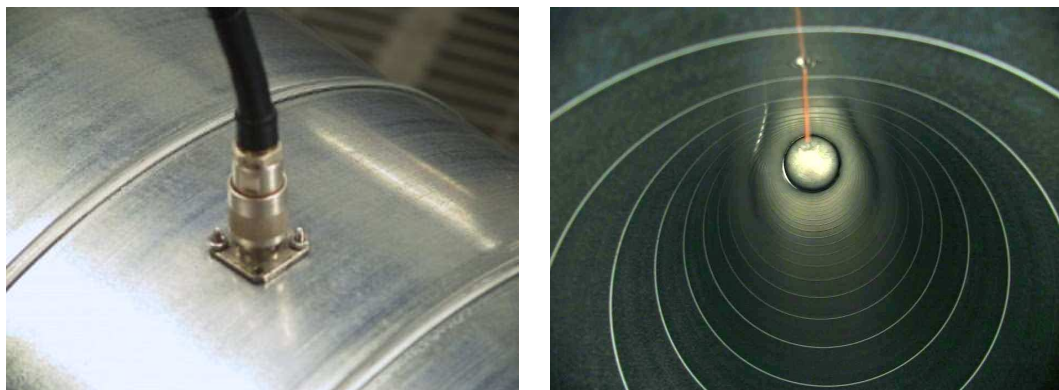


Figure 6.9: Outside and inside view of the monopole probe antenna mounted on the duct.

Table 6.3: Parameters of the frequency response experiments.

Figure	Setup	Duct type	Antenna type	l, r_d (cm)	L (m)	L_1 (m)	G_1	L_2 (m)	G_2
6.10A	straight	I	monopole	3.5	4.58	0.25	0	10.39	0
6.10B	straight	I	monopole	3.5	7.54	0.32	0	1.24	0
6.10C	straight	I	monopole	3.5	9.20	0.25	0	5.77	0
6.10D	straight	I	monopole	3.5	11.63	0.25	0	3.33	0
6.11A	straight	I	monopole	3.5	4.58	0.25	0	10.39	0
6.11B	straight	I	monopole	3.5	4.58	0.25	0.2	10.39	0.2
6.11C	straight	I	monopole	3.5	4.58	0.25	0.4	10.39	0.4
6.11D	straight	I	monopole	3.5	4.58	0.25	0.6	10.39	0.6
6.12A	straight	I	monopole	3.5	4.58	0.25	0	10.39	0
6.12B	straight	I	monopole	3.5	4.53	0.29	0	1.24	0
6.13A	straight	I	monopole	0.9	5.18	0.45	0	0.45	0
6.13B	straight	I	monopole	14.8	5.18	0.45	0.4	0.45	0.4
6.14A	straight	I	dipole	2.6, 6.4	8.34	0.46	0	0.46	0
6.15A	straight	I	monopole	3.5	2.44	0.31	-0.9	0.31	0
6.15B	straight	I	monopole	3.5	4.53	0.31	-0.9	1.24	0
6.16	straight	I	monopole	3.5	14.67	0.33	-0.9	0.26	-0.9
6.17A	bend	I	monopole	3.2	6.10	3.35	0	6.44	0
6.17B	taper	I, II	monopole	3.2	4.51	0.44	0	1.34	0
6.18	T (A \rightarrow B)	I	monopole	3.1	4.88	6.41	0	4.29	0
6.18	T (A \rightarrow C)	I	monopole	3.1	5.79	6.41	0	3.35	0
6.14B	straight	III	monopole	4	0.71	0.10	0	0.10	0

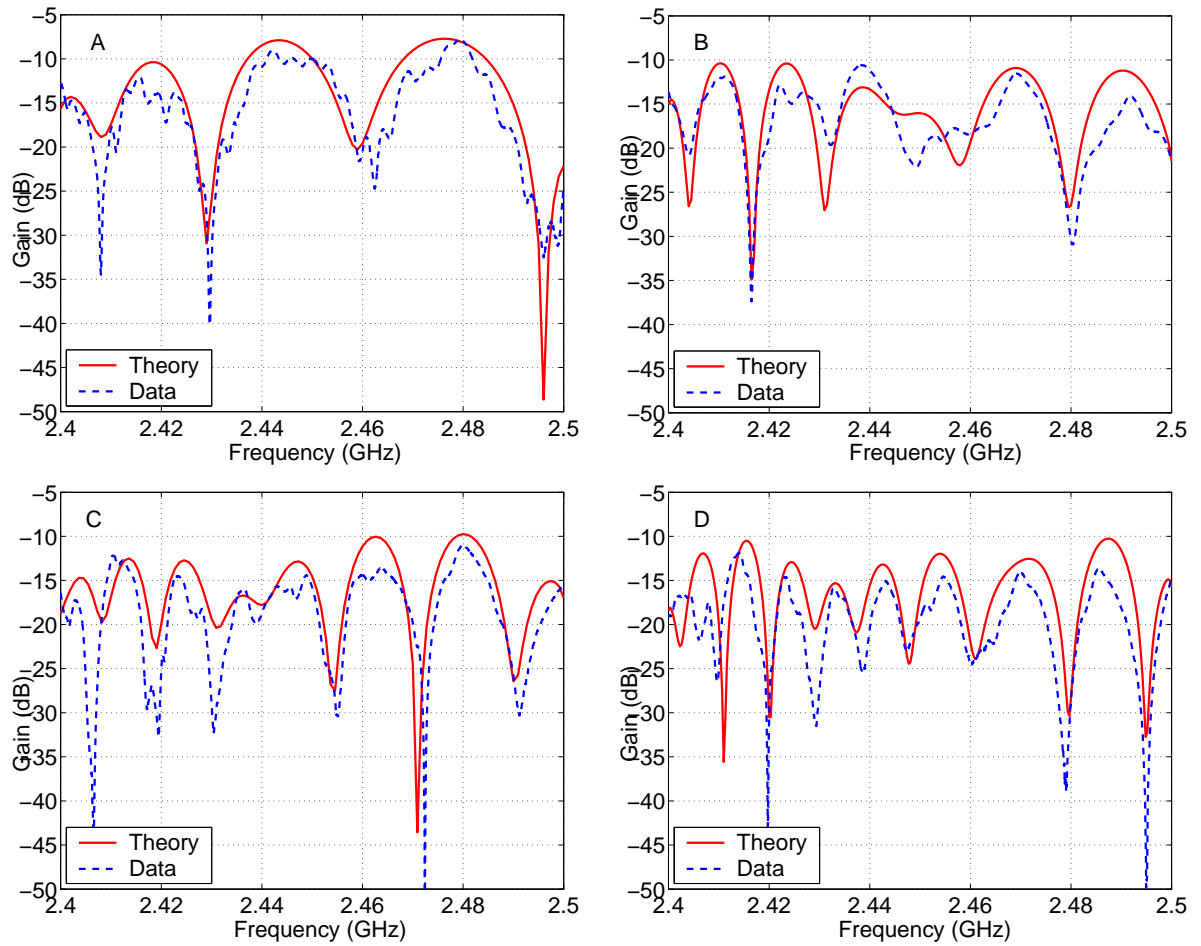


Figure 6.10: Theoretical and experimental frequency responses for two monopole antennas in a straight open-ended duct with antenna separation distance 4.58 m (A), 7.54 m (B), 9.20 m (C), 11.63 m (D), and other parameters given in Table 6.3.

we will assume that the reflection coefficient is constant for all modes.

The effect of the reflection coefficient is shown in Figure 6.11, which compares the experimental frequency response measured in an open-ended duct for one particular setup and the theoretical frequency responses for the same setup, computed for different values of the duct end reflection coefficient G . One can see that the reflection coefficient 0.2 reproduces fairly well the frequency response ripples caused by reflections from the open ends. The exact spacing and amplitude of the ripples are strong functions of G , L_1 , and L_2 .

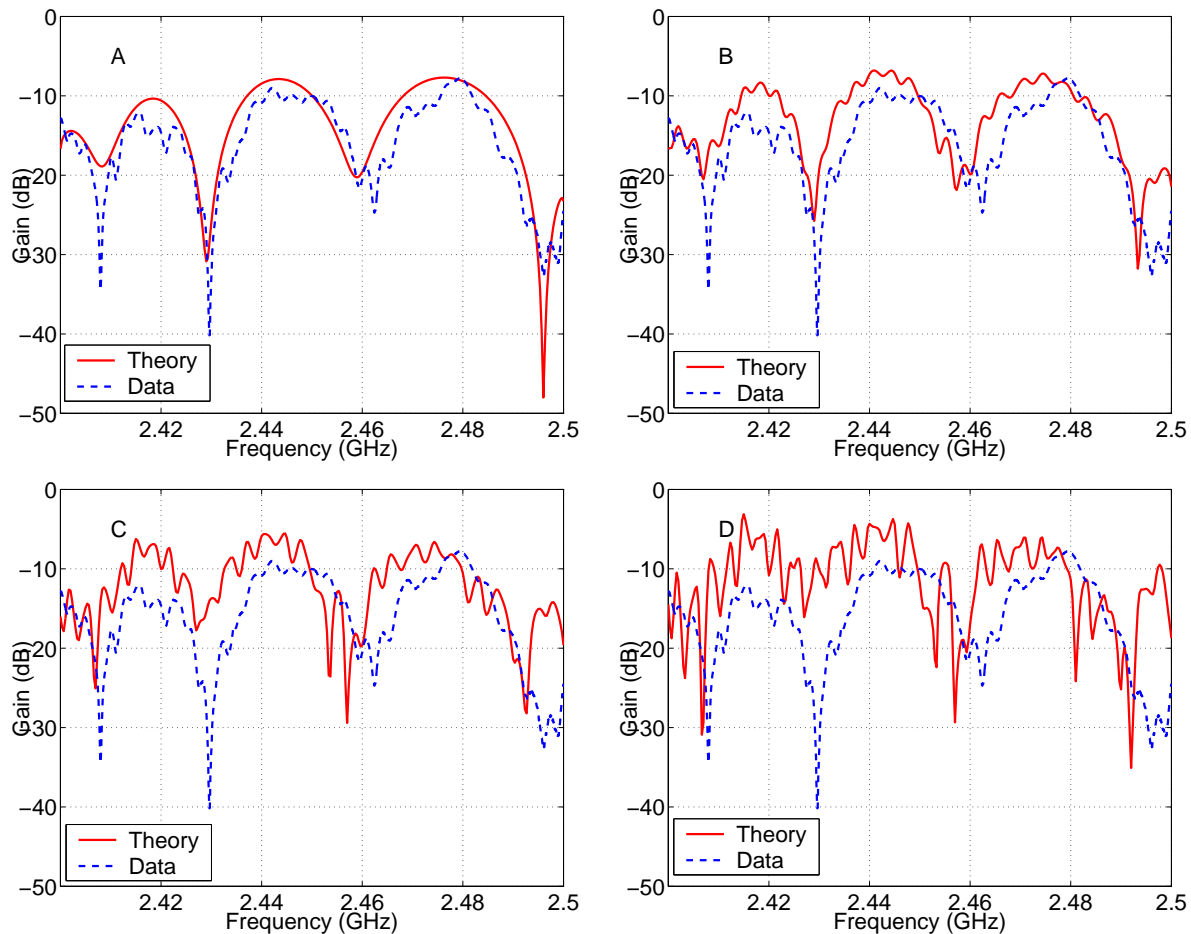


Figure 6.11: Comparison of the experimental frequency response for two monopole antennas in a straight open-ended duct and the theoretical frequency response computed using the end reflection coefficient $G = 0$ (A), $G = 0.2$ (B), $G = 0.4$ (C), $G = 0.6$ (D), and other parameters given in Table 6.3.

The effect of the distance on the reflections is shown in Figure 6.12, which compares the experimental and theoretical frequency responses measured in an open-ended duct for two setups with different distances to the open end. One can see that if the open end is close to the antenna, the effect of the reflection is about the same in magnitude as when the open end is far from the antenna. However, there are fewer small-scale oscillations because the reflected modes do not accumulate enough of the phase difference while travelling from the open end to the antenna.

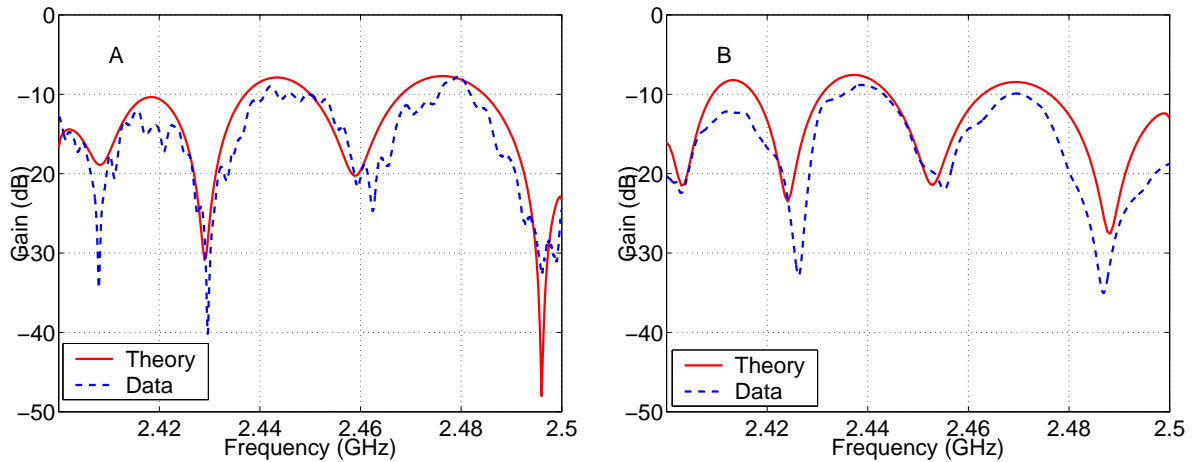


Figure 6.12: Comparison of the theoretical and experimental frequency responses for two monopole antennas in a straight open-ended duct with distance to the farthest open end 10.39 m (A) and 1.24 m (B), with other parameters given in Table 6.3.

To validate the model for monopoles of different length, we performed experiments with short and long monopole antennas in a straight duct. Figure 6.13 shows experimental and theoretical frequency responses for two monopole antennas with antenna length varied and other parameters given in Table 6.3. A very long monopole antenna excites a current distribution very different from the one excited by a shorter monopole. It appears that the open end reflection coefficient of the excited mode pack in this case can be approximated by the value 0.4.

To verify the validity of the model for different antennas and duct cross-sections, an experiment with dipole antennas in an open-ended cylindrical duct and an experiment with monopole antennas in an open-ended rectangular duct were performed. Figure 6.14 shows experimental and theoretical frequency responses for these cases, with other parameters given in Table 6.3. The disagreement

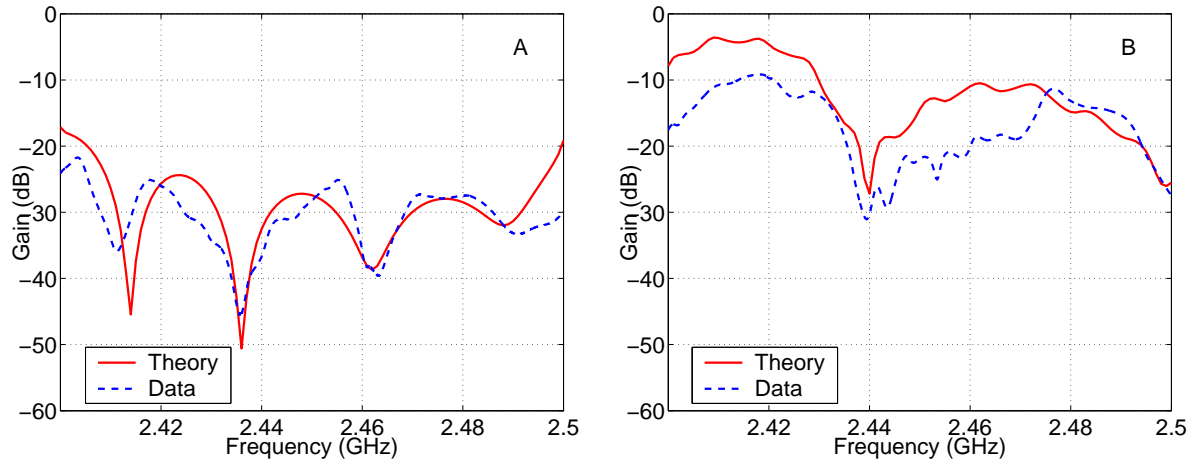


Figure 6.13: Theoretical and experimental frequency responses for two monopole antennas in a straight open-ended duct with antenna length 0.9 cm (A) and 14.8 cm (B), and other parameters given in Table 6.3.

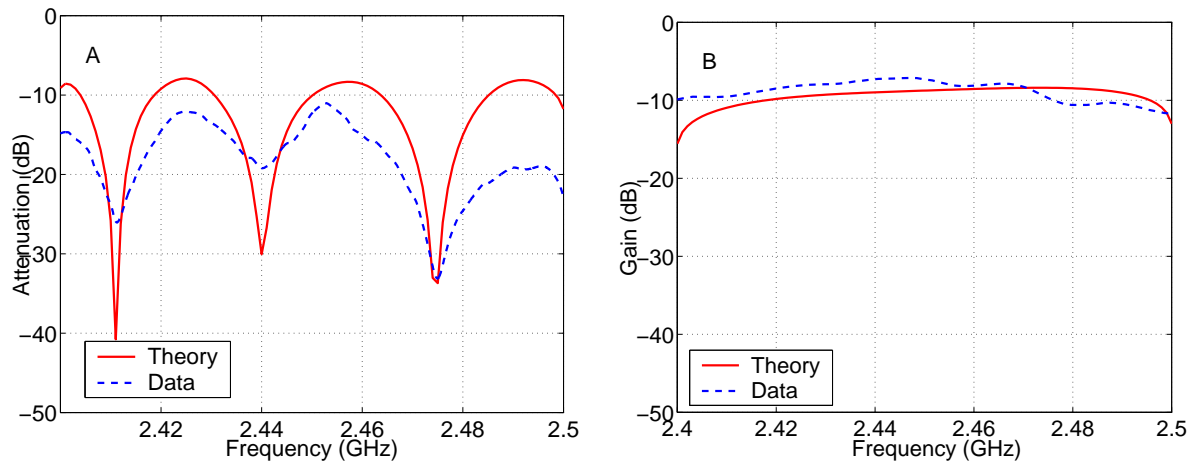


Figure 6.14: Theoretical and experimental frequency responses for two dipole antennas in a straight cylindrical open-ended duct (A) and for two monopole antennas in a straight rectangular open-ended duct (B), with other parameters given in Table 6.3.

between the curves shown in Figure 6.14A is partially due to the fact that the physical dipole has a more complicated structure than an ideal dipole with two circumferential arms fed by a point current source, considered in the model. The actual dipole has a balun structure together with a small radial section of coaxial cable with two perpendicularly soldered straight arms. Still, the model reproduces all major maxima and minima in the experimental curve. The two curves for a small rectangular duct agree well.

Figure 6.15 shows experimental and theoretical frequency responses for two monopole antennas in a straight duct short-terminated on one end, with other parameters given in Table 6.3. The model

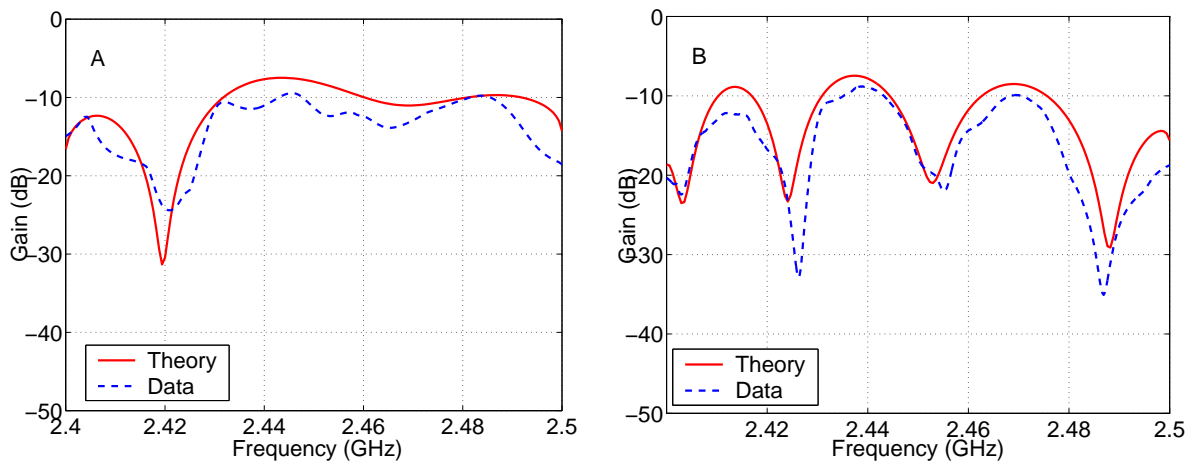


Figure 6.15: Theoretical and experimental frequency responses for two monopole antennas in a straight duct short-terminated on one end with separation distance 2.44 m (A) and 4.53 m (B), with other parameters given in Table 6.3.

used the reflection coefficient $G = -0.9$ (-0.92 dB) for a duct end terminated with the metal end cap. This value approximates the loss due to non-ideality of the reflection (e.g., the cap fit onto the duct is not tight) and seems to deliver the best agreement between experimental and theoretical curves.

If both ends of the duct are terminated with metal caps, the duct behaves as a resonator. A duct resonator cannot be compared in precision with carefully manufactured microwave resonators, and the frequency response measured in it is affected by any imperfections present in real HVAC ducts (dents, cross-section distortions, spiral corrugation, etc.). Figure 6.16 shows experimental and

theoretical frequency responses for two monopole antennas in a straight duct capped on both ends, with other parameters given in Table 6.3.

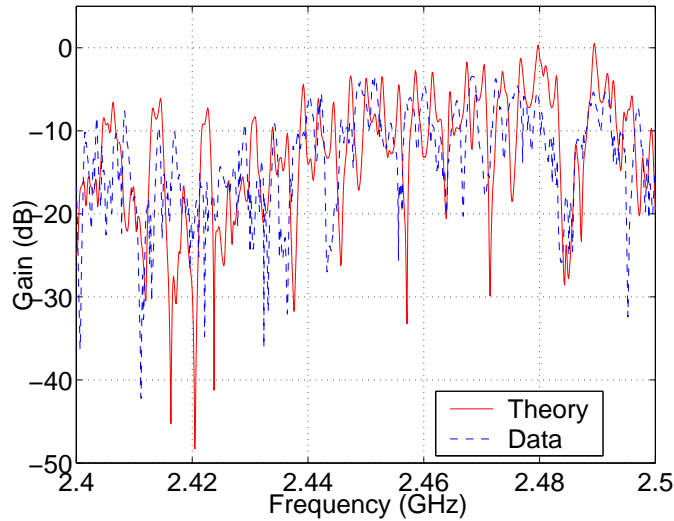


Figure 6.16: Theoretical and experimental frequency responses for two monopole antennas in a straight duct short-terminated on both ends, with other parameters given in Table 6.3.

To verify the validity of the model for bends and tapers, the experiments were performed using the configurations shown in Figure 6.4 with other parameters given in Table 6.3. Figure 6.17 shows experimental and theoretical frequency responses for two monopole antennas in a cascaded configuration involving straight sections and a bend, with both ends open. The model predicts well the average shape of the frequency response. The disagreement is partially due to internal reflections from duct open ends and the bend/taper discontinuity itself and partially to the imperfections of ducts which are not precision waveguides. Experiments with the taper verified that the measured channel response is the same if transmitting and receiving antenna are interchanged.

To analyze the effect of T-junctions on propagation, the experiments were performed using the configurations shown in Figure 6.5 with other parameters given in Table 6.3. Figure 6.18 shows experimental frequency responses for two monopole antennas in a cascaded configuration involving straight sections and a T-junction, with both ends open. The frequency responses shown in Figure 6.18 were used to extract the mode distributions discussed in Chapter 4. The lack of knowledge

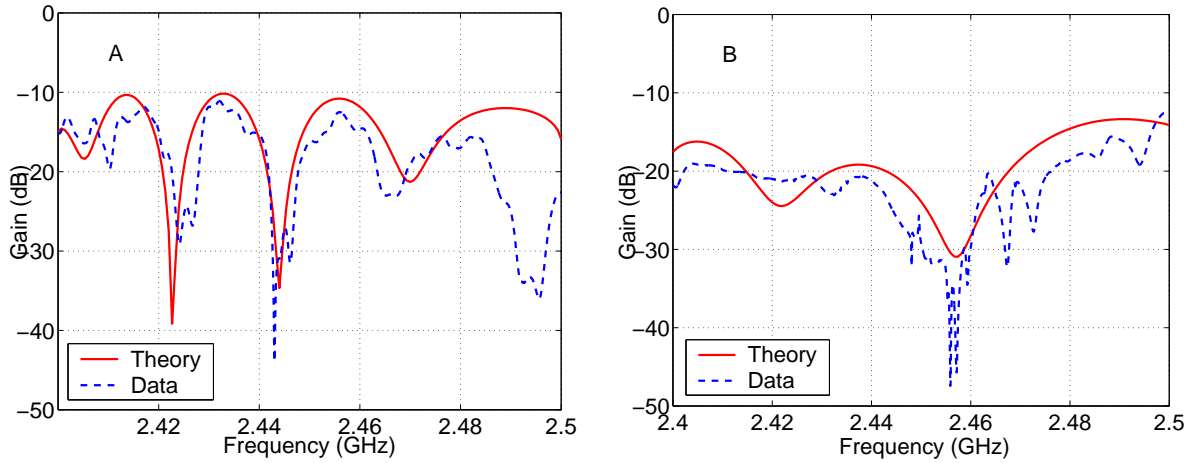


Figure 6.17: Theoretical and experimental frequency responses for two monopole antennas in an open-ended bent duct (A) and tapered duct (B), with other parameters given in Table 6.3.

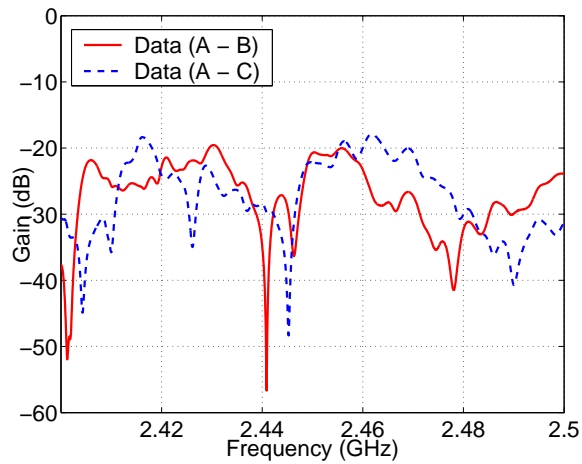


Figure 6.18: Experimental frequency responses for two monopole antennas in an open-ended duct with a T-junction and other parameters given in Table 6.3.

of the transfer matrix for the T-junction does not presently permit one to perform a comparison of experiment with the model.

Table 6.4: Comparison of theoretical predictions and experimental measurements of the average channel gain in the band.

Figure	Theoretical gain	Measured gain
6.10A	-11.63 dB	-13.46 dB
6.10B	-14.22 dB	-15.58 dB
6.10C	-14.56 dB	-16.82 dB
6.10D	-14.99 dB	-17.96 dB
6.12A	-11.63 dB	-13.46 dB
6.12B	-11.69 dB	-13.88 dB
6.13A	-26.06 dB	-28.81 dB
6.13B	-9.25 dB	-14.47 dB
6.14A	-10.98 dB	-16.29 dB
6.15A	-10.52 dB	-12.69 dB
6.15B	-8.45 dB	-10.35 dB
6.16	-8.78 dB	-10.43 dB
6.17A	-13.53 dB	-16.21 dB
6.17B	-17.56 dB	-19.99 dB
6.14B	-9.33 dB	-8.72 dB

One of the important channel characteristics is an average attenuation in the band computed as

$$L_{av} (dB) = 10 \log_{10} \left[\frac{1}{N} \sum_{k=1}^N |H(\omega_k)|^2 \right], \quad (6.1)$$

where N is the number of frequency points and $H(\omega_k)$ is the transfer function at the frequency ω_k . Average attenuation in the band affects the Signal-to-Noise Ratio (SNR) at the receiver. Table 6.4 compares theoretically predicted and experimentally measured average channel gain for all cases considered. One can see that with the exception of a few cases, namely dipole and long monopole antennas, the agreement between theoretical prediction of the average attenuation and experimentally measured one is about 3 dB.

6.4 Impulse response

This section compares the measured and predicted power delay profiles and RMS delay spread values predicted by the model over accessible distances in straight ducts with open and closed ends. The power delay profiles were calculated from impulse responses, which were obtained from the predicted frequency responses via an inverse Fourier transform.

The parameters of the experiments are given in Table 6.5, which lists antenna length l , separation distance L , distances L_1 and L_2 from the antennas to the respective duct ends, and terminal reflection coefficients G_1 and G_2 used for theoretical calculations.

Table 6.5: Parameters of the impulse response experiments.

Figure	Setup	Duct type	Antenna type	l, r_d (cm)	L (m)	L_1 (m)	G_1	L_2 (m)	G_2
6.19A	straight	I	monopole	3.5	4.58	0.25	0.2	10.39	0.2
6.19B	straight	I	monopole	3.5	14.67	0.25	-0.9	0.32	-0.9
6.20A	straight	I	monopole	3.5	2.44	0.32	0	0.28	0
6.20B	straight	I	monopole	3.5	5.39	0.32	0	0.38	0
6.20C	straight	I	monopole	3.5	7.58	0.32	0	1.24	0
6.20D	straight	I	monopole	3.5	10.94	0.32	0	0.93	0
6.20E	straight	I	monopole	3.5	14.67	0.32	0	0.25	0

Figure 6.19 shows measured and calculated power delay profiles for two monopole antennas in a straight cylindrical duct with both ends open (A) and closed (B). In case A, one can see that the general agreement is good. The first peak corresponds to the time of the first arrival, which is about 15 ns. In case B, the ringing time is very long. Waves travel multiple times back and forth between end caps before decaying out. Experimentally, we have found that the multimode power delay profile decays approximately exponentially in time. For modes propagating near the velocity of light, the measured time delay corresponds to an attenuation rate of about 6.6 dB/100 m. This value is lower than the attenuation constant of the most excited mode (11.71 dB/100 m for TE_{61}), but higher than the attenuation constant of the next excited mode (5.54 dB/100 m for TE_{51}). The

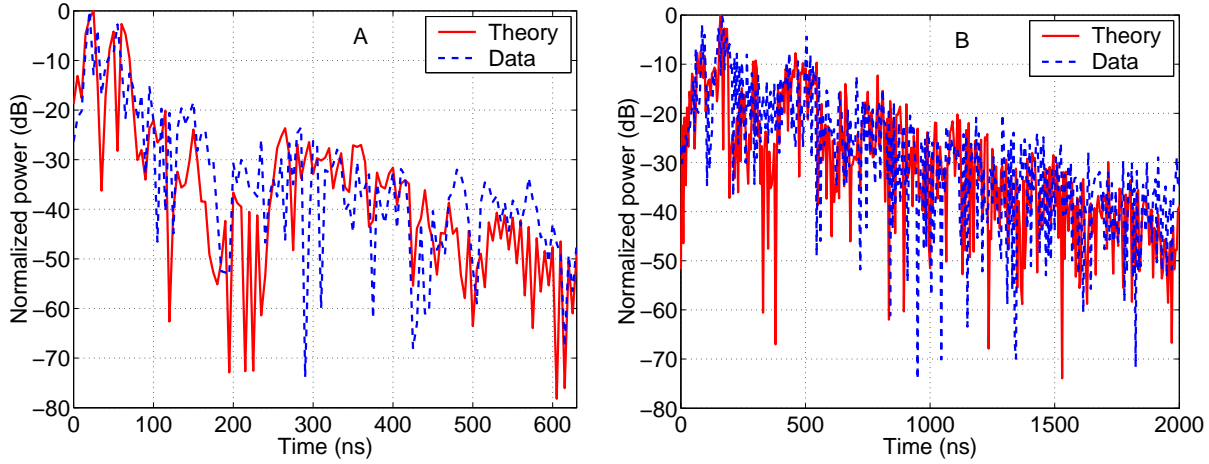


Figure 6.19: Theoretical and experimental power delay profiles for two monopole antennas in a straight duct with open ends (A) and closed ends (B) (other parameters are given in Table 6.5).

lowest loss mode in a cylindrical waveguide is TE_{01} . It has an attenuation constant of 0.39 dB/100 m but is not excited by a vertical monopole probe antenna.

Figure 6.20 shows measured and calculated RMS delay spread values for two monopole antennas in a straight cylindrical duct with both ends open and closed. One can see that theoretical results agree well with experimental data for distances up to 15 m. Although validation at longer distances is ultimately needed as well, this result gives confidence in the basic elements of the model.

6.5 Discussion

Theoretical curves presented in this Chapter are generally in good agreement (within a few dB) with the experimental curves and reproduce all major maxima and minima observed in the experiments. Observed differences are due primarily to three reasons.

First, real HVAC ducts are not manufactured and joined together with the same degree of precision as microwave guides, so some degree of parameter uncertainty (e.g., stochastic geometry perturbations, such as surface and shape imperfections) will always be present.

Second, in derivation of the model, several approximations were made, which allowed one to obtain an analytical expression for the frequency response. For example, the field in a waveguide

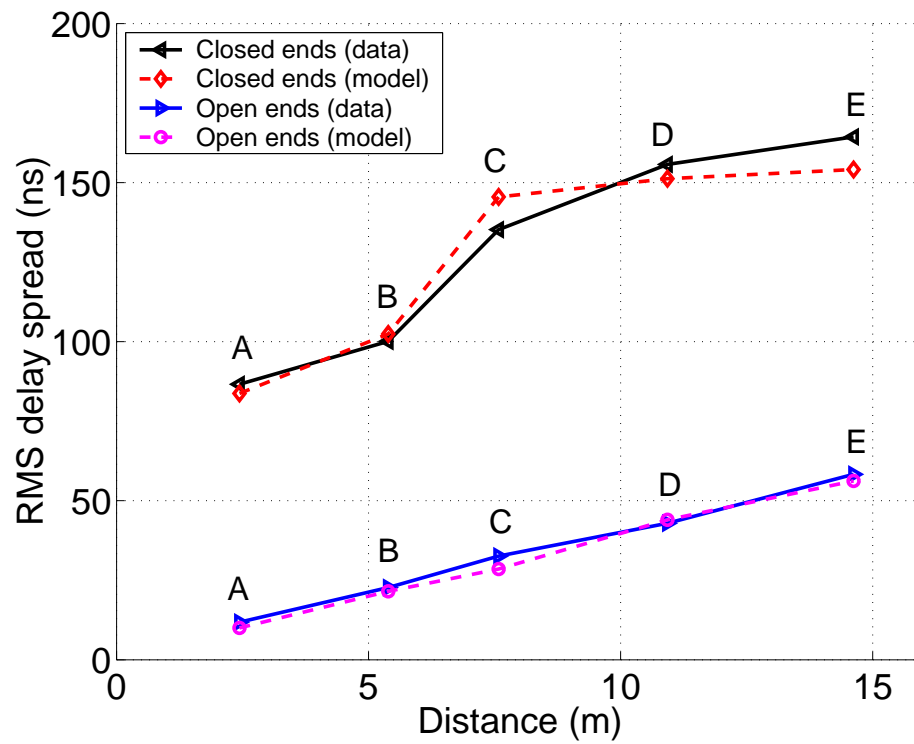


Figure 6.20: RMS delay spread: comparison of theoretical model with experimental data for two 3.5 cm monopole antennas in a 30.5 cm steel cylindrical duct with open ends ($G =$) and closed ends ($G = -0.9$).

is perturbed by the presence of the probe [174]. While more rigorous solutions would give a more accurate prediction for the frequency response in an ideal waveguide system, in a real HVAC duct system with parameter uncertainties, mentioned above, it may not result in significantly better agreement with experimental data.

Third, reflections from open ends are not calculated exactly. Exact mode reflection coefficients computed for an open-ended circular waveguide could further improve the agreement between data and theory, but this task is beyond the scope of this work.

Overall, the agreement between the theoretical and experimental results presented here is sufficiently good to use the model for estimating the quality of the HVAC duct communication channel. The model is simple but allows one to reliably predict the general shape of a channel frequency response and power delay profile as well as some average quantities, such as the average attenuation in the band and the RMS delay spread.

6.6 Summary

This Chapter described the experimental setup for measuring the HVAC duct channel response. The measurements were performed for a number of different configurations: cylindrical and rectangular ducts, various transmitter-receiver separation distances, various antenna types, open or short-terminated duct ends, and cascaded systems with bends or tapers. The experimental and theoretical results are in good agreement and show that the model can be used for analyzing the HVAC duct system behavior at radio frequencies.

Chapter 7

Summary

7.1 Summary

A typical HVAC duct system is a network of interconnected hollow metal pipes which can carry electromagnetic waves at radio frequencies and thus presents an attractive medium to be used for indoor communications. A promising use of the HVAC communication channel is providing high-speed network access to the offices in a large building. The HVAC channel is practical and economically viable since it uses an already existing infrastructure.

At radio frequencies, an HVAC duct system behaves as a complex network of multimode waveguides, which is a unique communication environment. To design a wireless HVAC distribution system, a reliable channel model is needed.

This work presents an analysis of an HVAC duct system as a radio frequency communication channel. Various physical mechanisms which affect the transfer function of this channel include antenna coupling, attenuation, and dispersion. Two main parts of the analysis include channel modelling and antenna design. The approach used here is based on the waveguide mode theory and employs the transfer matrix method to describe propagation through various cascaded HVAC elements (straight sections, bends, tapers, etc.). The transfer matrix of a specific HVAC element can be found analytically, numerically, or experimentally, depending on the element complexity.

The model presented in this work can predict both channel characteristics and antenna characteristics for a given geometry and dimensions of the duct system and the antennas. The model is computationally efficient and can potentially be applied to duct systems of multiple story buildings. The accuracy of the model has been validated with extensive experimental measurements on real HVAC ducts.

An important characteristic of the communication channel is the maximum data capacity, which is directly related to the coherence bandwidth of the channel. The coherence bandwidth of the HVAC channel generally reduces with an increase in transmitter-receiver distance due to interference between multiple propagating modes and their reflections in the duct system. The optimal transmission scheme under these circumstances is multicarrier modulation. The actual achievable data rate depends on specific coding, modulation, and equalization schemes and can potentially far exceed the maximum achievable data rate over phonelines and powerlines, while providing an efficient RF distribution.

7.2 Suggestions for future work

Several topics present an interest for future research related to using HVAC ducts for communications. One is the further investigation of selective mode excitation and channel response optimization techniques using various antennas, including array antennas and a single frequency-swept antenna. Those antennas can also be used for mode content measurement. Another is the determination of transfer matrices of complicated HVAC elements, such as T-junctions and Y-junctions. Third, finding the optimal coding and modulation technique, best suited for use in HVAC ducts, is a topic of interest as well. One other research topic is empirical modelling of important quantities (e.g., RMS delay spread) as functions of dependent parameters (e.g., duct diameter or operating frequency).

Real HVAC duct systems are very complicated, and efficient modelling of RF propagation in such systems is a challenging task. The model presented here should be perceived as a first step

towards the development of a tool for planning a wireless distribution system using building HVAC ducts.

The software tool "Duct Explorer" based on the presented model allows one to simulate frequency responses of various HVAC duct systems excited by various antennas and to perform parametric modelling. The next step would be to add an optimization capability and to integrate it with other functional pieces that perform, e.g. channel capacity calculations. This would allow to progress towards creating a system-level design tool.

Appendix A

Fields in waveguides

A.1 Introduction

HVAC ducts are essentially hollow metal waveguides of rectangular or circular cross-section. Maxwell's equations inside a hollow waveguide take the following form:

$$\nabla \times \vec{E} = -j\omega\mu_o\vec{H}, \quad (\text{A.1})$$

$$\nabla \times \vec{H} = j\omega\epsilon_o\vec{E}, \quad (\text{A.2})$$

where \vec{E} is an electric field inside the waveguide, \vec{H} is the magnetic field inside the waveguide, μ_o is the magnetic permeability of free space, ϵ_o is the dielectric permittivity of free space, and ω is the frequency of a time-harmonic field. Equations A.1 and A.2 allows one to solve for either \vec{E} or \vec{H} from the wave equation (Helmholtz equation), which is obtained as a result of simplification of Maxwell's equations:

$$\nabla^2 \vec{E} + \omega^2\mu_o\epsilon_o\vec{E} = 0, \quad (\text{A.3})$$

$$\nabla^2 \vec{H} + \omega^2\mu_o\epsilon_o\vec{H} = 0. \quad (\text{A.4})$$

An arbitrary field excited in a rectangular or a cylindrical waveguide can be represented as a superposition of normal orthogonal waveguide modes, which are solutions to the Equations A.3 and A.4 with boundary conditions imposed by the shape of a waveguide.

A mode is a specific pattern of electric and magnetic fields that maintains its shape with distance. Each mode has a cutoff frequency associated with it. If the excitation frequency is above the cutoff frequency, the mode is propagating (non-evanescent). Otherwise, the mode is evanescent, with power decaying exponentially with the distance. The lowest cutoff frequency of all modes is the cutoff frequency of the waveguide, below which the signal can not propagate. The mode propagation constant is

$$\gamma = \alpha + j\beta, \quad (\text{A.5})$$

where α is the attenuation constant and β is the propagation constant (wave number). Attenuation and propagation constants α and β are mode-dependent, which means that different modes propagate along the waveguide with different group velocities and attenuation. In a hollow metal waveguide, attenuation is due to losses in non-ideally conducting waveguide walls. Attenuation can be characterized by the wall resistance R_s , defined as

$$R_s = \sqrt{\frac{\omega\mu}{2\sigma}}, \quad (\text{A.6})$$

where μ is the magnetic permeability of the waveguide walls, and σ is the electrical conductivity of the walls. The wave number k is

$$\beta = \sqrt{k^2 - g^2}, \quad (\text{A.7})$$

where g is the cutoff wave number and k is the free-space wave number. The free-space wave number can be expressed as

$$k = \frac{\omega}{c} = \frac{2\pi}{\lambda}, \quad (\text{A.8})$$

where c is the speed of light and λ is the free-space wavelength. The mode cutoff frequency ω_c is given by

$$\omega_c = c g. \quad (\text{A.9})$$

Two types of modes can exist in a rectangular or a cylindrical waveguide: transverse electric (TE) modes and transverse magnetic (TM) modes. In TE modes, the electric field is always

perpendicular to the direction of propagation, and the magnetic field has a longitudinal component. In TM modes, the magnetic field is always perpendicular to the direction of propagation, and the electric field has a longitudinal component. A mode is denoted as TE_{nm} or TM_{nm} , where a pair of indices n and m specifies the pattern of the mode field. The mode electric and magnetic fields can be represented as

$$\vec{E} = C\vec{e}, \quad (\text{A.10})$$

$$\vec{H} = \frac{C}{\eta}\vec{h}, \quad (\text{A.11})$$

where C is the mode coefficient (amplitude of the electric field measured in V/m), η is the free-space impedance, and \vec{e} and \vec{h} are the normalized mode electric and magnetic fields.

Below, we give mode field expressions for rectangular and cylindrical waveguides. The notation used here and throughout this work is largely based on notation used by Pozar [32]. Some formulas (e.g., mode attenuation constants) are reproduced from Collin [72] and Kraus [33].

A.2 Rectangular waveguide

Consider a rectangular waveguide with horizontal and vertical dimensions a and b , as shown in Figure A.1. The coordinate system used here is Cartesian (x, y, z) . The cutoff wave numbers g in

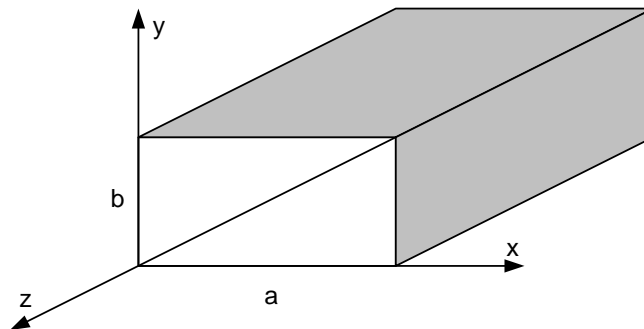


Figure A.1: Rectangular waveguide.

this waveguide are given by

$$g = \sqrt{\left(\frac{n\pi}{a}\right)^2 + \left(\frac{m\pi}{b}\right)^2}. \quad (\text{A.12})$$

Figure A.2 shows the cutoff frequencies of modes in a rectangular 2:1 waveguide ($a = 2b$). The horizontal axis is a unitless parameter ga .

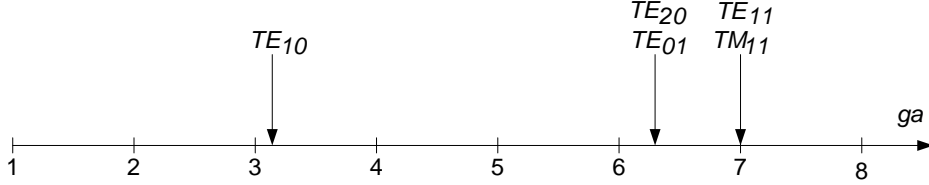


Figure A.2: Mode cutoff frequencies in a 2:1 rectangular waveguide.

For TE modes in a rectangular waveguide, both n and m cannot be simultaneously equal to zero. Normalized electric and magnetic field components of a TE mode are

$$\epsilon_x = \frac{jk}{g^2} \frac{m\pi}{b} \cos \frac{n\pi x}{a} \sin \frac{m\pi y}{b} e^{-\gamma z}, \quad (\text{A.13})$$

$$\epsilon_y = -\frac{jk}{g^2} \frac{n\pi}{a} \sin \frac{n\pi x}{a} \cos \frac{m\pi y}{b} e^{-\gamma z}, \quad (\text{A.14})$$

$$h_x = \frac{j\beta}{g^2} \frac{n\pi}{a} \sin \frac{n\pi x}{a} \cos \frac{m\pi y}{b} e^{-\gamma z}, \quad (\text{A.15})$$

$$h_y = \frac{j\beta}{g^2} \frac{m\pi}{b} \cos \frac{n\pi x}{a} \sin \frac{m\pi y}{b} e^{-\gamma z}, \quad (\text{A.16})$$

$$h_z = \cos \frac{n\pi x}{a} \cos \frac{m\pi y}{b} e^{-\gamma z}. \quad (\text{A.17})$$

For TM modes in a rectangular waveguide, neither n nor m can be equal to zero. Normalized electric and magnetic field components of a TM mode are

$$\epsilon_x = -\frac{j\beta}{g^2} \frac{n\pi}{a} \cos \frac{n\pi x}{a} \sin \frac{m\pi y}{b} e^{-\gamma z}, \quad (\text{A.18})$$

$$\epsilon_y = -\frac{j\beta}{g^2} \frac{m\pi}{b} \sin \frac{n\pi x}{a} \cos \frac{m\pi y}{b} e^{-\gamma z}, \quad (\text{A.19})$$

$$\epsilon_z = \sin \frac{n\pi x}{a} \sin \frac{m\pi y}{b} e^{-\gamma z}, \quad (\text{A.20})$$

$$h_x = \frac{jk}{g^2} \frac{m\pi}{b} \sin \frac{n\pi x}{a} \cos \frac{m\pi y}{b} e^{-\gamma z}, \quad (\text{A.21})$$

$$h_y = -\frac{j\omega k}{g^2} \frac{n\pi}{a} \cos \frac{n\pi x}{a} \sin \frac{m\pi y}{b} e^{-\gamma z}. \quad (\text{A.22})$$

The attenuation constant of a mode is

$$\alpha = \frac{2R_s k}{\eta b \beta} \times \begin{cases} \left(1 + \frac{b}{a}\right) \frac{\omega_c^2}{\omega^2} + \frac{b}{a} \left(\frac{\chi_m}{2} - \frac{\omega_c^2}{\omega^2}\right) \left(\frac{n^2 ab + m^2 a^2}{n^2 b^2 + m^2 a^2}\right) & \text{if } TE \\ \frac{n^2 b^3 + m^2 a^3}{n^2 b^2 a + m^2 a^3} & \text{if } TM \end{cases}, \quad (\text{A.23})$$

where χ_m is

$$\chi_m = \begin{cases} 1 & m = 0 \\ 2 & m > 0 \end{cases} = 1 + \text{sign}(m). \quad (\text{A.24})$$

The normalized time-average power carried by a mode is the same for TE and TM modes:

$$p = \frac{k\beta ab}{2\chi_n \chi_m g^2 \eta}. \quad (\text{A.25})$$

The characteristic wave impedance of a mode is

$$Z = \eta \frac{\epsilon_x}{h_y} = -\eta \frac{\epsilon_y}{h_x} = \eta \times \begin{cases} \frac{k}{\beta} & \text{if } TE \\ \frac{\beta}{k} & \text{if } TM \end{cases}. \quad (\text{A.26})$$

Figure A.3 shows the field structure of the first 18 modes of a 2:1 rectangular waveguide (courtesy Andrew Greenwood, University of Illinois at Urbana-Champaign). Plots shown in Figure A.3 are also given in [175].

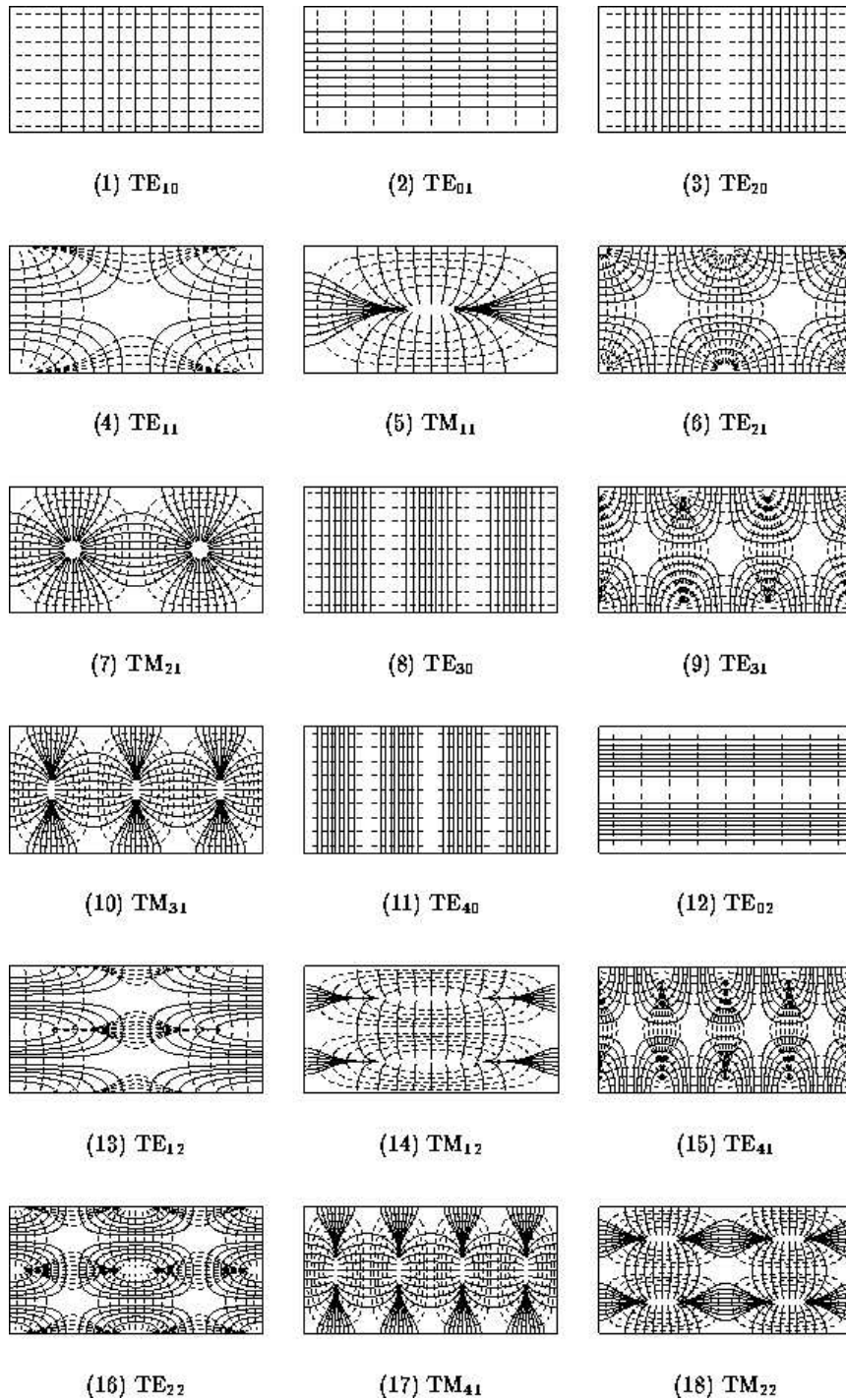


Figure A.3: First 18 modes of a 2:1 rectangular waveguide (courtesy Andrew Greenwood, University of Illinois at Urbana-Champaign).

A.3 Cylindrical waveguide

Consider a cylindrical waveguide with radius a , as shown in Figure A.4. The coordinate system used here is cylindrical (r, ϕ, z) . In this waveguide, the cutoff wave numbers are given by roots of

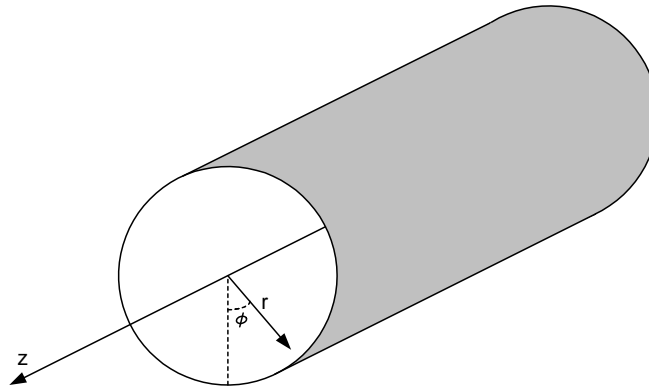


Figure A.4: Cylindrical waveguide.

the Bessel function of the first kind of order n $J_n(x)$ and its first derivative $J'_n(x)$:

$$g = \begin{cases} \frac{p'_{nm}}{a} & \text{if } TE \\ \frac{p_{nm}}{a} & \text{if } TM \end{cases}, \quad (\text{A.27})$$

where p'_{nm} and p_{nm} are the m -th nulls of equations $J'_n(x) = 0$ and $J_n(x) = 0$. Figure A.5 shows the cutoff frequencies of modes in a cylindrical waveguide. The horizontal axis is again a unitless parameter ga .

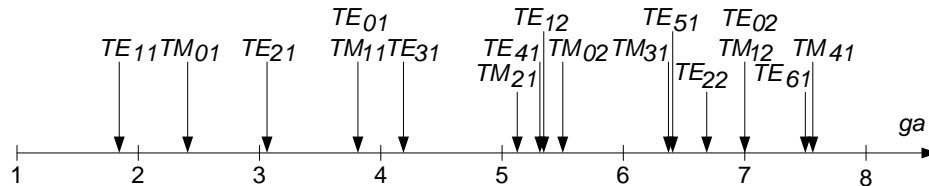


Figure A.5: Mode cutoff frequencies in a cylindrical waveguide.

The normalized electric and magnetic field components of a TE mode are

$$\epsilon_r = -\frac{jk n}{g^2 r} \cos(n\phi + a_{nm}) J_n(gr) e^{-\gamma z}, \quad (\text{A.28})$$

$$\epsilon_\phi = \frac{jk}{g} \sin(n\phi + a_{nm}) J'_n(gr) e^{-\gamma z}, \quad (\text{A.29})$$

$$h_r = -\frac{j\beta}{g} \sin(n\phi + a_{nm}) J'_n(gr) e^{-\gamma z}, \quad (\text{A.30})$$

$$h_\phi = -\frac{j\beta n}{g^2 r} \cos(n\phi + a_{nm}) J_n(gr) e^{-\gamma z}, \quad (\text{A.31})$$

$$h_z = \sin(n\phi + a_{nm}) J_n(gr) e^{-\gamma z}. \quad (\text{A.32})$$

Normalized electric and magnetic field components of a TM mode are

$$\epsilon_r = -\frac{j\beta}{g} \sin(n\phi + b_{nm}) J'_n(gr) e^{-\gamma z}, \quad (\text{A.33})$$

$$\epsilon_\phi = -\frac{j\beta n}{g^2 r} \cos(n\phi + b_{nm}) J_n(gr) e^{-\gamma z}, \quad (\text{A.34})$$

$$\epsilon_z = \sin(n\phi + b_{nm}) J_n(gr) e^{-\gamma z}, \quad (\text{A.35})$$

$$h_r = \frac{jk n}{g^2 r} \cos(n\phi + b_{nm}) J_n(gr) e^{-\gamma z}, \quad (\text{A.36})$$

$$h_\phi = -\frac{jk}{g} \sin(n\phi + b_{nm}) J'_n(gr) e^{-\gamma z}. \quad (\text{A.37})$$

The attenuation constant of a mode is

$$\alpha = \frac{R_s k}{\eta a \beta} \times \begin{cases} \frac{\omega_c^2}{\omega^2} + \frac{n^2}{(p'_{nm})^2 - n^2} & \text{if } TE \\ 1 & \text{if } TM \end{cases}. \quad (\text{A.38})$$

The normalized time-average power carried by a mode is

$$p = \frac{k\beta\pi}{4g^4\eta} \times \begin{cases} J_n^2(p'_{nm}) [(p'_{nm})^2 - n^2] & \text{if } TE \\ J_n'^2(p_{nm}) p_{nm}^2 & \text{if } TM \end{cases}. \quad (\text{A.39})$$

The characteristic wave impedance of a mode is

$$Z = \eta \frac{\epsilon_r}{h_\phi} = -\eta \frac{\epsilon_\phi}{h_r} = \eta \times \begin{cases} \frac{k}{\beta} & \text{if } TE \\ \frac{\beta}{k} & \text{if } TM \end{cases}. \quad (\text{A.40})$$

The field structure of the first 15 modes of a cylindrical waveguide is shown in Figure A.6 (courtesy Andrew Greenwood, University of Illinois at Urbana-Champaign). Plots shown in Figure A.6 are also given in [175].

A.4 Bessel function roots

The Bessel function of the first kind of order n can be written as

$$J_n(x) = \sum_{m=0}^{\infty} \frac{(-1)^m x^{n+2m}}{m!(n+m)!2^{n+2m}}. \quad (\text{A.41})$$

The first derivative of $J_n(x)$ can be calculated directly by differentiating the series given by Equation A.41:

$$J'_n(x) = \sum_{m=0}^{\infty} (n+2m) \frac{(-1)^m x^{n+2m-1}}{m!(n+m)!2^{n+2m}} = \frac{n}{x} J_n(x) + \sum_{m=1}^{\infty} 2m \frac{(-1)^m x^{n+2m-1}}{m!(n+m)!2^{n+2m}}. \quad (\text{A.42})$$

Using a new summation index $s = m - 1$ allows one to rewrite $J'_n(x)$ as

$$J'_n(x) = \frac{n}{x} J_n(x) + \sum_{s=0}^{\infty} \frac{(-1)^{s+1} x^{n+1+2s}}{s!(n+1+s)!2^{n+1+2s}}. \quad (\text{A.43})$$

Recognizing that the last term is also a Bessel function of the first kind of order n allows one to express $J'_n(x)$ in terms of $J_n(x)$ and $J_{n+1}(x)$ as

$$J'_n(x) = \frac{n}{x} J_n(x) - J_{n+1}(x). \quad (\text{A.44})$$

This formula is often used to calculate the derivatives of Bessel functions. Tables A.1 and A.2 list roots of $J'_n(x)$ and $J_n(x)$ used for calculating wave numbers of TE and TM modes in cylindrical waveguides.

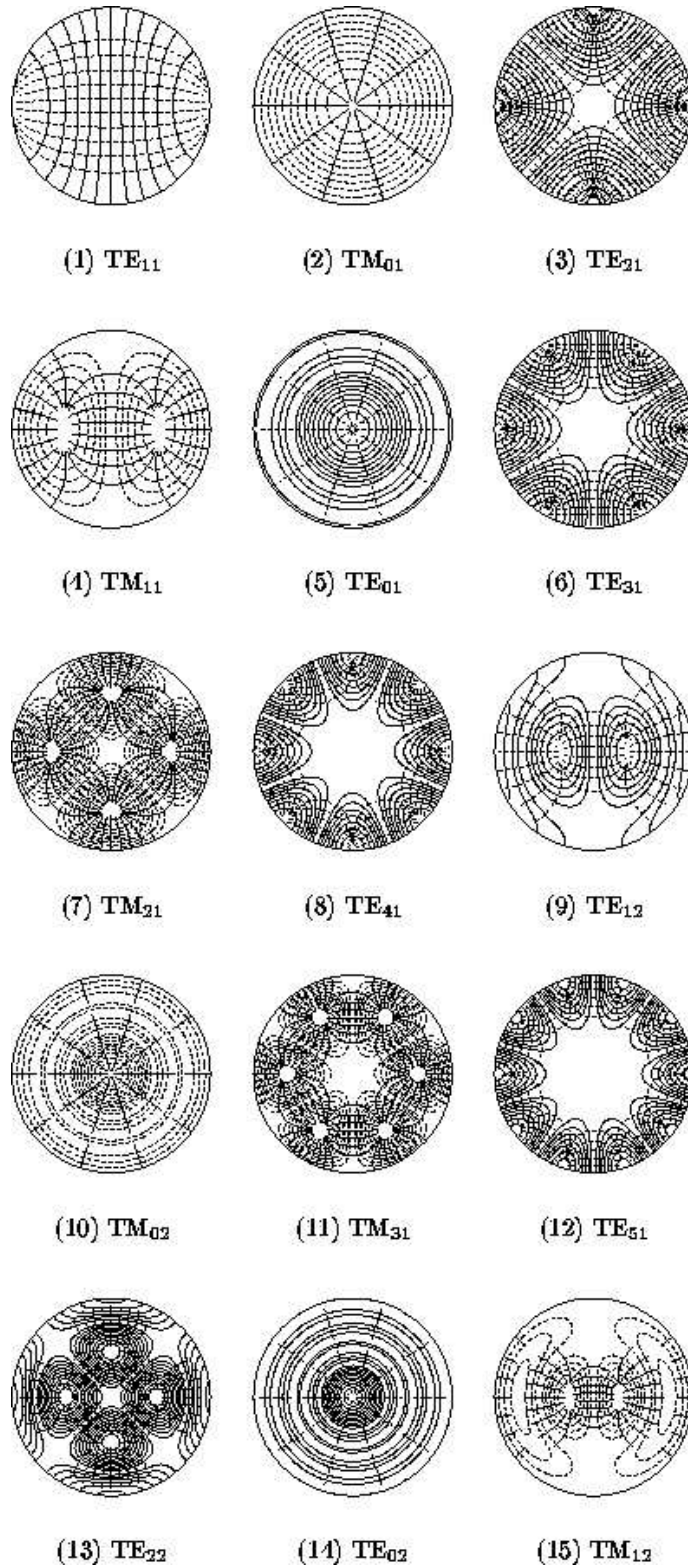


Figure A.6: First 15 modes of a cylindrical waveguide (courtesy Andrew Greenwood, University of Illinois at Urbana-Champaign).

n	p'_{n1}	p'_{n2}	p'_{n3}	p'_{n4}	p'_{n5}	p'_{n6}	p'_{n7}
0	3.832	7.016	10.173	13.324	16.471	19.616	22.760
1	1.841	5.331	8.536	11.706	14.864	18.016	21.164
2	3.054	6.706	9.969	13.170	16.348	19.513	22.672
3	4.201	8.015	11.346	14.586	17.789	20.972	24.145
4	5.318	9.282	12.682	15.964	19.196	22.401	25.590
5	6.416	10.520	13.987	17.313	20.576	23.804	27.010
6	7.501	11.735	15.268	18.637	21.932	25.184	28.410
7	8.578	12.932	16.529	19.942	23.268	26.545	29.791
8	9.647	14.116	17.774	21.229	24.587	27.889	31.155
9	10.711	15.287	19.005	22.501	25.891	29.219	32.505
10	11.771	16.448	20.223	23.761	27.182	30.535	33.842
11	12.826	17.600	21.431	25.009	28.461	31.838	35.167
12	13.879	18.745	22.629	26.246	29.729	33.131	36.481
13	14.928	19.883	23.819	27.474	30.987	34.415	37.784
14	15.975	21.015	25.002	28.694	32.237	35.689	39.079
15	17.020	22.142	26.178	29.907	33.478	36.954	40.365

Table A.1: Values of p'_{nm} for TE modes in a cylindrical waveguide

n	p_{n1}	p_{n2}	p_{n3}	p_{n4}	p_{n5}	p_{n6}	p_{n7}
0	2.405	5.520	8.654	11.792	14.931	18.071	21.212
1	3.832	7.016	10.173	13.324	16.471	19.616	22.760
2	5.136	8.417	11.620	14.796	17.960	21.117	24.270
3	6.380	9.761	13.015	16.223	19.409	22.583	25.748
4	7.588	11.065	14.373	17.616	20.827	24.019	27.199
5	8.771	12.339	15.700	18.980	22.218	25.430	28.627
6	9.936	13.589	17.004	20.321	23.586	26.820	30.034
7	11.086	14.821	18.288	21.642	24.935	28.191	31.423
8	12.225	16.038	19.555	22.945	26.267	29.546	32.796
9	13.354	17.241	20.807	24.234	27.584	30.885	34.154
10	14.476	18.433	22.047	25.509	28.887	32.212	35.500
11	15.590	19.616	23.276	26.773	30.179	33.526	36.834
12	16.698	20.790	24.495	28.027	31.460	34.830	38.156
13	17.801	21.956	25.705	29.271	32.731	36.124	39.469
14	18.900	23.116	26.907	30.506	33.993	37.408	40.773
15	19.994	24.269	28.102	31.733	35.247	38.684	42.068

Table A.2: Values of p_{nm} for TM modes in a cylindrical waveguide

Appendix B

Design tool

An interactive software tool "Duct Explorer" was developed in Matlab 6 to model the properties of the HVAC duct channel. The program has an easy graphical user interface and allows one to compute channel parameters for various duct and antenna configurations. The structure of the Duct Explorer is shown in Figure B.1.

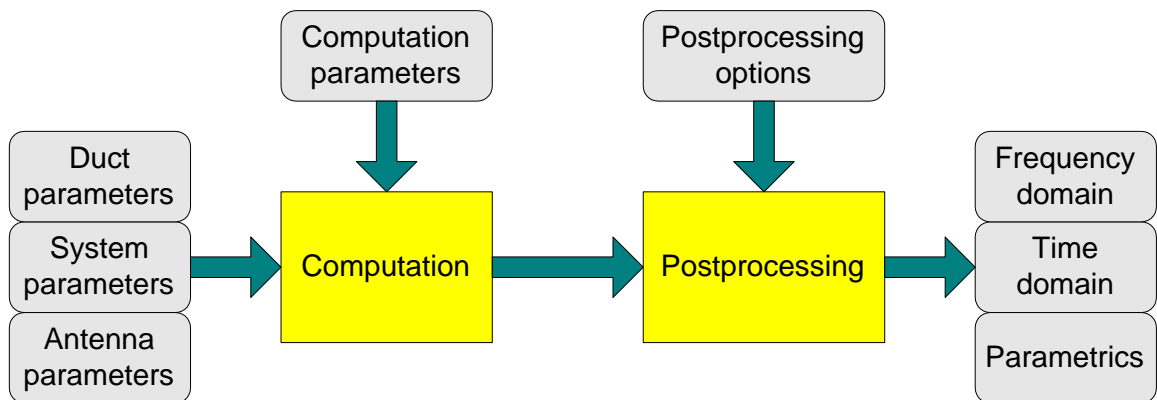


Figure B.1: The program structure of the Duct Explorer.

Prior to starting computations, the following input parameters must be supplied to the program:

1. Duct parameters.
 - Type (cylindrical or rectangular).

- Size (diameter or width and height).
- Wall conductivity.

2. Antenna parameters.

- Type (monopole, dipole, or array).
- Size (arm length, number of elements, element spacing).
- Position (distance to the wall, curvature radius).

3. System parameters.

- Transmitter-receiver separation distance.
- Distance to the ends.
- Reflection coefficients of the ends.
- Transmitter and receiver impedances.
- Whether the system includes bends or tapers.

4. Computation parameters.

- Frequency band of interest (start frequency, stop frequency, number of points).
- Parametric computations (what is the parameter, start value, stop value, number of points).
- Threshold for computing the RMS delay spread.

After the program finishes computations, a number of postprocessing options can be chosen:

1. Frequency domain.

- Magnitude frequency response.
- Antenna impedance.
- Mode distribution.

- Frequency autocorrelation function.
2. Time domain.
 - Power delay profile.
 3. Parametrics.
 - Attenuation, parameters \mathcal{P} and \mathcal{T} , or RMS delay spread vs. chosen parameter.
 - Spatial autocorrelation function.

Postprocessing options also allow the user to compare theoretical results with the specified experimental data file, which is selected by a built-in file browser. When frequency domain post-processing is performed, the average attenuation in the band for both theoretical and experimental responses is computed and posted into the output window. When time domain post-processing is performed, the RMS delay spread for both theoretical and experimental responses is computed and posted into the output window. The graphical user interface of the program is shown in Figure B.2.

Duct Explorer

<p>Duct</p> <p>type: cylindrical</p> <p>diameter: 0.305</p> <p>width: 0.61</p> <p>height: 0.305</p> <p>conductivity: 1e6 (S/m)</p>	<p>Antenna</p> <p>type: monopole</p> <p>arm length: 0.035</p> <p>dist. to wall: 0.305</p> <p>dipole radius: 0.05</p> <p>elements: 5</p> <p>spacing: 0.13</p>	<p style="text-align: center;">System</p> <table style="width: 100%; border-collapse: collapse;"> <tr> <td style="width: 50%;">Distances</td> <td style="width: 50%;">Terminations</td> </tr> <tr> <td>transmitter -- receiver: 4.58</td> <td>left load: 0</td> </tr> <tr> <td>left load -- transmitter: 0.25</td> <td>right load: 0</td> </tr> <tr> <td>receiver -- right load: 10.39</td> <td></td> </tr> </table> <div style="text-align: center; margin: 10px 0;"> </div>		Distances	Terminations	transmitter -- receiver: 4.58	left load: 0	left load -- transmitter: 0.25	right load: 0	receiver -- right load: 10.39		
Distances	Terminations											
transmitter -- receiver: 4.58	left load: 0											
left load -- transmitter: 0.25	right load: 0											
receiver -- right load: 10.39												
<p>Computation</p> <p>Frequency</p> <p>start: 2.4 GHz points</p> <p>stop: 2.5 GHz 101</p> <p>Parametric</p> <p>start: 1 points</p> <p>stop: 2 10</p> <p>parameter: none</p> <p>RMS threshold: dB</p> <p><input type="checkbox"/> mode content</p>	<p style="text-align: center;">Postprocessing</p> <table style="width: 100%; border-collapse: collapse;"> <tr> <td style="width: 30%;">Theory (mag)</td> <td style="border: 1px solid black; padding: 2px;">magnitude.prn</td> </tr> <tr> <td>Theory (pha)</td> <td style="border: 1px solid black; padding: 2px;">phase.prn</td> </tr> <tr> <td>Data (mag)</td> <td style="border: 1px solid black; padding: 2px;">data/data_mag.prn</td> </tr> <tr> <td>Data (pha)</td> <td style="border: 1px solid black; padding: 2px;">data/data_pha.prn</td> </tr> </table> <p>Frequency</p> <p><input checked="" type="checkbox"/> magnitude compare <input type="checkbox"/> power compare</p> <p><input type="checkbox"/> impedance</p> <p><input type="checkbox"/> mode distribution</p> <p><input type="checkbox"/> autocorrelate</p> <p style="text-align: right;">Time</p> <p style="text-align: right;"><input type="checkbox"/> autocorrelate</p> <p style="text-align: right;">Parameters</p> <p style="text-align: right;">none vs. parameter</p> <p style="text-align: right;"><input type="checkbox"/> autocorrelate</p>		Theory (mag)	magnitude.prn	Theory (pha)	phase.prn	Data (mag)	data/data_mag.prn	Data (pha)	data/data_pha.prn	<p>Outputs</p> <p>Average attenuation (dB)</p> <p> Theory</p> <p> Data</p> <p>RMS delay spread (ns)</p> <p> Theory</p> <p> Data</p>	<p>Controls</p> <p style="text-align: center;">Compute</p> <p style="text-align: center;">Plot</p> <p style="text-align: center;">units</p> <p style="text-align: center;">m</p>
Theory (mag)	magnitude.prn											
Theory (pha)	phase.prn											
Data (mag)	data/data_mag.prn											
Data (pha)	data/data_pha.prn											

Figure B.2: The graphical user interface of the Duct Explorer

Bibliography

- [1] D. F. Bantz and F. J. Bauchot, “Wireless LAN design alternatives,” *IEEE Network*, vol. 8, no. 2, pp. 43–53, March-April 1994.
- [2] A. Hills, “Large-scale wireless LAN design,” *IEEE Communications Magazine*, vol. 39, no. 11, pp. 98–107, November 2001.
- [3] W. Gibbs, “The network in every room,” *Scientific American*, pp. 38–43, February 2002.
- [4] D. Clark, “Powerline communications: finally ready for prime time?,” *IEEE Internet Computing*, vol. 2, no. 1, pp. 10–11, January-February 1998.
- [5] A. Broadbridge, “Power line modems and networks,” *Second IEE National Conference on Telecommunications*, pp. 294–296, 1989.
- [6] J. Newbury and W. Miller, “Potential communication services using power line carriers and broadband integrated services digital network,” *IEEE Transactions on Power Delivery*, vol. 14, no. 4, pp. 1197–1201, October 1999.
- [7] “Plug and play at home,” *Economist: Science Technology Quarterly*, p. 8, March 14 2002.
- [8] E. H. Frank and J. Holloway, “Connecting the home with a phone line network chip set,” *IEEE Micro*, vol. 20, no. 2, pp. 27–37, 39, March-April 2000.
- [9] D. Liu, E. Flint, B. Gaucher, and Y. Kwark, “Wide band home phone line characterization,” *IEEE Transactions on Consumer Electronics*, vol. 46, no. 1, pp. 76–86, February 2000.

- [10] D. D. Stancil and C. P. Diehl, "Wireless signal distribution in a building HVAC system," *U. S. Patent 5,994,984*, November 30 1999.
- [11] C. P. Diehl, B. E. Henty, N. Kanodia, and D. D. Stancil, "Wireless RF distribution in buildings using heating and ventilation ducts," *Proceedings of 8th Virginia Tech/MPRG Symposium on Wireless Personal Communications*, June 1998, Also included in the volume, *Wireless Personal Communications: Emerging Technologies for Enhanced Communications*, W. H. Tranter, T.S. Rappaport, B. D. Woerner and J. H. Reed, Eds., pp. 61-70 (Kluwer, 1999).
- [12] D. D. Stancil, O. K. Tonguz, A. Xhafa, A. Cepni, P. Nikitin, and D. Brodtkorb, "High-speed internet access via HVAC ducts: a new approach," *Proceedings of the IEEE Global Telecommunications Conference (GLOBECOM'01)*, vol. 6, pp. 3604–3607, San Antonio, TX, November 2001.
- [13] H. Goldstein, "Radio contact in high-rises can quit on firefighters," *IEEE Spectrum*, vol. 39, no. 4, pp. 2002, April 2000.
- [14] Kwok-Wai Cheung, J. H.-M. Sau, and R. D. Murch, "A new empirical model for indoor propagation prediction," *IEEE Transactions on Vehicular Technology*, vol. 47, no. 3, pp. 996–1001, August 1998.
- [15] H. Hashemi and D. Tholl, "Statistical modeling and simulation of the RMS delay spread of indoor radio propagation channels," *IEEE Transactions on Vehicular Technology*, vol. 43, no. 1, pp. 110–120, February 1994.
- [16] J. Walfisch and H. L. Bertoni, "A theoretical model of UHF propagation in urban environments," *IEEE Transactions on Antennas and Propagation*, vol. 36, no. 12, pp. 1788–1796, December 1988.
- [17] T. S. Rappaport, "Indoor radio communications for factories of the future," *IEEE Communications Magazine*, vol. 27, no. 5, pp. 15–24, May 1989.

- [18] H. Hashemi, "The indoor radio propagation channel," *Proceedings of the IEEE*, vol. 81, no. 7, pp. 943–968, July 1993.
- [19] H. Hashemi, "Impulse response modeling of indoor radio propagation channels," *IEEE Journal on Selected Areas in Communications*, vol. 11, no. 7, pp. 967–978, September 1993.
- [20] S. Y. Tan and H. S. Tan, "Modelling and measurements of channel impulse response for an indoor wireless communication system," *IEE Proceedings*, vol. 142, no. 5, pp. 405–410, October 1995.
- [21] L. Dossi, G. Tartara, and F. Tallone, "Statistical analysis of measured impulse response functions of 2.0 GHz indoor radio channels," *IEEE Journal on Selected Areas in Communications*, vol. 14, no. 3, pp. 405–410, April 1996.
- [22] J. D. Parsons, *The Mobile Radio Propagation Channel.*, John Wiley & Sons, 1996.
- [23] T. Kurner, D. J. Cichon, and W. Wiesbeck, "Concepts and results for 3D digital terrain-based wave propagation models: An overview," *IEEE Journal on Selected Areas in Communications*, vol. 11, no. 7, pp. 1002–1012, September 1993.
- [24] T. Bierhoff, A. Wallrabenstein, A. Himmler, E. Griese, and G. Mrozynski, "Ray tracing technique and its verification for the analysis of highly multimode optical waveguides with rough surfaces," *IEEE Transactions on Magnetics*, vol. 37, no. 5, pp. 3307–3310, September 2001.
- [25] L. Nuno, J. V. Balbastre, and H. Castane, "Analysis of general lossy inhomogeneous and anisotropic waveguides by the finite-element method (FEM) using edge elements," *IEEE Transactions on Microwave Theory and Techniques*, vol. 45, no. 3, pp. 446–449, March 1997.
- [26] A.V. Popov and N.Y.Zhu, "Curved oversized EM waveguides: Adiabatic modes and parabolic equation," *Day on Diffraction, International Seminar*, pp. 220–231, 1999.

- [27] A. V. Popov and Y. Z. Ning, "Modeling radio wave propagation in tunnels with a vectorial parabolic equation," *IEEE Transactions on Antennas and Propagation*, vol. 48, no. 9, pp. 1403–1412, September 2000.
- [28] S. R. Seshadri, "Ideal normal mode theory of a serpentine cylindrical waveguide," *IEE Proceedings on Microwaves, Antennas and Propagation*, vol. 136, no. 6, pp. 480–486, December 1989.
- [29] C. Boulas, S. Valette, E. Parrens, and A. Fournier, "Low loss multimode waveguides on silicon substrate," *Electronics Letters*, vol. 28, no. 17, pp. 1648–1649, August 1992.
- [30] R. Yoshimura, M. Hikita, S. Tomaru, and S. Imamura, "Very low loss multimode polymeric optical waveguides," *Electronics Letters*, vol. 33, no. 14, pp. 1240–1242, July 1997.
- [31] M. Oz and R. R. Krchnavek, "Power loss analysis at a step discontinuity of a multimode optical waveguide," *Journal of Lightwave Technology*, vol. 16, no. 12, pp. 2451–2457, December 1998.
- [32] D. M. Pozar, *Microwave Engineering*, John Wiley & Sons, Inc., 1998.
- [33] J. D. Kraus, *Electromagnetics*, McGraw-Hill Inc., 1992.
- [34] S. E. Miller, "Waveguide as a communication medium," *The Bell System Technical Journal*, vol. 33, no. 6, pp. 1209–1265, 1954.
- [35] S. E. Miller and A. C. Beck, "Low-loss waveguide transmission," *Proceedings of the IRE*, vol. 41, no. 3, pp. 348–358, 1953.
- [36] E. A. J. Marcatili and R. A. Schmeltzer, "Hollow metallic and dielectric waveguides for long distance optical transmission and lasers," *The Bell System Technical Journal*, pp. 1783–1809, July 1964.
- [37] R. Vacek, "Electromagnetic wave propagation in general multimode waveguide structures exhibiting simultaneously attenuation, dispersion and coupling phenomena," *Proceedings of*

- the SBMO/IEEE MTT-S Microwave and Optoelectronics Conference*, vol. 2, pp. 599–605, 1997.
- [38] C. D. Nantista and S. G. Tantawi, “Overmoded rectangular waveguide components for a multi-moded RF power distribution system,” *Proceedings of EPAC*, pp. 318–320, 2000.
- [39] W. A. Imbriale, T. Y. Otoshi, and C. Yeh, “Power loss for multimode waveguides and its application to beam-waveguide system,” *IEEE Transactions on Microwave Theory and Techniques*, vol. 46, no. 5, pp. 523–529, May 1998.
- [40] S. G. Tantawi, N. M. Kroll, and K. Fant, “RF components using over-moded rectangular waveguides for the next linear collider multi-moded delay line RF distribution system,” *Proceedings of the Particle Accelerator Conference*, vol. 2, pp. 1435–1437, 1999.
- [41] F. L. Whetten and C. A. Balanis, “Meandering long slot leaky-wave waveguide-antennas,” *IEEE Transactions on Antennas and Propagation*, vol. 39, no. 11, pp. 1553–1560, November 1991.
- [42] P. Pannier, L. Kadri, C. Seguinot, P. Kennis, and F. Huret, “Accurate and efficient numerical method for the analysis of multimode waveguide discontinuities,” *IEEE Transactions on Microwave Theory and Techniques*, vol. 48, no. 2, pp. 295–304, February 2000.
- [43] Y. P. Zhang and Y. Hwang, “Theory of the radio-wave propagation in railway tunnels,” *IEEE Transactions on Vehicular Technology*, vol. 47, no. 3, pp. 1027–1036, August 1998.
- [44] P. Delogne, “EM propagation in tunnels,” *IEEE Transactions on Antennas and Propagation*, vol. 39, no. 3, pp. 401–406, March 1991.
- [45] A.G. Emslie, R.L. Lagace, and P.F. Strong, “Theory of the propagation of UHF radio waves in coal mine tunnels,” *IEEE Transactions on Antennas and Propagation*, vol. AP-23, no. 2, pp. 192–205, March 1975.

- [46] S.F. Mahmoud and J. R. Wait, "Guided electromagnetic waves in a curved rectangular mine tunnel," *Radio Science*, vol. 9, no. 5, pp. 567–572, May 1974.
- [47] Y. Yamaguchi, T. Abe, T. Sekiguchi, and J. Chiba, "Attenuation constants of UHF radio waves in arched tunnels," *IEEE Transactions on Microwave Theory and Techniques*, vol. MT-33, no. 8, pp. 714–718, August 1985.
- [48] A. Coraiola and B. Sturani, "Using a pair of phased antennas to improve UHF reception/transmission in tunnels," *IEEE Antennas and Propagation Magazine*, vol. 42, no. 5, October 2000.
- [49] C. L. Holloway, D. A. Hill, R. A. Dalke, and G. A. Hufford, "Radio wave propagation characteristics in lossy circular waveguides such as tunnels, mine shafts, and boreholes," *IEEE Transactions on Antennas and Propagation*, vol. 48, no. 9, pp. 1354–1366, September 2000.
- [50] J.S. Lamminmaki and J. J. A. Lempiainen, "Radio propagation characteristics in curved tunnels," *IEE Proceedings on Microwaves, Antennas and Propagation*, vol. 145, pp. 327–331, August 1998.
- [51] Y.P. Zhang, Y. Hwang, and R. G. Kouyomjian, "Ray-optical prediction of radio-wave propagation characteristics in tunnel environments - part 1: Theory, part 2: Analysis and measurements," *IEEE Transactions on Antennas and Propagation*, vol. 46, no. 9, pp. 1328–1345, September 1998.
- [52] S.F. Mahmoud and J. R. Wait, "Geometrical optical approach for electromagnetic wave propagation in rectangular mine tunnels," *Radio Science*, vol. 9, no. 12, pp. 1147–1158, December 1974.
- [53] Y. Ohtaki, M. Sengoku, K. Sakurai, Y. Yamaguchi, and T. Abe, "Propagation characteristics in open-groove waveguides surrounded by rough walls," *IEEE Transactions on Electromagnetic Compatibility*, vol. 32, no. 3, pp. 177–184, August 1990.

- [54] P. MARIage, M. Lienard, and P. Degauque, "Theoretical and experimental approach of the propagation of high frequency waves in road tunnels," *IEEE Transactions on Antennas and Propagation*, vol. 42, no. 1, pp. 75–81, January 1994.
- [55] M. Lienard, S. Betrencourt, and P. Degauque, "Theoretical and experimental approach of the propagation at 2.5 GHz and 10 GHz in straight and curved tunnels," *IEEE Vehicular Technology Conference*, vol. 4, pp. 2268–2271, September 1999.
- [56] M. Lienard and P. Degauque, "Propagation in wide tunnels at 2 GHz: A statistical analysis," *IEEE Transactions on Vehicular Technology*, vol. 47, no. 4, pp. 1322–1328, November 1998.
- [57] S. Betrencourt, M. Lienard, and P. Degauque, "Mobile communication in road tunnels: Influence of the traffic conditions on the channel statistics," *10th Mediterranean Electrotechnical Conference*, pp. 432–435, 2000.
- [58] J. Lee and H. L. Bertoni, "Coupling at L, T and cross junctions in tunnels and urban street canyons," *IEEE Vehicular Technology Conference*, vol. 1, pp. 274–278, 2001.
- [59] O. Ercan and L. Sevgi, "The PE solution of natural waveguides in atmosphere: ducts and elevated ducts," *Seventh Mediterranean Electrotechnical Conference*, pp. 394–397, 1994.
- [60] M. L. Skolnik, *Introduction to Radar Systems*, pp. 502–518, McGraw-Hill Inc., 2000.
- [61] A. S. Kulesa, G. S. Woods, B. Piper, and M. L. Heron, "Line-of-sight EM propagation experiment at 10.25 GHz in the tropical ocean evaporation duct," *IEE Proceedings on Microwaves, Antennas and Propagation*, vol. 145, no. 1, pp. 65–69, February 1998.
- [62] A. G. Bessios, "Compound compensation strategies for wireless data communications over the multimodal acoustic ocean waveguide," *IEEE Journal of Oceanic Engineering*, vol. 21, no. 2, pp. 167–180, April 1996.

- [63] Jin-Yuan Liu and Chen-Fen Huang, "Effect of a transition density layer on wave propagation in a seismo-acoustic ocean waveguide," *Proceedings of the International Symposium on Underwater Technology*, pp. 47–52, 1998.
- [64] M. Nardin, F. Glangeaud, J. M. Vanpe, R. Ancey, P. Pignot, L. Royer, and S. Gafet, "Ocean waveguide effects on acoustic and seismic ULF propagation," *OCEANS MTS/IEEE Conference Proceedings*, vol. 1, pp. 586–591, 1997.
- [65] A. Ittipiboon and L. Shafai, "Probe mutual impedance in a rectangular waveguide," *IEEE Transactions on Microwave Theory and Techniques*, vol. 33, pp. 327–335, April 1985.
- [66] B. Wang, "Mutual impedance between probes in a waveguide," *IEEE Transactions on Microwave Theory and Techniques*, vol. 36, no. 1, pp. 53–60, January 1988.
- [67] B. Wang, "Mutual impedance between probes in a circular waveguide," *IEEE Transactions on Microwave Theory and Techniques*, vol. 37, no. 6, pp. 1006–1012, June 1989.
- [68] L. W. Li, P. S. Kooi, M. S. Leong, and T. S. Yeo, "Full-wave analysis of antenna radiation in a rectangular waveguide with discontinuity. II. probe mutual impedance," *Proceedings of the IEEE Conference on Communication Systems*, vol. 2, pp. 464–468, 1994.
- [69] L. W. Li, P. S. Kooi, M. S. Leong, and T. S. Yeo, "Mutual impedance of two probes located in two different waveguide regions separated by a homogeneous dielectric slab: fullwave analysis," *IEE Transactions on Microwaves, Antennas and Propagation*, vol. 144, no. 5, pp. 329–336, October 1997.
- [70] Y. Huang, "Current distribution along a probe in waveguide," *IEEE Antennas and Propagation Society International Symposium*, vol. 1, pp. 513–516, 1990.
- [71] J.-F. Mao and O. Wing, "Time-domain transmission matrix of lossy transmission lines," *IEEE Microwave and Guided Wave Letters*, vol. 8, no. 2, pp. 90–92, February 1998.
- [72] R. E. Collin, *Field Theory of Guided Waves*, IEEE Press, 1990.

- [73] G. F. Edelmann, W. S. Hodgkiss, S. Kim, W. A. Kuperman, H. C. Song, and T. Akal, "Underwater acoustic communication using time reversal," *OCEANS MTS/IEEE Conference and Exhibition*, vol. 4, pp. 2231–2235, 2001.
- [74] C. G. Montgomery, R. H. Dicke, and E.M. Parcell, *Principles of Microwave Circuits*, vol. 8 of *MIT Rad. Lab.*, McGraw-Hill, 1948.
- [75] H. Cox, Hung Lai, and M. Hirano, "Reciprocity based channel compensation for wideband communications in a multipath environment," *Conference Record of The Twenty-Seventh Asilomar Conference on Signals, Systems and Computers*, vol. 1, pp. 593–597, 1993.
- [76] C. Ozzaim and C. M. Butler, "Coupling to a probe in a metal can by an electric dipole," *IEEE International Symposium of Antennas and Propagation Society*, vol. 2, pp. 838–841, 1999.
- [77] J. P. Karst and H. Garbe, "Characterization of loaded TEM-waveguides using time-domain reflectometry," *IEEE International Symposium on Electromagnetic Compatibility*, , no. 1, pp. 127–132, 1999.
- [78] M. Nakazawa, H. Kubota, A. Sahara, and K. Tamura, "Time-domain ABCD matrix formalism for laser mode-locking and optical pulse transmission," *IEEE Journal of Quantum Electronics*, vol. 34, no. 7, pp. 1075–1081, July 1998.
- [79] Hsue Ching-Wen Hsue and Pan Te-Wen, "Reconstruction of nonuniform transmission lines from time-domain reflectometry," *IEEE Transactions on Microwave Theory and Techniques*, vol. 45, no. 1, pp. 32–38, January 1997.
- [80] S. D. Corey and A. T. Yang, "Interconnect characterization using time-domain reflectometry," *IEEE Transactions on Microwave Theory and Techniques*, vol. 43, no. 9, pp. 2151–2156, September 1995.

- [81] P. V. Nikitin, D. D. Stancil, A. G. Cepni, O. K. Tonguz, A. E. Xhafa, and D. Brodtkorb, "Propagation model for the HVAC duct as a communication channel," *IEEE Transactions on Antennas and Propagation*, To appear in May, 2003.
- [82] N. Marcuvitz, *Waveguide Handbook*, vol. 10 of *MIT Rad. Lab.*, McGraw-Hill, 1948.
- [83] N. Marchand, *Ultrahigh Frequency Transmission and Radiation*, John Wiley & Sons, 1947.
- [84] L. Lewin, "A contribution to the theory of probes in waveguide," *IEE Proceedings*, vol. 105, pp. 109–116, October 1958.
- [85] D. V. Otto, "The admittance of cylindrical antennas driven from a coaxial line," *Radio Science*, vol. 2, no. 9, pp. 1031–1042, September 1967.
- [86] A. G. Williamson and D. V. Otto, "Cylindrical antenna in a rectangular waveguide driven from a coaxial line," *IEE Electronics Letters*, vol. 9, no. 10, pp. 545–547, November 1972.
- [87] A. G. Williamson and D. V. Otto, "Coaxially fed hollow cylindrical monopole in a rectangular waveguide," *IEE Electronics Letters*, vol. 9, no. 10, pp. 218–220, May 1973.
- [88] A. G. Williamson, "Analysis and modeling of a coaxial-line/rectangular-waveguide junction," *IEE Proceedings*, vol. 129, no. 5, pp. 262–270, October 1982.
- [89] A. G. Williamson, "Coaxially fed hollow probe in a rectangular waveguide," *IEE Proceedings*, vol. 132, no. 5, pp. 273–285, August 1985.
- [90] R. B. Keam and A. G. Williamson, "Analysis of coaxial-line/rectangular waveguide junction with dielectrically sheathed probe," *Electronics Letters*, vol. 28, no. 3, pp. 240–241, January 1992.
- [91] J. M. Rollins and J. M. Jarem, "The input impedance of a hollow-probe fed, semi-infinite rectangular waveguide," *IEEE Transactions on Microwave Theory and Techniques*, vol. 37, no. 7, pp. 1144–1146, July 1989.

- [92] J. M. Jarem, "A method of moments analysis and a finite-difference time-domain analysis of a probe-sleeve fed rectangular cavity," *IEEE Transactions on Microwave Theory and Techniques*, vol. 39, no. 3, pp. 444–451, March 1991.
- [93] J. M. Jarem, "Analysis of a probe-metallic sleeve feed system for a rectangular waveguide," *IEEE Antennas and Propagation Society International Symposium*, vol. 2, pp. 942–945, 1989.
- [94] J. F. Liang, H. C. Chang, and K. A. Zaki, "Coaxial probe modeling in waveguides and cavities," *IEEE Transactions on Microwave Theory and Techniques*, vol. 40, no. 12, pp. 2172–2180, December 1992.
- [95] W. S. Lee and E. K. Yung, "The input impedance of a coaxial line fed probe in a cylindrical waveguide," *IEEE Transactions on Microwave Theory and Techniques*, vol. 42, no. 8, pp. 1468–1473, August 1994.
- [96] H. J. Eom, Y. H. Cho, and M. S. Kwon, "Monopole antenna radiation into a parallel-plate waveguide," *IEEE Transactions on Antennas and Propagation*, vol. 48, no. 7, pp. 1142–1144, July 2000.
- [97] H. A. N. Hejase, H. L. Duncan, K. Naishadham, H. Gangl, C. Trad, and A. Hejase, "Characteristics of a thin-wire circular loop antenna in a parallel-plate waveguide," *Proceedings of Twenty-Third Southeastern Symposium on System Theory*, pp. 414–418, 1991.
- [98] R. Jin, J. Hirokawa, and M. Ando, "Accelerant method for green's function of horizontal dipole in parallel plate waveguide," *IEE Transactions on Microwaves, Antennas and Propagation*, vol. 145, no. 5, pp. 430–432, October 1998.
- [99] A. R. Adams, R. D. Pollard, and C. M. Snowden, "A method-of-moments study of strip dipole antennas in rectangular waveguide," *IEEE Transactions on Microwave Theory and Techniques*, vol. 45, no. 10, pp. 1756–1766, October 1997.

- [100] A. E. Gera, "Linking resistance and reactance via Hilbert transforms," *Proceedings of Electrical and Electronics Engineers in Israel*, pp. 141–144, 1991.
- [101] S. M. Narayana, G. Rao, R. Adve, T. K. Sarkar, V. C. Vannicola, M. C. Wicks, and S. A. Scott, "Interpolation/extrapolation of frequency domain responses using the Hilbert transform," *IEEE Transactions on Microwave Theory and Techniques*, vol. 44, no. 10, pp. 1621–1627, October 1996.
- [102] R. W. Donaldson, B. P. Donaldson, M. Fattouche, "In-building wireless radio channel characterization based on energy measurements and the Hilbert transform," *Proceedings of the IEEE Communications, Computers, and Signal Processing Conference*, pp. 224–229, 1995.
- [103] O. M. Ramahi and R. Mittra, "Design of a matching network for an HF antenna using the real frequency method," *IEEE Transactions on Antennas and Propagation*, vol. 37, no. 4, pp. 506–509, April 1989.
- [104] M. I. Petelin, "Mode selection in high power microwave sources," *IEEE Transactions on Electron Devices*, vol. 48, no. 1, pp. 129–133, January 2001.
- [105] D. H. Roper and J. M. Baird, "Analysis of overmoded waveguides using the finite-difference time domain method," *IEEE MTT-S International Microwave Symposium Digest*, vol. 1, pp. 401–404, 1992.
- [106] J. M. Baird, D. H. Roper, and R. W. Grow, "Surface array waveguide mode analyzer," *IEEE MTT-S International Microwave Symposium Digest*, vol. 1, pp. 137–140, 1992.
- [107] B. Tomasic and A. Hessel, "Linear array of coaxially fed monopole elements in a parallel plate waveguide. I. Theory," *IEEE Transactions on Antennas and Propagation*, vol. 36, no. 4, pp. 449–462, April 1988.

- [108] B. Tomasic and A. Hessel, "Linear array of coaxially fed monopole elements in a parallel plate waveguide. II. Experiment," *IEEE Transactions on Antennas and Propagation*, vol. 36, no. 4, pp. 463–467, April 1988.
- [109] V. V. Stepanov, "Using of multielement excitation for improvement of uniformity of microwave energy distribution in partly filled rectangular microwave chamber," *9th International Crimean Microwave Conference*, pp. 418–419, 1999.
- [110] M. Lienard, J. Baudet, D. Degardin, and P. Degauque, "Capacity of multi-antenna array systems in tunnel environment," *IEEE Vehicular Technology Conference*, vol. 2, pp. 552–555, 2002.
- [111] K. Demarest, R. Plumb, and Z. Huang, "Modeling baluns with the method of moments," *IEEE Transactions on Antennas and Propagation*, vol. 42, no. 8, pp. 1195–1198, August 1994.
- [112] C. Icheln and P. Vainikainen, "Dual-frequency balun to decrease influence of rf feed cables in small antenna measurements," *Electronics Letters*, vol. 21, no. 12, pp. 1760–1761, October 2000.
- [113] "<http://www.univie.ac.at/future.media/moe/onlinewerkzeuge.html>," .
- [114] D. A. Frickey, "Conversions between S, Z, Y, H, ABCD, and T parameters which are valid for complex source and load impedances," *IEEE Transactions on Microwave Theory and Techniques*, vol. 42, no. 2, pp. 205–211, February 1994.
- [115] R. B. Marks and D. F. Williams, "Comments on "conversions between S, Z, Y, h, ABCD, and T parameters which are valid for complex source and load impedances"," *IEEE Transactions on Microwave Theory and Techniques*, vol. 43, no. 4, pp. 914–915, April 1995.
- [116] H.-W. Glock and U. van Rienen, "An iterative algorithm to evaluate multimodal S-parameter measurements," *IEEE Transactions on Magnetics*, vol. 36, no. 4, pp. 1841–1845, July 2000.

- [117] H.-W. Glock, F. Marhauser, P. Hulsman, M. Kurz, and H. Klein, "Analysis of HOM interaction between cavities by multimodal s-parameter measurements," *Proceedings of the 1997 Particle Accelerator Conference*, vol. 1, no. 1, pp. 521–523, 1997.
- [118] J. Hong, W. Huang, and T. Makino, "On the transfer matrix method for distributed-feedback waveguide devices," *Journal of Lightwave Technology*, vol. 10, no. 12, pp. 1860–1868, December 1992.
- [119] W. Huang and J. Hong, "A transfer matrix approach based on local normal modes for coupled waveguides with periodic perturbations," *Journal of Lightwave Technology*, vol. 10, no. 10, pp. 1367–1375, October 1992.
- [120] Joong-Ho Kim and M. Swaminathan, "Modeling of irregular shaped power distribution planes using transmission matrix method," *IEEE Transactions on Advanced Packaging*, vol. 24, no. 3, pp. 334–346, August 2001.
- [121] Z. Menachem and E. Jerby, "Transfer matrix function (TMF) for wave propagation in dielectric waveguides with arbitrary transverse profiles," *IEEE Transactions on Microwave Theory and Techniques*, vol. 46, no. 7, pp. 975–982, July 1998.
- [122] Jin-Fa Lee, "Advances in finite element methods for microwave engineering," *Asia-Pacific Microwave Conference*, vol. 1, no. 2, pp. 193–198, 2001.
- [123] P. Krauss and F. Arndt, "Rigorous mode-matching method for the modal analysis of the T-junction circular to sidecoupled rectangular waveguide," *Microwave Symposium Digest*, vol. 3, pp. 1355–1357, 1995.
- [124] J. M. Reiter and F. Arndt, "A boundary contour mode-matching method for the rigorous analysis of cascaded arbitrarily shaped H-plane discontinuities in rectangular waveguides," *IEEE Microwave and Guided Wave Letters*, vol. 2, no. 10, pp. 403–405, October 1992.

- [125] F. Arndt, R. Beyer, J. M. Reiter, T. Sieverding, and T. Wolf, "Automated design of waveguide components using hybrid mode-matching/numerical EM building-blocks in optimization-oriented CAD frameworks-state of the art and recent advances," *IEEE Transactions on Microwave Theory and Techniques*, vol. 45, no. 5, pp. 747–760, May 1997.
- [126] A. C. Beck, "Measurement techniques for multimode waveguides," *IRE Transactions on Microwave Theory and Techniques*, pp. 35–42, 1955.
- [127] M. P. Forrer and K. Tomiyasu, "Determination of higher order propagating modes in waveguide systems," *Journal of Applied Physics*, vol. 29, pp. 1040–1045, July 1958.
- [128] V. G. Price, "Measurement of harmonic power generated by microwave transmitters," *IRE Transactions on Microwave Theory and Techniques*, vol. MTT-7, pp. 116–120, January 1959.
- [129] A. J. Taub, "A new technique for multimode power measurement," *IRE Transactions on Microwave Theory and Techniques*, vol. MTT-10, pp. 496–505, November 1962.
- [130] D. S. Levinson and I. Rubinstein, "A technique for measuring individual modes propagating in overmoded waveguide," *IRE Transactions on Microwave Theory and Techniques*, vol. MTT-14, no. 7, pp. 310–322, July 1966.
- [131] Y. Klinger, "The measurement of spurious modes in overmoded waveguides," *IEE Proceedings*, vol. 106B, pp. 89–93, September 1959.
- [132] D. J. Lewis, "Mode couplers and multimode measurement techniques," *IRE Transactions on Microwave Theory and Techniques*, vol. MTT-7, pp. 110–116, January 1959.
- [133] C. Seguinot, P. Kennis, J.-F. Legier, F. Huret, E. Paleczny, and L. Hayden, "Multimode TRL - a new concept in microwave measurements: theory and experimental verification," *IEEE Transactions on Microwave Theory and Techniques*, vol. 46, no. 5, pp. 536–542, May 1998.

- [134] J. A. Lorbeck and R. J. Vernon, "Determination of mode content and relative phase in highly overmoded circular waveguides by open-ended radiation pattern measurement," *Antennas and Propagation Society International Symposium*, vol. 3, pp. 1251–1254, 1989.
- [135] R. H. Johnston, "Measurement of modes in an overmoded circular waveguide," *Proceedings of the 40th Midwest Symposium on Circuits and Systems*, vol. 1, pp. 599–602, 1998.
- [136] G. V. Eleftheriades, A. S. Omar, and L. P. B. Katehi G. M. Rebeiz, "Some important properties of waveguide junction generalized scattering matrices in the context of the mode matching technique," *IEEE Transactions on Microwave Theory and Techniques*, vol. 42, no. 10, pp. 1896–1903, October 1984.
- [137] R. T. Deck, M. Mirkov, and B. G. Bagley, "Determination of bending losses in rectangular waveguides," *Journal of Lightwave Technology*, vol. 16, no. 9, pp. 1703–1714, September 1998.
- [138] B. Gimeno and M. Guglielmi, "Multimode equivalent network representation for H- and E-plane uniform bends in rectangular waveguide," *IEEE Transactions on Microwave Theory and Techniques*, vol. 44, no. 10, pp. 1679–1687, October 1996.
- [139] C. Nantista, N. M. Kroll, and E. M. Nelson, "Design of a 90 degrees overmoded waveguide bend," *Proceedings of the Particle Accelerator Conference*, vol. 2, pp. 983–985, 1993.
- [140] M. Miyagi, K. Harada, and S. Kawakami, "Wave propagation and attenuation in the general class of circular hollow waveguides with uniform curvature," *IEEE Transactions on Microwave Theory and Techniques*, vol. 32, no. 5, pp. 513–521, 1984.
- [141] A. Weisshaar, S. M. Goodnick, and V. K. Tripathi, "A rigorous and efficient method of moments solution for curved waveguide bends," *IEEE Transactions on Microwave Theory and Techniques*, vol. 40, no. 12, pp. 2200–2206, 1992.

- [142] Guo-Xin Fan and Qing Huo Liu, "Dyadic Green's functions for curved waveguides and cavities and their reformulation," *Antennas and Propagation Society International Symposium*, no. 3, pp. 1504–1507, 1998.
- [143] A. Weisshaar, M. Mongiardo, and V. K. Tripathi, "Accurate and efficient CAD-oriented modeling of circular waveguide bends," *MTT-S International Microwave Symposium Digest*, vol. 3, pp. 1591–1594, 1997.
- [144] M. Brambilla and U. Finzi, "Electro-magnetic modes of the toroidal cavity," *IEEE Transactions on Plasma Science*, vol. PS-2, pp. 112–114, September 1974.
- [145] F. Cap and R. Deutsch, "Toroidal resonators for electromagnetic waves," *IEEE Transactions on Microwave Theory and Techniques*, vol. MTT-26, no. 7, pp. 478–486, July 1978.
- [146] K. W. Kark, "Perturbation analysis of electromagnetic eigenmodes in toroidal waveguides," *IEEE Transactions on Microwave Theory and Techniques*, vol. 39, no. 4, pp. 631–637, April 1991.
- [147] M. S. Janaki and B. Dasgupta, "Eigenmodes for electromagnetic waves propagating in a toroidal cavity," *IEEE Transactions on Plasma Science*, vol. 18, no. 1, pp. 78–85, February 1990.
- [148] A. Melloni, F. Carniel, R. Costa, and M. Martinelli, "Determination of bend mode characteristics in dielectric waveguides," *Journal of Lightwave Technology*, vol. 19, no. 4, pp. 571–577, April 2001.
- [149] H. Flugel and E. Kuhn, "Computer-aided analysis and design of circular waveguide tapers," *IEEE Transactions on Microwave Theory and Techniques*, vol. 36, no. 2, pp. 332–336, February 1988.
- [150] W. A. Huting and K. J. Webb, "Numerical analysis of rectangular and circular waveguide tapers," *IEEE Transactions on Magnetics*, vol. 25, no. 4, pp. 3095–3097, July 1989.

- [151] G. R. Branner, B. P. Kumar, and D. G. Thomas, "Design of microstrip T-junction power divider circuits for enhanced performance," *Proceedings of the 38th Midwest Symposium on Circuits and Systems*, vol. 2, pp. 1213–1215, 1996.
- [152] F. Boone and K. Wu, "Full-wave modal analysis of NRD guide T-junction," *IEEE Microwave and Guided Wave Letters*, vol. 10, pp. 228–230, June 2000.
- [153] X.-P. Liang, K. A. Zaki, and A. E. Atia, "A rigorous three plane mode-matching technique for characterizing waveguide T-junctions, and its application in multiplexer design," *IEEE Transactions on Microwave Theory and Techniques*, vol. 39, no. 12, pp. 2138–2147, December 1991.
- [154] Ke-Li Wu, Ming Yu, and Apu Sivadas, "Novel modal analysis of a circular-to-rectangular waveguide T-junction and its application to design of circular waveguide dual-mode filters," *IEEE Transactions on Microwave Theory and Techniques*, vol. 50, no. 2, pp. 465–473, February 2002.
- [155] P. V. Nikitin, D. D. Stancil, O. K. Tonguz, A. E. Xhafa, A. G. Cepni, and D. Brodtkorb, "RF propagation in an HVAC duct system: impulse response characteristics of the channel," *IEEE AP-S Symposium and USNC/URSI Meeting*, vol. 2, pp. 726–729, San Antonio, TX, June 2002.
- [156] M. V. Davidovich, V. P. Meschanov, and N. F. Popova, "Waveguide probe structure on microwave," *9th International Crimean Microwave Conference*, pp. 362–363, 1999.
- [157] M. R. Chatterjee and L. S. Green, "Derivation of impulse response and transfer function of an optical fiber under chromatic dispersion and application to a linear fiber-optic communication system," *Proceedings of the IEEE Southern Tier Technical Conference*, vol. 1, pp. 209–216, 1990.

- [158] K. C. Byron and D. M. Ashworth, "Intermodal and intramodal dispersion measurements on 1.3 μm single-mode fibre for use at 0.85 μm ," *IEE Proceedings on Optoelectronics*, vol. 135, no. 3, pp. 220–222, June 1998.
- [159] T. Zwick, F. Demmerle, and W. Wiesbeck, "Comparison of channel impulse response measurements and calculations in indoor environment," *Antennas and Propagation Society International Symposium*, vol. 2, pp. 1498–1501, 1996.
- [160] S. Jungling, "The impulse model including waveguiding effects using modal analysis," *Proceedings of the IEEE Ultrasonics Conference*, vol. 1, pp. 95–99, 1991.
- [161] K. A. Wear, "The effects of frequency-dependent attenuation and dispersion on sound speed measurements: applications in human trabecular bone," *IEEE Transactions on Ultrasonics, Ferroelectrics and Frequency Control*, vol. 47, no. 1, pp. 265–273, January 2000.
- [162] M. Lienard and P. Degauque, "Propagation in road tunnels: from modeling to experiments," *Proceedings of the Fourth IEEE International Caracas Conference on Devices, Circuits and Systems*, pp. 509–512, 2002.
- [163] A. M. Kawalec, "Dispersive filter having long impulse response," *International Conference on Microwaves, Radar and Wireless Communications*, vol. 1, pp. 74–77, 2000.
- [164] T. S. Rappaport, *Wireless Communications: Principles and Practice.*, Prentice-Hall, 1996.
- [165] A. E. Xhafa, O. K. Tonguz, , A. G. Cepni, D. D. Stancil, P. V. Nikitin, and D. Brodtkorb, "Theoretical estimates of HVAC duct capacity for high-speed Internet access," *Proceedings of the IEEE International Conference on Communications (ICC'02)*, vol. 2, pp. 936–939, New York, NY, May 2002.
- [166] A. V. Shishkova, "Application of the spherical wave theory to the calculation of the near-field radiation from an open-ended circular waveguide," *The Fourth International Kharkov*

Symposium on Physics and Engineering of Millimeter and Sub-Millimeter Waves, , no. 2, pp. 645–647, June 2001.

- [167] S. Maci, P. Ya. Ufimtsev, and R. Tiberio, “Equivalence between physical optics and aperture integration for radiation from open-ended waveguides,” *IEEE Transactions on Antennas and Propagation*, vol. 45, no. 1, pp. 183–185, January 1997.
- [168] A. Altintas, P. H. Pathak, and M.-C. Liang, “A selective modal scheme for the analysis of EM coupling into or radiation from large open-ended waveguides,” *IEEE Transactions on Antennas and Propagation*, vol. 36, no. 1, pp. 84–96, January 1988.
- [169] K. J. Bois, A. D. Benally, and R. Zoughi, “Multimode solution for the reflection properties of an open-ended rectangular waveguide radiating into a dielectric half-space: the forward and inverse problems,” *IEEE Transactions on Instrumentation and Measurement*, vol. 48, no. 6, pp. 1131–1140, December 1999.
- [170] C.-W. Chang, K.-M. Chen, and J. Qian, “Nondestructive determination of electromagnetic parameters of dielectric materials at X-band frequencies using a waveguide probe system,” *IEEE Transactions on Instrumentation and Measurement*, vol. 46, no. 5, pp. 1084–1092, October 1997.
- [171] J. K. Piotrowski, “Analysis of a coaxial line-circular waveguide junction used for measurement of materials,” *International Conference on Microwaves, Radar and Wireless Communications*, vol. 1, pp. 333–336, 2000.
- [172] Z. X. Shen and R. H. MacPhie, “A simple method for calculating the reflection coefficient of open-ended waveguides,” *IEEE Transactions on Microwave Theory and Techniques*, vol. 45, no. 4, pp. 546–548, April 1997.
- [173] C. W. Chuang and P. H. Pathak, “Ray analysis of modal reflection for three-dimensional open-ended waveguides,” *IEEE Transactions on Antennas and Propagation*, vol. 37, no. 3, pp. 339–346, March 1989.

- [174] S. L. Lopuch and T. K. Ishii, "Field distribution of two conducting posts in a waveguide," *IEEE Transactions on Microwave Theory and Techniques*, vol. 32, no. 1, pp. 29–33, January 1984.
- [175] C. S. Lee, S. W. Lee, and S. L. Chuang, "Plot of modal field distribution in rectangular and circular waveguides," *IEEE Transactions on Microwave Theory and Techniques*, vol. 33, no. 3, pp. 271–274, March 1985.